MicroRNAs in neural stem cell proliferation and differentiation

Dissertation
zur
Erlangung des Doktorgrades (Dr. rer. nat.)
der
Mathematisch-Naturwissenschaftlichen Fakultät
der
Rheinischen Friedrich-Wilhelms-Universität Bonn

vorgelegt von

Beate Katharina Roese-Koerner

aus
Bonn

Bonn 2015

Angefertigt mit Genehmigung der Mathematisch-Naturwissenschaftlichen
Fakultät der Rheinischen Friedrich-Wilhelms-Universität Bonn

1. Gutachter: Prof. Dr. Oliver Brüstle

2. Gutachter: Prof. Dr. Waldemar Kolanus

Tag der Promotion: 13.05.2015

Erscheinungsjahr: 2015

TABLE OF CONTENTS

ABBREVATIONS

°C	Degree Celsius
3'UTR	3' untranslated region
AA	L-Ascorbic Acid
ADAM protease	A disintegrin and metalloproteinase
Ago	Argonoute protein
APS	Ammonium persulfate
AT	Austria
ATP	Adenosine triphosphate
BAF53	Transcriptional regulator actin-like 6
BDNF	Brain-derived neurotrophic factor
BES	N,N-Bis(2-hydroxyethyl)-2-aminoethanesulfonic acid, N,N-Bis(2-hydroxyethyl)taurine
bp	Basepair
cAMP	Cyclic adenosine monophosphate
cDNA	Copy Deoxyribonucleic Acid
CEBP-β	CCAAT/enhancer binding protein beta
C. Elegans	Caenorhabditis elegans
CH	Switzerland
ChIP	Chromatin immuno precipitation
CHIR99021	6-(2-(4-(2,4-Dichlorophenyl)-5-(4-methyl-1H-imidazol-2-yl)-pyrimidin-2-ylamino)ethyl-amino)-nicotinonitrile
c-Myc	Myelocytomatosis viral oncogene homolog
CREB	cAMP-response binding protein
CNS	Central nervous system
CoR	Corepressor
CSPD	Chloro-5-substituted adamantyl-1,2-dioxetane phosphate
ct	Threshold cycle
Cy3	Cyanin 3
d	Day
DAPI	4′,6-diamidino-2-phenylindole
dbcAMP	N6,2′-O-Dibutyryladenosine 3′,5′-cyclic monophosphate sodium salt
ddH_2O	Double-destilled water
DE	Germany
DEPC	Diethylpyrocarbonate
DGCR8	DiGeorge syndrome critical region gene 8
DIG	Digoxigenin
DIG-11-UTP	Digoxigenin-11-uridine-5'-triphosphate
DLL	Delta-like
dLMO	Drosophila LIM-only protein
DMEM	Dulbecco's Modified Eagle Medium
DMSO	Dimethylsulfoxid
DN	Dominant negative
DNA	Desoxyribonucleic acid
dNTPs	Desoxynucleosid-triphosphate mix
DPBS	Dulbeccos phosphate buffered saline

ds	Double-stranded
EDTA	Ethylenediaminetetraacetic acid
EGF	Epidermal growth factor
EGFR	Epidermal growth factor receptor
EN2	Engrailed 2
FCS	Fetal calf serum
FGF	Fibroblast growth factor
FLS	Formamide-loading buffer suspension
FN	Fibronectin
FOXA2	Forkhead box A2
FOXG1	Forkhead box G1
FR	France
g	Gram
GABA	γ-Aminobutyric acid
GDNF	Glial cell line-derived neurotrophic factor
GFAP	Glial fibrillary acidic protein
GFP	Green fluorescent protein
h	Homo sapiens
HAc	Histone acetyltransferases
HDAc	Histone deacetylase
HeLa	Henrietta Lacks
HER	HES-related
HES	Hairy and enhancer of split
hESCs	Human embryonic stem cells
HEY	Hairy/enhancer-of-split related with YRPW motif 1
ICM	Inner cell mass
iPSCs	Induced pluripotent stem cells
JAG	Jagged
JAK	Janus kinase
Kb	Kilobases
Klf4	Krüppel-like factor 4
KO-DMEM	Knockout DMEM
KO-SR	Knockout serum replacement
KO-SRM	KO-SR containing medium
LMX1A	LIM homeobox transcription factor 1A
LN	Laminin
LNA	Locked nucleic acid
Log	Logarithm
M	Molar
MAML	Mastermind-like
MEFs	Mouse embryonic fibroblasts
mg	Milligram
MG	Matrigel
MHB	Midbrain-hindbrain boundary
min	Minute
miRNA, miR	MicroRNA
miRISC	miRNA induced silencing complex
ml	Milliliter
mM	Millimolar

mRNA	Messenger RNA
ms	Mouse
MSX1	Msh homeobox 1
mV	Millivolt
MYB	Myeloblastosis viral oncogene homolog
NaCl	Natrium chloride
ND	Neuronal differentiation
ND15	15 days differentiated lt-NES cultures
ND30	30 days differentiated lt-NES cultures
NEUROG	Neurogenin
ng	Nanogramm
NICD	Notch intracellular domain
NL	Netherlands
nM	Nanomolar
NSC	Neural stem cells
nt	Nucleotide(s)
Oct4	Octamer-binding transcription factor 4
PCR	Polymerase chain reaction
PAX6	Paired box 6
Pen/Strep	Penicillin/Streptomycin
PFA	Paraformaldehyd
PI	Protease inhibitor cocktail
PO	Poly-L-ornithine
Pol II / Pol III	RNA Polymerase II or III
Pre-miRNA	Precursor microRNA
Pri-miRNA	Primary microRNAs
PSCs	Pluripotent stem cells
PSEN	Presenilin
qRT-PCR	Quantitative real-time polymerase chain reaction
rb	Rabbit
RBPj	Recombination signal binding protein for immunoglobulin kappa J region
REL	Reticuloendotheliosis viral oncogene homolog
REST	RE1-silencing transcription factor
RNA	Ribonucleic acid
RNAi	RNA interference
rpm	Rounds per minute
RT	Room temperature
rRNA	Ribosomal RNA
s	Second
SDS	Sodium dodecyl sulfate
SEM	Standard error of the mean
SHH	Sonic hedgehog
siRNA	Small interfering RNA
SIRT1	Sirtuin 1
snoRNA	Small nucleolar RNA
snRNA	Small nuclear RNA
SOX2	Sex determining region Y-box 2
STAT	Signal-transducer and activator of transcription protein

STMN1	Stathmin1
SSC	Solution of sodium chloride and sodium citrate
Taq DNA polymerase	Thermus aquaticus DNA polymerase
TBE	Tris-borate-EDTA
TC	Tissue culture
TEMED	N,N,N′,N′-Tetramethylethylenediamine
TGFβ	Transforming growth factor β
TH	Tyrosin hydroxylase
TLX	Nuclear receptor subfamily 2, group E, member 1
Tris	Tris(hydroxymethyl)aminomethane
tRNA	Transfer RNA
Tween20	Polyoxyethylensorbitanmonolaurat
UK	United Kingdom of Great Britain and Northern Ireland
US	United States of America
µg	Microgram
µl	Microliter
µm	Micrometer
µM	Micromolar

ABSTRACT

MicroRNAs (miRNAs) are post-transcriptional regulators of gene expression that are emerging as key regulators of neural (stem) cell properties. Due to their ability to regulate a broad repertoire of targets, they represent an exciting tool to modulate stem cell fate. Brain-enriched miR-9/9* has been described to enhance neural stem cell differentiation and impact on regionalization. Furthermore, it was suggested to interact with the Notch signaling pathway, which is well known to play a fundamental role in neural stem cell maintenance and differentiation.

To investigate a potential miRNA-Notch-interplay, a Notch-dependent population of neuroepithelial stem cells derived from human embryonic stem (lt-NES) cells was chosen as a model system. In line with previous findings, ectopic expression of miR-9/9* impaired self-renewal and promoted differentiation of lt-NES cells. Our analysis revealed that this impact of miR-9/9* is, at least in part, due to a feedback loop between miR-9/9* and Notch activity. Notch directly controls miR-9/9* expression on a transcriptional level, while miR-9/9* in turn regulates Notch signaling by targeting of HES1 and NOTCH2. However, elevated levels of individual miR-9 and miR-9* revealed a separate way of action. While miR-9 enhanced differentiation and targeted HES1 and NOTCH2, miR-9* enhanced differentiation, impaired self-renewal of lt-NES cells and was shown to target NOTCH2 and SOX2.

Compared to other miRNAs identified in a miRNA expression profiling during lt-NES cell differentiation (i.e. miR-7, miR-128, and miR-130b), only elevated levels of miR-9/9* induced significant changes in lt-NES proliferation and spontaneous differentiation. Nevertheless, long-term (15 days) lt-NES cell differentiation was enhanced by miR-9/9* as well as miR-7. Detailed analysis revealed that they even affect neuronal subtype specification. While the overall number of differentiated neurons increased, the generation of neurons positive for dopaminergic marker TH was impaired upon miR-9/9* and miR-7 overexpression. In line with this, miR-9, miR-9*, and miR-7 were downregulated during the time course of a floor plate precursor based differentiation protocol for the generation of mesencephalic dopaminergic neurons from human pluripotent stem cells. Futhermore, overexpression of miR-9/9* and miR-7 reduced mRNA expression levels of EN2 and FOXA2, two additional dopaminergic markers.

Taken together, these results show that miRNAs can be used to modulate human neural stem cell maintenance, differentiation and subtype specification. Specifically, miR-9 and miR-9* act on human neural stem cell maintenance and spontaneous differentiation – to some extent by their interplay with the Notch signaling pathway. In addition, miR-9/9* as well as miR-7 impact on neural stem cell differentiation and lineage decision.

1. Introduction

1.1 Human pluripotent stem cells

The unique potential to self-renew and to differentiate into diverse cell types are hallmarks defining stem cells. In early mammalian development, a specific class of stem cells called pluripotent stem cells (PSCs) is able to give rise to cells of all three germ layers. These cells can be isolated from the inner cell mass (ICM) of a human blastocyst and expanded in cell culture maintaining their potential to proliferate and differentiate depending on the signals provided by their environment [1]. Once isolated and propagated *in vitro*, these pluripotent stem cells are called human embryonic stem cells (hESCs, Fig. 1.1).

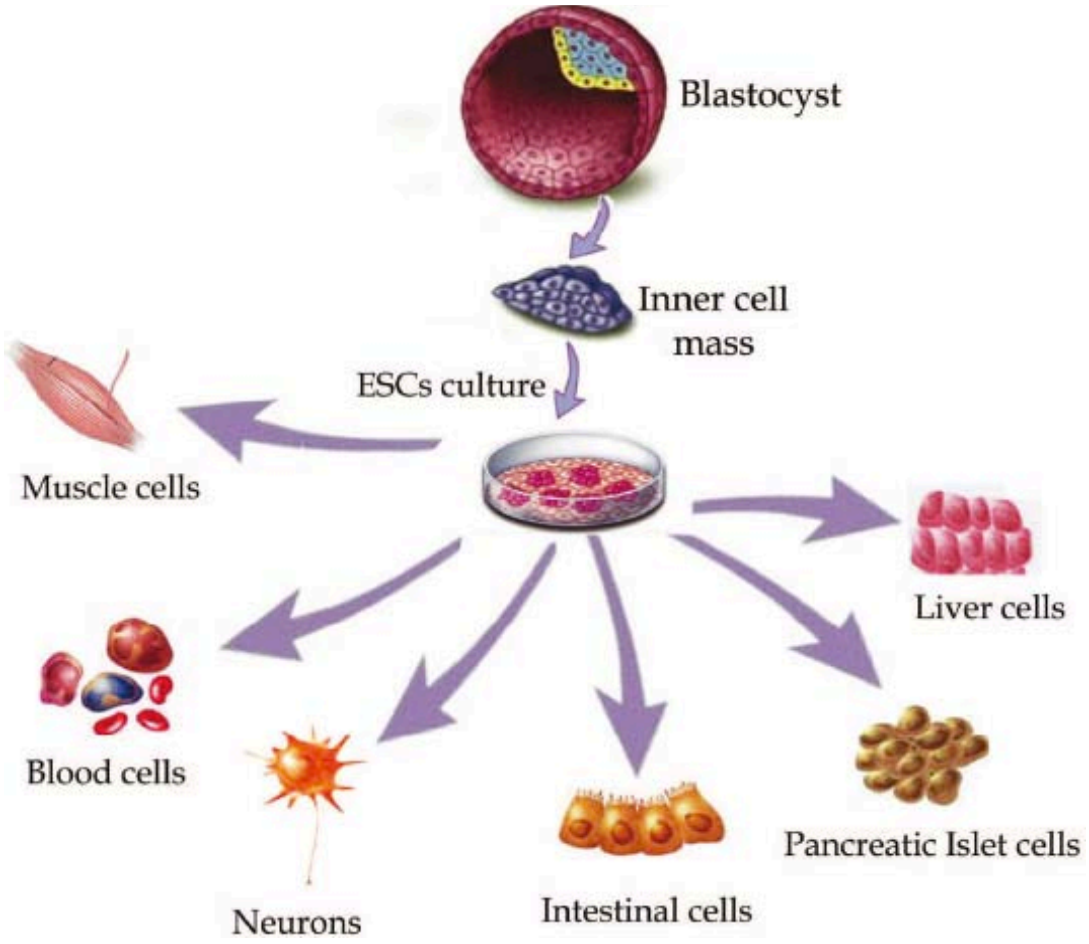

Fig. 1.1: Derivation of human embryonic stem cells.
The isolated inner cell mass of a human blastocyst is cultured on a layer of mitotically inactivated mouse embryonic fibroblasts as hESCs. Under defined conditions, these hESCs are able to differentiate into tissues of all three embryonic germ layers. Image taken from [2].

Due to their ability of almost unlimited self-renewal hESCs can be used as a reliable cell source to gain insight into early processes of human development as well as to define signals for the derivation of specific somatic cell types. The access to many

human tissues is restricted due to obvious ethical reasons. Therefore, the generation of defined somatic cell types is of major importance for future drug screening and therapeutic cell replacement strategies [3].

In 2007, Takahashi and Yamanaka were able to identify four transcription factors that were sufficient to induce pluripotency in somatic cells. They showed that short-term overexpression of Oct4 (Octamer-binding transcription factor 4), Sox2 (Sex determining region Y-box 2), Klf4 (Krüppel-like factor 4) and c-Myc (myelocytomatosis viral oncogene homolog) in adult human fibroblasts induces a cell population capable of expansion and differentiation similar to hESCs. The cells resulting from this protocol are called induced pluripotent stem cells (iPSCs, [4], Fig. 1.2).

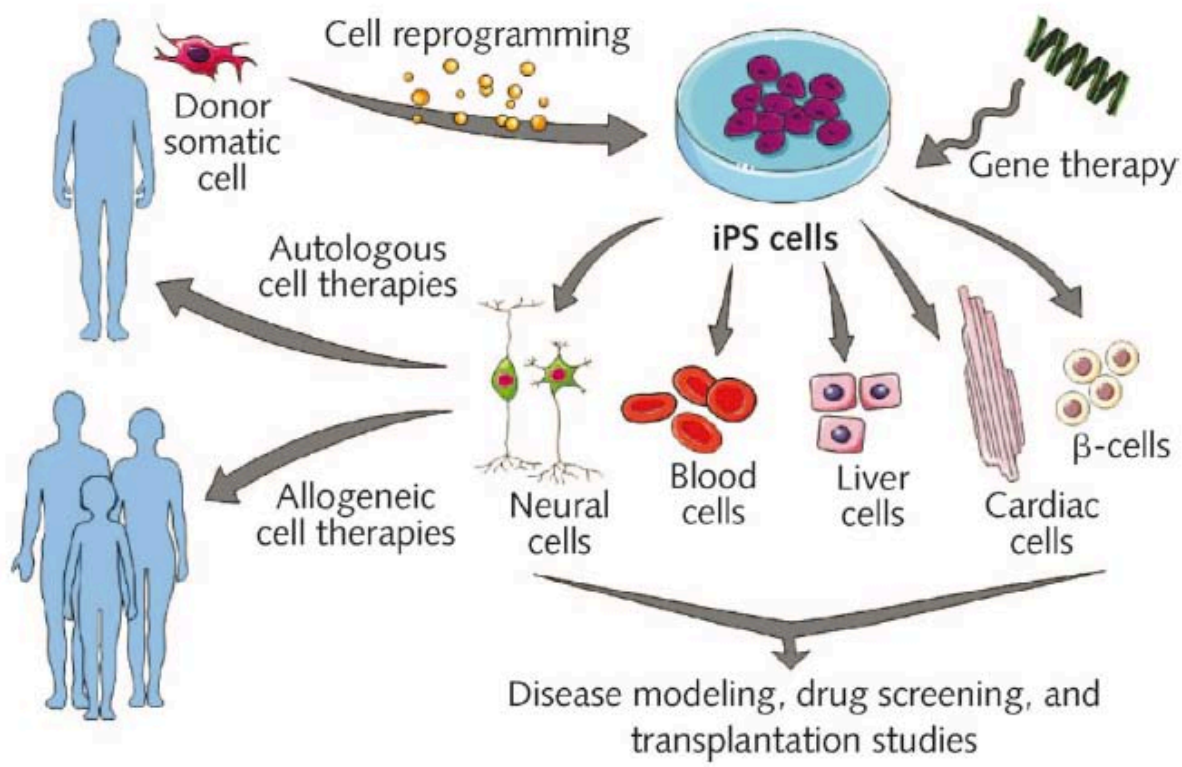

Fig. 1.2: Derivation of human induced pluripotent stem cells.
Donor somatic cells can be reprogrammed into iPSCs by defined factors. From the resulting iPSCs desired functional cell types from all three germ layers could be derived. These cells could potentially be used for *in vitro* disease modeling and drug screening as well as autologous and allogeneic cell transplantation in combination with gene therapy. Image taken from [5].

Theoretically, both ESCs and iPSCs could be used to produce all cell types present in the human body (Fig. 1.1, Fig. 1.2). Most hESC/iPSC differentiation paradigms represent ‘‘run-through’’ procedures (reviewed in [3, 6]), which means that no stable intermediate cultures are generated. In these protocols, undifferentiated pluripotent

stem cells (PSCs) are exposed to complex differentiation protocols including addition of extrinsic factors or genetic modifications to achieve the desired cell types [7]. The outcome of these paradigms can be highly variable. Long term-expandable tissue-specific stem cells derived from PSCs as an intermediate can be used to reduce this variability. Most expandable populations show a broad and stable differentiation potential into the desired cell types. Due to the limited regenerative capacity of the central nervous system (CNS) and the restricted access to primary human neural tissue there is an increased need to generate stably expandable neural stem cells of defined spatial and temporal identity.

1.2 Long-term self-renewing neuroepithelial-like stem cells derived from human embryonic stem cells

Many attempts have been made to generate neural stem cells from hESCs [8-10]. In 2009, *Koch et al.* generated a long-term, self-renewing neuroepithelial stem cell population from hESCs (lt-NES cells), which can be expanded extensively in the presence of fibroblast growth factor 2 (FGF2) and epidermal growth factor (EGF). Although in the phenotypic and regional identity of lt-NES cells is well defined, these cells maintain the ability to form neuroepithelial rosette architectures *in vitro* and express rosette-specific genes (Fig. 1.3, [7]). Even after long-term proliferation, they still remain responsive to extrinsic morphogens and retain sufficient plasticity to be recruited into different neural subtypes such as neurons and glial cell types in a controlled manner [7].

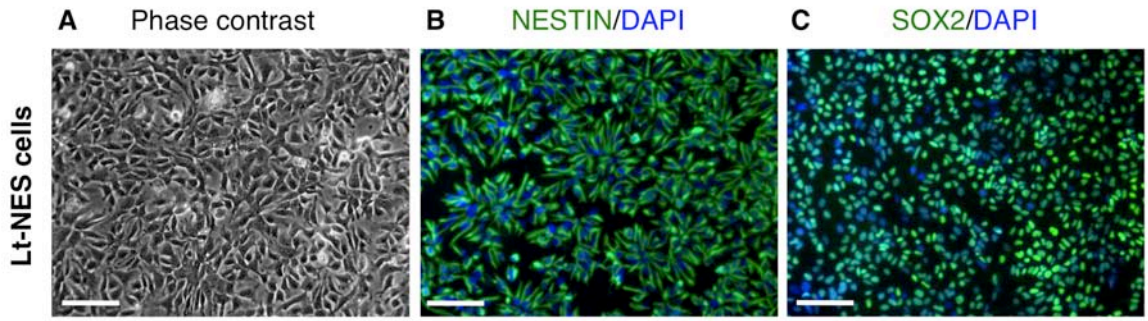

Fig. 1.3: Morphology of lt-NES cells.
(A) Phase contrast pictures showing the homogenous, rosette-like morphology of lt-NES cells in high density cultures. **(B,C)** Representative immunostainings for neural stem cell markers NESTIN **(B)** and SOX2 **(C)** in proliferating lt-NES cells. DAPI (blue) stains nuclei. Scale bars indicate 100 μm.

Upon differentiation into neurons, lt-NES cells are able to form functional neuronal networks and undergo synaptic integration upon transplantation into the brain of immuno-deficient mice [7]. Taking this broad and stable neuronal differentiation potential into account lt-NES cells represent a suitable model system to study the biology of human neural stem cells.

1.3 Notch signaling and neural stem cells

Data from various model organisms showed that neural stem cells depend on Notch signaling for their maintenance and differentiation (reviewed in [11, 12]). In early mouse development, constitutive activation of Notch signaling inhibits neuronal differentiation [13] and maintains neural stem cells in a proliferative state [14]. Accordingly, inactivation of Notch receptor antagonist Numb delays cell cycle arrest, impairs differentiation and induces hyperproliferation in the developing mouse cortex [15].

Notch is a transmembrane receptor whose signaling is initiated by binding to its ligands (eg. Delta or Jagged) on a neighboring cell. In humans, four isoforms of the Notch receptor, namely NOTCH 1-4, can be found as well as three isoforms of Delta (DLL1, 3 and 4) and two isoforms of Jagged (JAG1 and JAG2) [16]. Canonical Notch signaling is mediated via sequential proteolytic cleavage carried out by ADAM protease (a disintegrin and metalloproteinase) and the γ-secretase complex (Fig. 1.4). Thereby, the intracellular domain of Notch (NICD) is released and able to translocate into the nucleus. In the nucleus, cleaved NICD displaces the HDAc (histone deacetylase)-CoR (co-repressor) complex, which is bound to RBPj (DNA binding protein transcriptional regulator recombination signal binding protein for immunoglobulin kappa J region). Once NICD and RBPj form a complex, they recruit transcriptional coactivators like MAML (mastermind-like) and HAc (histone acetyltransferases). By binding to the RBPj motifs located in promoter regions, this complex promotes the transcription of Notch downstream targets like the HES (hairy and enhancer of split) and HEY (hairy/enhancer-of-split related with YRPW motif) [17] family (Fig. 1.4) as well as cell cycle regulators like Cyclin E1 (reviewed in [18]).

However, the effect of Notch on proliferation and differentiation depends on its activation level [19]. Even though Notch signaling is needed for stem cell

maintenance and proliferation, it has been shown that its activation can also lead to quiescence in adult neural stem cells [20].

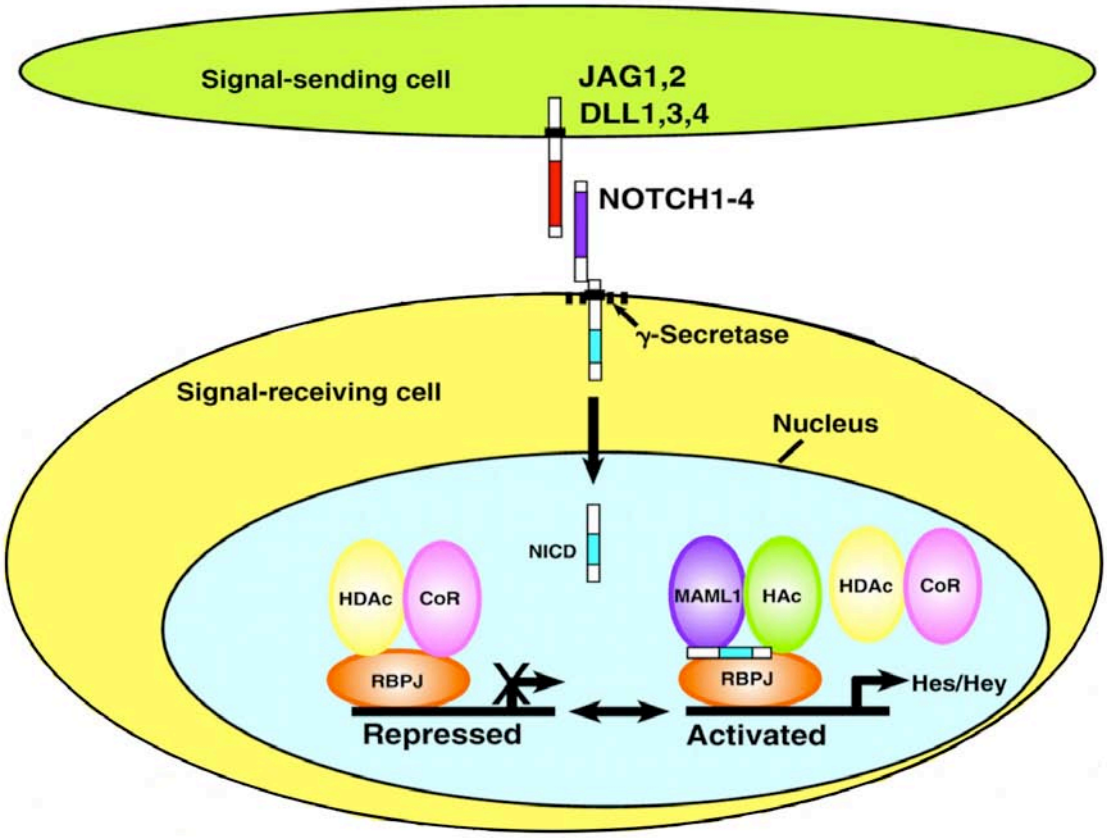

Fig. 1.4: Core components of the canonical Notch signaling pathway.
Notch signaling is activated by interaction of the Notch family receptors on one cell with ligands of the Jagged and Delta-like families on another cell. Subsequently the transmembrane receptor Notch is proteolytically cleaved freeing its intracellular domain. NICD translocates to the nucleus (blue), where it displaces the HDAc-CoR complex from the RBPj protein. NICD and RBPj form an activation complex recruiting MAML and HAc that triggers transcriptional activation of Notch target genes like the HEY and HES families. Image taken from [21].

In lt-NES cells, Notch contributes to the maintenance of a self-renewing undifferentiated state in part through its impact on G1/S-phase transition [22]. In line with this, Notch inhibition triggers an early onset of neuronal differentiation in lt-NES cells [22].

1.4 MiRNA biogenesis and mechanisms of action

One mechanism potentially influencing neural stem cell behavior is post-transcriptional regulation of genes involved in their maintenance and differentiation. In 1993 it was found that short non-coding RNAs are able to regulate gene activity in *C. Elegans* by binding to the 3´untranslated regions of genes [23]. This was the first discovery of RNA interference – a mechanism regulating global messenger RNA

(mRNA) levels. Since then, many classes of small regulatory RNAs were identified. MicroRNAs (miRNAs) present one endogenously expressed class and their mature form is of 21-25 nucleotides (nt) in length. About half of all known human miRNA genes are located in introns of protein-coding genes, while others are found in untranslated regions [24]. Their first transcript is called primary miRNA (pri-miRNA) and mainly produced by polymerase II [25]. Only a small subset of miRNAs located in repetitive regions of the genome is transcribed by polymerase III [26] (Fig. 1.5A).

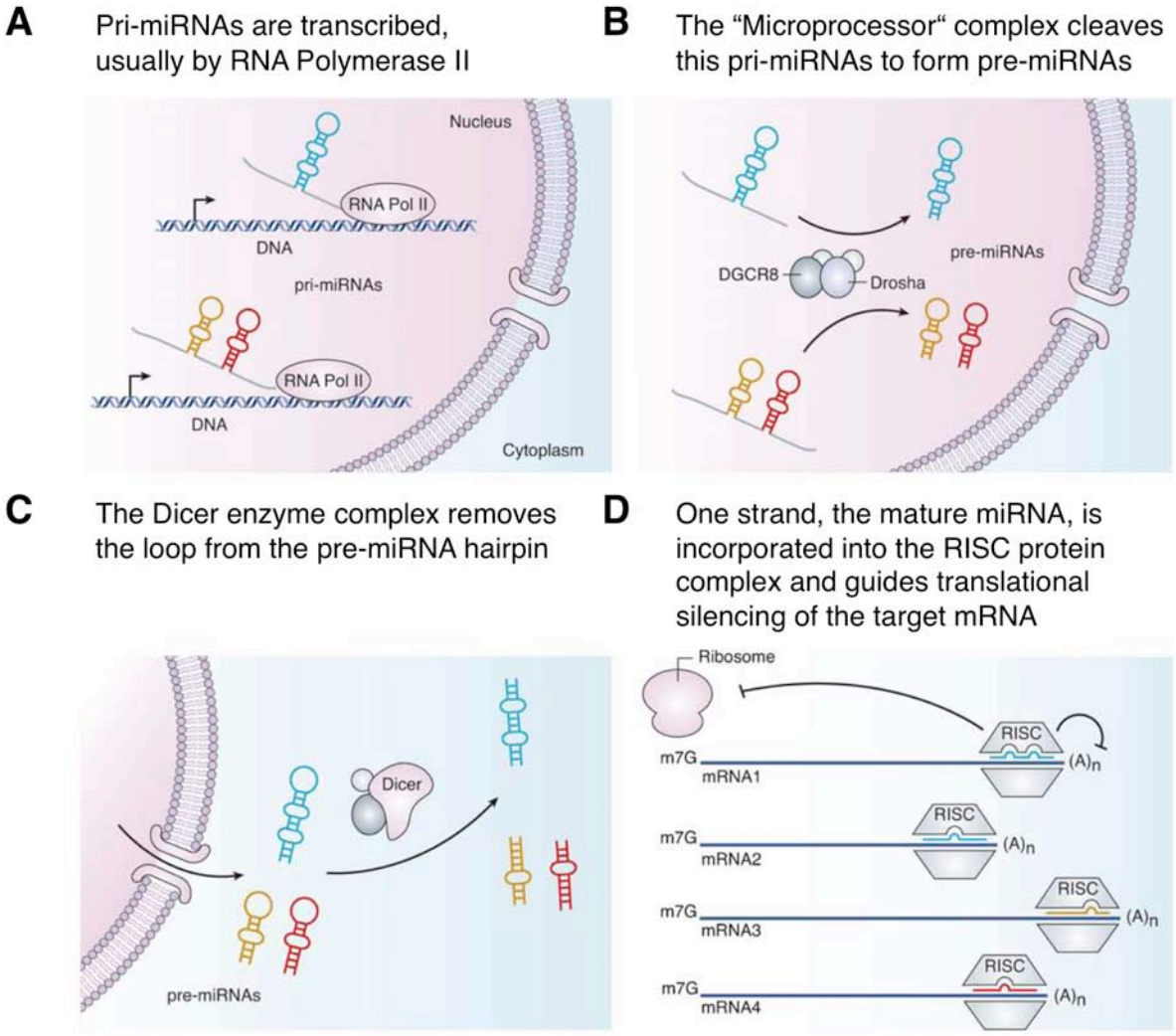

Fig. 1.5: MiRNA biogenesis and mechanism of action.
(A) A pri-form of the miRNAs is transcribed from genomic loci by RNA polymerase II or III **(B)** and further processed by an enzymatic complex containing DGCR8 and Drosha. **(C)** The resulting pre-form is exported to the cytosol and cleaved into the mature form by Dicer. **(D)** Mature miRNAs are incorporated into the miRISC complex and guide it to specific mRNAs. Once bound the miRISC complex triggers mRNA silencing. Image taken from [27].

The primary transcripts produced by the two polymerases form imperfect hairpin structures. These hairpins can encode either one single or a cluster of several mature

miRNAs. The „microprocessor“ protein complex containing a Drosha Type 3 RNase and cofactor DGCR8 recognizes and cleaves the hairpin structures (Fig. 1.5B) generating a second precursor form of the mature miRNA called pre-miRNA. This cleavage permits the export of the pre-miRNA into the cytoplasm through nuclear pore complexes [28-30]. In the cytoplasm, the pre-miRNA is further processed into its mature form by a protein complex including the Dicer type 3 RNase (Fig. 1.5C). This mature miRNA is then incorporated into the miRNA induced silencing complex (miRISC) guiding the complex to complementary or imperfectly complementary target mRNAs. The main binding to the mRNA target is carried out by a stretch of 7-8 nucleotides located at the 5´end of the miRNA called the seed region. Once the mRNA is bound by the miRISC complex, silencing is carried out by an enclosed Argonaute protein (Ago) [31-33] (Fig. 1.5D).

Binding of the miRISC complex can result in reduction of protein levels by either degradation or translational repression of the target mRNA [34-37]. The effects induced by modulation of a target mRNA differ due to cell type specific miRNA and mRNA expression profiles. The regulatory effect of miRNAs can be divided into three subgroups: (1) Switch interactions: the miRNA causes a drop of protein levels to amounts low enough to impair its function. An extreme case of switch interactions is called failsafe interaction. Here, the regulation by a miRNA is employed as a safety net. Target genes regulated by other repressors – even in absence of the specific miRNA – carry target sites for this miRNA to ensure additional translational repression of aberrant transcripts. (2) Tuning interactions: The miRNA reduces the protein produced to optimal, functional levels ensuring cell type-specific expression. (3) Neutral interactions: Even though the miRNA regulates protein levels, this modulation is tolerated by the cell or readjusted by feedback mechanisms (reviewed in [38]).

MiRNAs can exhibit their function even in case of imperfect (bulged) binding, which enable them to modulate multiple targets at once [36, 39]. Therefore, these endogenous regulators provide elegant mechanisms to act on single targets as well as to control whole signaling cascades.

1.5 MiRNAs in neuronal development

In neural development, post-transcriptional regulation by miRNAs is of major importance, which is reflected in the high enrichment of specific miRNAs in the CNS [40]. Approximately 70 percent of all known miRNAs are expressed in the brain, and expression levels of many amongst them change dramatically during brain development [41-43]. Their importance was underlined by Dicer knockout studies in mice [29, 44]. Ablation of Dicer induced an impairment of neuronal differentiation, neuronal cell death and, in some cases, embryonic lethality [45-48]. The phenotypes observed upon Dicer ablation have to be interpreted carefully though as they may not be solely due to miRNA depletion. First, the blockade of the downstream maturation may lead to an enrichment of precursor forms, which could also affect the behavior of the cells [49] (reviewed in [40]). Second, Dicer is also known to be needed for the maturation of other small RNA classes – like snoRNAs [50] and endo-si-RNAs [51].

However – at least in *Zebrafish* embryos – it has been shown that the severe defects in brain morphogenesis induced by the lack of Dicer can be rescued by reinjection of the miR-430 family pointing to a significant role of miRNAs in neural development [52]. Accordingly, several studies in various model organisms demonstrated critical roles for a number of miRNAs in neuronal function or development (reviewed in [40, 53]). In mammals, miRNAs were found to play a role in neural tube closure [54], regulation of dendritic spine morphogenesis [55], terminal differentiation of olfactory precursors [56] and neural progenitor proliferation [57].

In addition to data obtained in model organisms, the participation of miRNAs in the control of neuronal differentiation is supported by results from studies in various cell culture models [58-62]. Their enormous impact on neuronal gene expression was illustrated by ectopic expression of miR-124 in HeLa cells, which switched the expression profile of this cervical tumor cell line towards neuron-specific gene sets [36]. Recently, elevated levels of miR-124 and miR-9/9* were even used to induce the conversion of fibroblasts into neurons [63], underlining the potential of specific miRNAs to define somatic cell types.

In line with these findings, many neuronal subtypes have been shown to depend on miRNA expression (reviewed in [64]). For instance, miRNA depleted mouse ESCs failed to differentiate towards the dopaminergic phenotype, which was partially rescued by transfection of an embryonic mouse midbrain derived small RNA fraction

[65]. In the same study, miR-133b was identified as a specific inhibitor of dopaminergic differentiation [65]. However, this phenotype was not supported by data from a miR-133b knock out mouse model [17]. Further studies on the derivation of dopaminergic neurons revealed additional miRNAs involved in their specification. MiR-7 and miR-132 were shown to inhibit the generation of dopaminergic neurons in mice [66, 67] and, very recently, miR-181a and miR-125b were reported to enhance dopaminergic lineage choice in lt-NES cells [68].

To gain further insight into the specific regulation of miRNAs in human neural development, a miRNA expression profiling of hESCs, proliferating hESC-derived lt-NES cells and their differentiated progeny obtained after 15 and 30 days of growth factor withdrawal was carried out [68]. In this profiling, the miRNAs were grouped in three categories according to their expression dynamic compared to hESCs. Group 1: miRNAs up-regulated in lt-NES cells and upon induction of neural differentiation; Group 2: miRNAs down-regulated in lt-NES cells and upon induction of neural differentiation; Group 3: miRNAs specifically expressed in hESCs. Expression profiles in group 1 confirmed the upregulation of miRNAs known to be most highly and specifically expressed in the mammalian brain – including miR-124, miR-9/9*, miR-125b and miR-128 [69, 70]. In addition, it revealed increased expression of miRNAs less studied in the neural context – like miR-7, miR-130b, and miR-324 [68] – in the human system.

1.6 Role of miR-9/9* in neuronal development

Among the miRNAs up-regulated in the initial screening during neuronal ESC differentiation [68] miR-9 and miR-9* were particularly interesting (Tab. 1.1). These two miRNAs are derived from the same pri-miRNAs that are transcribed from 3 different loci located on different chromosomes in mammals and show a distinct expression pattern in different organs (reviewed in [71]). MiR-9 was first identified in *Drosophila* [72], where it is called miR-9a. In developing flies, miR-9a is expressed in epithelial cells of the peripheral nervous system but not in mature neurons [73]. Although its sequence is highly conserved between mammals and flies, the expression patterns were found vary between these organisms (reviewed in [74]). In the mammalian brain, miR-9 is among the most highly expressed miRNAs and was

found to be heavily regulated during neuronal differentiation and highly expressed in mature neurons [41, 43, 70, 75].

Many studies in model organisms indicate a role for miR-9 in the proliferation and differentiation of neural stem cells. In mice, it is expressed in a reciprocal gradient with forkhead box protein G1 (FoxG1), a transcription factor that promotes proliferation of cortical progenitor cells [75]. Furthermore, miR-9 was found to enhance neural precursor differentiation by targeting tailless homologue (TLX), a nuclear receptor that is required for maintenance of adult neural precursor cell self-renewal in the murine cortex [76]. In human neural precursors from an earlier developmental stage than lt-NES cells, miR-9 was reported to modulate migration and proliferation by targeting Stathmin (STMN1), a protein promoting microtubule instability [77]. Furthermore, miR-9 modulates regionalization within the CNS. In *Zebrafish*, it restricts the organizer activity at the midbrain-hindbrain boundary (MHB) by targeting several components of the fibroblast growth factor (FGF) pathway and promotes neurogenesis by repression of HES orthologs hairy-related 5 (Her5) and hairy-related 9 (Her9) [78]. Like in *Zebrafish, Xenopus* miR-9 is expressed in the neural tube and regions adjactant to the MHB but not in the spinal cord [79]. Knockdown of miR-9 using morpholinos leads to increased apoptosis in the *Xenopus* forebrain and reduced number of neurons produced in the *Xenopus* hindbrain region [79]. In addition, miR-9 regulates the specification and temporal identity of motor neurons and the columnar formation in the chick spinal cord [80, 81].

Like miR-9, miR-9* impacts on neuronal specification and triggers pro-neural gene expression. However, compared to miR-9, knowledge on miR-9* function in the brain is rather scarce. In mouse, miR-9* takes part in the switch from non-neuronal transcriptional regulator BAF53a (actin-like 6a) to BAF53b (proneural actin-like 6b) [57]. An interaction that may even contribute to the transdifferentiation of fibroblasts into functional neurons [63].

In addition, miR-9* and miR-9 cooperate to block transcription of non-neuronal genes by engaging into a feedback loop with the RE1 silencing transcription factor (REST). While miR-9 targets REST directly, miR-9* reduces levels of its co-factor CoREST. In turn, REST regulates expression of miR-9 and miR-9* by binding to their promoter regions [58]. Their role in neural development raised the question whether miR-9/9* impact on major developmental signaling pathways like Notch.

Table 1.1: Known targets and functions of miR-9 and miR-9* in the nervous system (adapted from [82]).

miRNAs	Functions	Targets	Organism	Reference
miR-9	Restriction of the midbrain-hindbrain boundary extent; promotion of neurogenesis	Fgf8, Fgfr1, Canopy1; Her5, Her9	Zebrafish	[78]
	Regulation of timing of neurogenesis	Her6, Zic5, Elavl3	Zebrafish	[83]
	Modulation of motor neuron subtype specification in the spinal cord	FoxP1	Chicken	[81]
	Specification of temporal motor neuron identity	OC1	Chicken	[80]
	Inhibition of neural progenitor proliferation and apoptosis; regulation of neural progenitor differentiation along the anterior-posterior axis	Hairy1	Xenopus	[79]
	Opposing oscillation to control neural progenitor differentiation	Hes1	Mouse	[84, 85]
	Regulation of Cajal-Retzius cell differentiation during corticogenesis	FoxG1	Mouse	[75, 86]
	Promotion of differentiation and migration in adult neural stem cells	TLX	Mouse	[76]
	Promotion of neuronal differentiation and reduction of glial differentiation	STAT3 phospho-rylation	Mouse	[59]
	Derepression of proneuronal genes	REST	Human	[87]
	Regulation of proliferation and migration of neural progenitors	STMN1	Human	[77]
miR-9*	Derepression of proneuronal genes	CoREST	Human	[87]
	Regulation of activity-dependent dendritic growth in hippocampal neurons	BAF53a	Mouse	[57]
miR-9/9*	Reprogramming of fibroblasts into neurons	BAF53a	Human	[63]

First evidence of a connection between miR-9 and the Notch signaling pathway was found in drosophila sensory organs. Here, miR-9a targets Notch downstream effector senseless, thereby controlling the number of neuronal precursors generated [73]. Most recently, an additional interaction of miR-9 with Notch downstream target Hes1 was suggested in neural development of *Xenopus* [79], *Zebrafish* [83] and *Mus Musculus* [84]. Another study in mouse even indicated that miR-9 is needed for

proper Notch1 signaling [88]. Interestingly, *Krichevsky et al.* found a reduction of mature miR-9 in mice deficient for the γ-secretase complex member Presinilin1 but did not identify the mechanism leading to this reduction [41]. However, the conservation and relevance of these connections between miR-9 and Notch signaling found in model organisms is still to be explored in human neural stem cells.

1.7 Aim of the thesis

Many miRNAs are specifically and differentially expressed during brain development. However, studies addressing their role in human neural development are rather scarce due to the limited availability of primary material and the variable outcomes of human embryonic stem cell (hESC) based differentiation protocols. In order to address these issues and achieve standardized neuronal differentiation, a homogenous population of stable hESC-derived neural precursor cells, i.e. rosette-type neural stem cells of ventral hindbrain identity (lt-NES cells), was chosen as a model system. An initial miRNA expression profiling covering the differentiation of hESCs into lt-NES cells and their neuronal progeny was employed to identify candidate miRNAs for further analysis of their role in neurogenesis. Compared to their levels in hESCs, miR-7, miR-9/9*, miR-128 and miR-130b were up-regulated during the course of this *in vitro* differentiation paradigm.

In this thesis, the expression levels of these candidate miRNAs picked from the screening will be validated and their impact on lt-NES cell proliferation and differentiation will be assessed. To that end, lentiviral constructs to modulate miRNA expression levels will be designed as stable overexpression of specific miRNAs can be used to explore their roles in neural stem cells and to identify targets underlying the observed effects.

Furthermore, the connection between miR-9/9* and the Notch signaling pathway – one of the major pathways regulating neural stem cell properties – will be explored. Due to the dose-dependency of its action, a tight regulation of the Notch activation status is crucial for neural stem cell maintenance. Post-transcriptional regulation by miRNAs is a mechanism well suited to assure proper expression levels of a variety of target genes at once. To unravel a potential interplay between miR-9/9* and Notch, the gain and loss of function phenotypes of both will be compared. In addition, post-

transcriptional regulation of the Notch pathway by miR-9/9* as well as potential Notch-dependent expression of miR-9/9* genomic loci will be analyzed.

In addition to lt-NES cell self-renewal and spontaneous differentiation, another focus of this work lay on the role of specific miRNAs (i.e. miR-9/9* and miR-7) in long-term neuronal differentiation and the specification of neuronal subtypes as knowledge on their involvement may prove useful in directed differentiation of specific neuronal subtypes.

2. Material and Methods

2.1 Material

2.1.1 Technical equipment

Appliance	Name	Manufacturer	Registered Office
Autoclave	D-150	Systec	Wettenberg, DE
Balance	LA310S	Satorius	Göttingen, DE
Balance	BL610	Satorius	Göttingen, DE
Block heater	Thermomixer compact	Eppendorf	Hamburg, DE
Cell culture centrifuge	Megafuge 1.0R	Kendro	Hanau, DE
Chemiluminometer	ChemiDoc	Bio-Rad	Munich, DE
Counting chamber	Neubauer	Roth	Karlsruhe, DE
Digital camera	Canon Power Shot G5	Canon	Krefeld, DE
Fluorescence lamp	HAL100	Carl Zeiss	Jena, DE
Fluorescence microscope	Axiovert 40 CFL	Carl Zeiss	Jena, DE
Fluorescence microscope	Axioskop 2	Carl Zeiss	Jena, DE
Freezer -80°C	HERAfreeze	Kendro	Hanau, DE
Gel electrophoresis chamber	Agagel	Biometra	Göttingen, DE
Gel documentation	Geldoc2000	Bio-Rad	Munich, DE
Incubator	HERAcell	Kendro	Hanau, DE
Inverse light microscope	Axiovert 25	Carl Zeiss	Jena, DE
Liquid nitrogen store	MVE 611	Chart Industries	Burnsville, US
Luminometer	Lumino2000	Bio-Rad	Munich, DE
Magnetic stirrer	SB162	Bibby Stuart	Staffordshire, UK
Micropipette	2µl, 10µl, 20µl, 100µl, 1000µl	Eppendorf	Hamburg, DE
Micro Spectro-photometer	Nanodrop ND-1000	Peqlab	Erlangen, DE
pH-meter	Microprocessor pH meter	Hanna-instruments	Woonsocket, US
Pipette-boy	Accu-Jet 2	Brand	Wertheim, DE
Power supply (agarose electrophoresis)	Standard Power Pack P25	Biometra	Göttingen, DE
Power supply (PAGE electrophoresis)	Powerpac Un2versal 500V	Bio-Rad	Munich, DE
Real-Time PCR Detection system	iCycler	Bio-Rad	Munich, DE
Radiation cassette	X-omatic casette	Kodak	Rochester, US

Appliance	Name	Manufacturer	Registered Office
Refrigerators 4°C/-20° -20°C	G 2013 Comfort	Liebherr	Lindau, DE
Hybridization oven	OV3	Biometra	Göttingen, DE
Speedvac	Concentrator 5301	Eppendorf	Hamburg, DE
Sterile laminar flow hood	HERAsafe	Kendro	Hanau, DE
Table centrifuge	Centrifuge 5415R	Eppendorf	Hamburg, DE
Thermocycler	T3000	Biometra	Göttingen, DE
Ultrasonic Homogenizer	Ultrasonic 1000	Bio-Rad	Munich, DE
UV Crosslinker	Stratalinker 2400	Stratagene	La Jolla, US
Vacuum pump	Vacuubrand	Brand	Wertheim, DE
Vertical slab gel electrophoresis units	SE 660	Amersham Biosciences	Buckinghamshire, UK
Vortexer	Genie 2	Scientific Industries	Bohemia, US
Water bath	1008	GFL	Burgwedel, DE
X-ray developing machine	XOMAT 1000 processor	Kodak	Rochester, US

2.1.2 Cell culture

2.1.2.1 Plastic ware

Product	Manufacturer	Registered Office
Cryovials (1 ml, 1.8 ml)	Nunc	Wiesbaden, DE
Falcon tubes 15 ml	Greiner Bio One	Frickenhausen, DE
Falcon tubes 50 ml	Greiner Bio One	Frickenhausen, DE
Multi Safe-Seal Tubes (0.65 ml, 1.7 ml, 2 ml)	Peqlab	Erlangen, DE
Petridish (6 cm, 10 cm)	Becton Dickinson	Heidelberg, DE
Serological pipettes (5 ml, 10 ml, 25 ml)	Becton Dickinson	Heidelberg, DE
Tissue culture dishes (3.5 cm, 6 cm, 10 cm)	Becton Dickinson	Heidelberg, DE
Tissue culture dishes (3.5 cm, 6 cm, 10 cm)	PAA Laboratories	Pasching, AT
Tissue culture dishes 15 cm	PAA Laboratories	Pasching, AT

2.1.2.2 Reagents, Media and Supplements

Product	Manufacturer	Registered Office
Accutase	Invitrogen	Karlsruhe, DE
Alfazyme	Invitrogen	Karlsruhe, DE
L-Ascorbic Acid	Sigma-Aldrich	Deisenhof, DE

Product	Manufacturer	Registered Office
B27 supplement	Invitrogen	Karlsruhe, DE
B27 supplement without vitamin A	Invitrogen	Karlsruhe, DE
BDNF	R&D systems	Wiesbaden, DE
BES	Sigma-Aldrich	Deisenhof, DE
CHIR99021	Axon Medchem	Groningen, NL
Collagenase type IV	Invitrogen	Karlsruhe, DE
cyclicAMP	Sigma-Aldrich	Deisenhof, DE
DAPT	Sigma-Aldrich	Deisenhof, DE
Dispase	Invitrogen	Karlsruhe, DE
DMEM/F12	Invitrogen	Karlsruhe, DE
DMEM high glucose	Invitrogen	Karlsruhe, DE
DMSO	Sigma-Aldrich	Deisenhof, DE
Dorsomorphin	R&D systems	Wiesbaden, DE
Doxycycline	PAA Laboratories	Pasching, AT
DPBS	Invitrogen	Karlsruhe, DE
EDTA	Sigma-Aldrich	Deisenhof, DE
EGF	Invitrogen	Karlsruhe, DE
FCS	Invitrogen	Karlsruhe, DE
FGF2	R&D systems	Wiesbaden, DE
FGF8b	R&D systems	Wiesbaden, DE
Fibronectin	Invitrogen	Karlsruhe, DE
GDNF	R&D systems	Wiesbaden, DE
Gelatine	Invitrogen	Karlsruhe, DE
Gentamycine	PAA Laboratories	Pasching, AT
D-Glucose	Sigma-Aldrich	Deisenhof, DE
L-Glutamine	Invitrogen	Karlsruhe, DE
GMEM medium	Invitrogen	Karlsruhe, DE
HBSS	Invitrogen	Karlsruhe, DE
Insulin	Sigma-Aldrich	Deisenhof, DE
Knockout DMEM	Invitrogen	Karlsruhe, DE
Knockout Serum Replacement	Invitrogen	Karlsruhe, DE
Laminin	Sigma-Aldrich	Deisenhof, DE
LDN193184	Axon Medchem	Groningen, NL
Lipofectamine 2000	Invitrogen	Karlsruhe, DE
Matrigel	BD Bioscience	Heidelberg, DE
β-Mercaptoethanol	Invitrogen	Karlsruhe, DE
mTESR	Stem Cell Technologies	Grenoble, FR
N2 supplement (100x)	Invitrogen	Karlsruhe, DE
Neurobasal medium	Invitrogen	Karlsruhe, DE
NGS	Sigma-Aldrich	Deisenhof, DE
Non-essential amino acids	Invitrogen	Karlsruhe, DE
OptimemI medium	Invitrogen	Karlsruhe, DE
Pen/Strep	Invitrogen	Karlsruhe, DE
Polybrene	Sigma-Aldrich	Deisenhof, DE
Poly-L-ornithine	Sigma-Aldrich	Deisenhof, DE

Product	Manufacturer	Registered Office
Purmorphamine	Merck	Darmstadt, DE
Puromycin	PAA Laboratories	Pasching, AT
RPMI medium	Invitrogen	Karlsruhe, DE
SB431542	Sigma-Aldrich	Deisenhof, DE
SHH-C225	R&D systems	Wiesbaden, DE
Sodium pyruvat	Invitrogen	Karlsruhe, DE
TGFβ3	R&D systems	Wiesbaden, DE
Trypan blue	Invitrogen	Karlsruhe, DE
Trypsin-EDTA (10x)	Invitrogen	Karlsruhe, DE
Trypsin Inhibitor (Soybean, Powder)	Invitrogen	Karlsruhe, DE

2.1.2.3 Cell lines

293FT cells: human embryonal kidney cell line 293FT
H9.2 hESCs: human embryonal stem cell line H9.2
H9.2 lt-NES cells: lt-NES cells derived from human embryonal stem cell line H9.2
HepG2 cells: human liver carcinoma cell line HepG2
I3 hESCs: human embryonal stem cell line I3
I3 lt-NES cells: lt-NES cells derived from human embryonal stem cell line I3
iPS cells: induced pluripotent stem cell line ILB-C-31F-R1
U87 cells: primary glioblastoma cell line U87

2.1.2.4 Cell culture media

Basal media were ordered from Invitrogen except mTESR, which was ordered ready to use from Stem Cell Technologies – see section 2.1.2.2 Reagents, Media and Supplements. All media mixtures were stored at 4°C and used within 4 weeks.

GMEM medium
87% GMEM, 10% KO-SR, 1% L-glutamine, 1% sodium pyruvat, 1% non-essential amino acids, 0.05% of β-mercaptoethanol

MEF medium
88% DMEM high glucose, 10% FCS, 1% Pen/Strep

RPMI medium
89% RPMI medium, 10% FCS, 1% Pen/Strep

lt-NES maintenance medium (N2)
96% DMEM-F12, 1% N2-Supplement, 1% Pen/Strep, 0.1% B27-supplement, 20 µg/ml Insulin, 1.6 mg/m D-Glucose

lt-NES differentiation medium (NgMc)
49% N2 medium, 49% Neurobasal medium, 1% B27-supplement, 100 ng/ml cAMP, 1% Pen/Strep

hESC maintenance medium (KO-SR): 82.95% Knockout DMEM, 15% Knockout Serum Replacement, 1% L-glutamine, 1% NEAA, 0.05% of β-mercaptoethanol, 10 ng/ml FGF

Neuronal differentiation medium according to [89] 98% NeuroBasal, 2% B27 supplement devoid of vitamin A (B27-RA), 20 ng/ml BDNF, 20 ng/ml GDNF, 200 µM AA, 0.5 mM dbcAMP, 1 ng/ml TGFβ3, 10 µM DAPT

2.1.2.5 Factors and coatings

AA (L-Ascorbic acid, stock solution)	200 mM in ddH_2O
BDNF (stock solution)	10 μg/ml BDNF, 0.1% BSA in ddH_2O
cAMP (stock solution)	100 μg/ml cAMP in ddH_2O
CHIR99021 (stock solution)	10 mM CHIR99021 in DMSO
DAPT (stock solution)	10 mM DAPT in DMSO
dbcAMP (stock solution)	100 mM dbcAMP in ddH_2O
Dorsomorphin (stock solution)	1 mM in DMSO
Doxycycline (stock solution)	10 mg/ml Doxycycline in ddH_2O
EGF (stock solution)	10 µg/ml EGF, 0.1 M Acetic acid, 0.1% BSA in ddH_2O
FGF2 (stock solution)	10 µg/ml FGF2, 0.1% BSA in ddH_2O
FGF8b (stock solution)	100 μg/ml FGF8b, 0.1% BSA in ddH_2O
Fibronectin (FN)	1 μg/ml in DPBS
GDNF (stock solution)	10 μg/ml GDNF, 0.1% BSA in ddH_2O
Gentamycine (stock solution)	200 mg/ml Gentamycine in ddH_2O
Gelatine	0.1% Gelatine Typ A in ddH_2O, autoclaved
Insulin (stock solution)	5 mg/ml Insulin, 10 mM NaOH in ddH_2O
Laminin (LN)	1 μg/ml in dPBS
LDN193189 (stock solution)	200 μM in DMSO
Matrigel [90]	33.3 μg/ml Matrigel in KO-DMEM
Poly-L-ornithine (PO)	15 μg/ml in ddH_2O, sterile-filtered
Purmorphamine (stock solution)	10 mM Purmorphamine in DMSO
Puromycine (stock solution)	10 mg/ml Puromycine in ddH_2O
SB431542 (stock solution)	50 mM SB431542 in DMSO
SHH-C252 (stock solution)	100 μg/ml SHH-C252, 0.1% BSA in ddH_2O
TGFβ3 (stock solution)	2 μg/ml TGFβ3, 0.1% BSA in ddH_2O
Trypsin-EDTA	1:10 Trypsin-EDTA (10x) in DPBS
Trypsin-Inhibitor 1x:	0.5 mg/ml Soybean Trypsin Inhibitor powder in DPBS, sterile filtration

2.1.2.6 miRNA mimics and inhibitors

All miRNA mimics and inhibitors were purchased from Qiagen and transfected using Lipofectamine 2000 (Qiagen).

Product	Catalogue Number
Syn-hsa-miR-9-5p miScript miRNA Mimic	MSY0000441
Syn-hsa-miR-9-3p miScript miRNA Mimic	MSY0000442
Syn-hsa-miR-7-5p miScript miRNA Mimic	MSY0000252
AllStars Negative Control siRNA	1027280
Anti-hsa-miR-9-5p miScript miRNA Inhibitor	MIN0000441
Anti-hsa-miR-9-3p miScript miRNA Inhibitor	MIN0000442
Anti-hsa-miR-7-5p miScript miRNA Inhibitor	MIN0000252
miScript Inhibitor Negative Control	1027271

2.1.3 Molecular biology

2.1.3.1 Consumables

Product	Manufacturer	Registered Office
Adhesive PCR film	Peqlab	Erlangen, DE
CLXPosure film	ThermoFischer Scientific	Waltham, US
Cryovials (1 ml, 1.8 ml)	Nunc	Wiesbaden, DE
Falcon tubes 15 ml	Greiner Bio One	Frickenhausen, DE
Falcon tubes 50 ml	Greiner Bio One	Frickenhausen, DE
Multi Safe-Seal Tubes (0.65 ml, 1.7 ml, 2 ml)	Peqlab	Erlangen, DE
Nitrocellulose membrane	Roth	Karlsruhe, DE
Nylon membrane	Roche	Basel, CH
Petridish (6 cm, 10 cm)	Becton Dickinson	Heidelberg, DE
Semi-Skirted 96 Well PCR Plate	Peqlab	Erlangen, DE
Serological pipettes (5 ml, 10 ml, 25 ml)	Becton Dickinson	Heidelberg, DE

2.1.3.2 Chemicals and Reagents

Product	Manufacturer	Registered Office
β-Mercaptoethanol	Invitrogen	Karlsruhe, DE
6x DNA loading buffer	Fermentas	St. Leon-Rot, DE
Acetic acid	Roth	Karlsruhe, DE
Acrylamide: Bisacrylamide (19:1)	Sigma-Aldrich	Deisenhof, DE
Agarose	PeqLab	Erlangen, DE
Ammonium acetate	Sigma-Aldrich	Deisenhof, DE
APS	Sigma-Aldrich	Deisenhof, DE
ATP	Sigma-Aldrich	Deisenhof, DE
Boric acid	Sigma-Aldrich	Deisenhof, DE
Bradford assay	Sigma-Aldrich	Deisenhof, DE
Bromophenol blue	Sigma-Aldrich	Deisenhof, DE
BES	Sigma-Aldrich	Deisenhof, DE
CaCl	Roth	Karlsruhe, DE
Chloroform	Sigma-Aldrich	Deisenhof, DE
Coenzyme A	Sigma-Aldrich	Deisenhof, DE
Colenterazine	PJK	Kleinblittersdorf, DE
Complete protease inhibitor cocktail tablets	Roche Applied Science	Mannheim, DE
Cyanocyanol blue	Sigma-Aldrich	Deisenhof, DE
DAPI	Sigma-Aldrich	Deisenhof, DE
Deoxycholic acid sodium salt	Sigma-Aldrich	Deisenhof, DE
Deionized Formamide	Applied Biosystems	Foster City, US
DEPC	Sigma-Aldrich	Deisenhof, DE
DIG-11-UTP	Roche Applied Science	Mannheim, DE

Product	Manufacturer	Registered Office
DMSO	Sigma-Aldrich	Deisenhof, DE
DNA Ladder (100 bp)	Peqlab	Erlangen, DE
DNA Ladder (1 kb)	Peqlab	Erlangen, DE
DPBS	Invitrogen	Karlsruhe, DE
DTT	Sigma-Aldrich	Deisenhof, DE
EDTA	Sigma-Aldrich	Deisenhof, DE
Ethanol for molecular biology	Merck	Darmstadt, DE
Ethidium bromide	Sigma-Aldrich	Deisenhof, DE
Human fetal brain RNA	Stratagene	La Jolla, US
FCS	Invitrogen	Karlsruhe, DE
Fluorescein calibration dye	Bio-Rad	Munich, DE
Glycine	Sigma-Aldrich	Deisenhof, DE
Glycerol	Sigma-Aldrich	Deisenhof, DE
Glycogen	Fermentas	Ontario, Canada
HBSS	Invitrogen	Karlsruhe, DE
Hydrochloric acide (1 mol/l)	Roth	Karlsruhe, DE
Igepal CA-630	Sigma-Aldrich	Deisenhof, DE
Lauryl sulfate sodium salt	Sigma-Aldrich	Deisenhof, DE
Luciferin sodium salt	PJK	Kleinblittersdorf, DE
Magnesium chloride	Invitrogen	Karlsruhe, DE
Magnesium sulfate	Roth	Karlsruhe, DE
Maleic acid	Fluka	Basel, CH
Methanol	Sigma-Aldrich	Deisenhof, DE
Methylene blue	Sigma-Aldrich	Deisenhof, DE
Milk powder blotting grade	Roth	Karlsruhe, DE
Mowiol 4-88	Merck	Darmstadt, DE
NaCl	Roth	Karlsruhe, DE
N-laurolysarcosine	Sigma-Aldrich	Deisenhof, DE
dNTPs	Peqlab	Erlangen, DE
Paraformaldehyde	Sigma-Aldrich	Deisenhof, DE
Passive lysis buffer 5x	Promega	Fitchburg, US
Restriction endonucleases	New England Biolabs	Frankfurt a. M., DE
RNA Ladder (Low Molecular Weight Marker 10-100nt)	USB	Cleveland, US
RNAse Exitus Plus	Applied Biosystems	Foster City, US
SDS	Roth	Karlsruhe, DE
Sodium acetate	Roth	Karlsruhe, DE
Sodium azide	Merck	Darmstadt, DE
Sodium chloride	Roth	Karlsruhe, DE
Sodium citrate	Fluka	Basel, CH
Sodium hydrogen carbonate	Merck	Darmstadt, DE
Sodium hydrogen phosphate	Roth	Karlsruhe, DE
Sodium hydroxide (1 mol/l)	Roth	Karlsruhe, DE
Sodium hydroxide pellets	Merck	Darmstadt, DE
SYBR-green I nucleic acid gel stain (10.000x)	Sigma-Aldrich	Deisenhof, DE

Product	Manufacturer	Registered Office
Taq DNA Polymerase Recombiant (5 U/µl)	Invitrogen	Karlsruhe, DE
TEMED	Sigma-Aldrich	Deisenhof, DE
Tricine	Sigma-Aldrich	Deisenhof, DE
Triton-X100	Sigma-Aldrich	Deisenhof, DE
Trizma Base (Tris)	Merck	Darmstadt, DE
Trizma Hydrochloride (Tris-HCl)	Sigma-Aldrich	Deisenhof, DE
Trypan blue	Invitrogen	Karlsruhe, DE
Tween 20	Sigma-Aldrich	Deisenhof, DE
Urea	Roth	Karlsruhe, DE
Xylene cyanol	Bio-Rad	Munich, DE
X-ray Developer	Tetenal	Norderstedt, DE
X-ray Fixing Solution	Tetenal	Norderstedt, DE

2.1.3.3 Kits and cloning material

Product	Manufacturer	Registered Office
DIG Luminescent Detection Kit	Roche Applied Science	Mannheim, DE
DNaseI	Invitrogen	Karlsruhe, DE
iScript Reverse Transcription Kit	Bio-Rad	Munich, DE
Lenti-X™ Tet-On® Advanced Inducible Expression System	Clontec Laboratories	Mountain View, US
Luminata Classico Western HRP substrate	Merck Millipore	Darmstadt, DE
Luminata Forte Western HRP substrate	Merck Millipore	Darmstadt, DE
Magna ChIP A/G Chromatin Immunoprecipitation Kit	Merck Millipore	Darmstadt, DE
MAX Efficiency® Stbl2™ Competent Cells	Invitrogen	Karlsruhe, DE
MAX Efficiency® Stbl3™ Competent Cells	Invitrogen	Karlsruhe, DE
miScript Reverse Transcription Kit	Qiagen	Hilden, DE
miScript SYBR Green PCR Kit	Qiagen	Hilden, DE
mirVana Probe Construction Kit	Applied Biosystems	Foster City, US
NucleoBond Xtra EF Maxiprep Kit	Machery-Nagel	Düren, DE
PeqGOLD Miniprep Kit	Peqlab	Erlangen, DE
PeqGOLD Trifast	Peqlab	Erlangen, DE
psiCHECK™-2 Vector	Promega	Fitchburg, US
Zymoclean™ Gel DNA Recovery Kit	Zymo Research	Orange, US

2.1.3.4 Oligonucleotides

2.1.3.4.1 Primers used for Realtime PCR

Gene	Forward Primer	Reverse Primer
18S rRNA	TTCCTTGGACCGGCGCAAG	GCCGCATCGCCGGTCGG
DLL1	GGAGAAGCATCTGAAAGAAAAAGG	GGGAGTCTTGCCATCTCACTT
DLL3	CCAATGGAGGCAGCTGTAGT	GTTGAAGCAGGGTCCATCTG
DLL4	GCAAACAGCAAAACCACACA	TCCGACACTCTGGCTTTTCA
EN2	CCAAAGAAGAAGAACCCGAAC	ACCTGTTGGTCTGGAACTCG
FOXA2	ACACCACTACGCCTTCAACC	GCCTTGAGGTCCATTTTGTG
HES1	AAGGCGGACATTCTGGAAAT	GTCACCTCGTTCATGCACTC
HES5	ACATCCTGGAGATGGCTGTC	AGCAGCTTCATCTGCGTGT
HEY1	CCGAGATCCTGCAGATGA	GCTCAGATAACGCGCAACT
HEY2	TGAAGATGCTTCAGGCAACA	GCGCAACTTCTGTTAGGCACT
JAGGED1	GTGGCTTGGATCTGTTGCTT	TTGGTGGTGTTGTCCTCAGA
JAGGED2	GACGCACCTGTGGTTGTTAGT	CAGTGGAGAGATCGCTGGAG
LIN28A	CGGGCATCTGTAAGTGGTTC	CTGATGCTCTGGCAGAAGTG
LIN28B	TCTTCCAAAGGCCTTGAGTC	TCAAGGCCACCACAGTTGTA
LMX1A	CCATCGAGCAGAGTGTCTACAG	GTCGTCGCTATCCAGGTCAT
miR-7	ACAACAAAATCACTAGTCTTCCA	Universal Primer (Qiagen)
miR-9	TCATACAGCTAGATAACCAAAGA	Universal Primer (Qiagen)
miR-9*	ACTTTCGGTTATCTAGCTTTAT	Universal Primer (Qiagen)
miR-16	CGCCAATATTTACGTGCTGCTA	Universal Primer (Qiagen)
miR-125b	TCACAAGTTAGGGTCTCAGGGA	Universal Primer (Qiagen)
miR-128	AAAGAGACCGGTTCACTGTGA	Universal Primer (Qiagen)
miR-130b	ATGCCCTTTCATCATTGCACTG	Universal Primer (Qiagen)
miR-133b	TAGCTGGTTGAAGGGGACCAAA	Universal Primer (Qiagen)
MAML1	CAGCAACAGCAGTTCCTTCA	GTGTCGGGTCTTGGTACTGG
MAML3	CAGCAGCAGCAGCAGATTTT	CTGCTGCACTGGGTATGGAT
MSX1	AAGTTCCGCCAGAAGCAGTA	TTCAGCTTCTCCAGCTCTGC
NESTIN	GGAGAAGGACCAAGAACTG	ACCTCCTCTGTGGCATTC
NEUROG2	CAGGCCAAAGTCACAGCAAC	CCGAGCAGCACTAACACGTC
NOTCH1	TGAAGAACGGGGCTAACAAA	TCCATATGATCCGTGATGTCC
NOTCH2	CTGCCCTTGGACCCATTTAT	CCAGTGGCTGGATCAGTAGC
NOTCH3	CCTCACTTCACTGCATTCCA	CCCTAGTTCCCAAAGGGAGA
NOTCH4	AGAACTGATTGCAGCCCAAG	TGTCCTGGGCATCTTTATCG
PAX6	AATAACCTGCCTATGCAACCC	AACTTGAACTGGAACTGACACAC
Pri-miR-9_2	CTTCGGTACTGCCAGAAAGG	GCAACAACCCCTCTCAAGAC
PSEN1	AAGACACTGTTGCAGAGAATG	CCAGCGAGGATACTGCTGG
SIRT1	CAGTGGCTGGAACAGTGAGA	TATACCTCAGCGCCATGGAA
SOX2	CACATGTCCCAGCACTACCA	CTCCCATTTCCCTGGTTTTT

2.1.3.4.2 Primers used for semiquantitative PCR

Gene	Forward Primer	Reverse Primer
18S rRNA	TTCCTTGGACCGGCGCAAG	GCCGCATCGCCGGTCGG
EN2	CCAAAGAAGAAGAACCCGAAC	ACCTGTTGGTCTGGAACTCG

Gene	Forward Primer	Reverse Primer
FOXA2	ACACCACTACGCCTTCAACC	GCCTTGAGGTCCATTTTGTG
Pri-miR-9_1	TGTCCCTTCCCTCCTACTCC	ATCCTCTGGTGCTGGTCAGT
Pri-miR-9_2	CTTCGGTACTGCCAGAAAGG	GCAACAACCCCTCTCAAGAC
Pri-miR-9_3	GTGTCTGTCCATCCCCTCTG	CTCGGCTCCTCTGGCTCT
Pri-miR-7_1	CATTTCTCTGGTGAAAACTGCTG	AATCGGACATTAGTAGAACAGAA TTAAGA
Pri-miR-7_2	TGAAGGAGCATCCAGACCG	AGAACACGTGGAAGGATAGCC
Pri-miR-7_3	ACTCAGGTGTCATAGCTTGGCTC	GAAGCGATTCTTCCCCGA
CHIP 9_1_1	TAGGAGCTGGGGGGAGAGA	TGGGGACCCCCCTAAATCT
CHIP 9_1_2	GGTGGAGACCAAAATTGGGA	CCTCCATTAGATGGGTGTGAAG
CHIP 9_1_3	TCCTACGGAAGGCCAGGA	CACAGCCCAGCAGGCA
CHIP 9_2_1	TAGAGTCTAGACCCGGCTGAGG	GAGCCTCCGGTCTAACTTCTGA
CHIP 9_2_2	TGGTAGTCTTGACTGTACTAGTGC ACTG	GGTTTGCCTGCTCATTCACTAATA
CHIP 9_3_1	TGGGCAGCTCAGGCAG	CTGTCTGCAGCCCCACAA
CHIP 125b2	TCCCCAGTGCCTATGCC	TGTACCATTTCACATTAGCTGCA
CHIP HES1	CAAGACCAAAGCGGAAAGAA	GGATCCTGTGTGATCCCTAGG

2.1.3.4.3 Primers used for cloning

Gene	Forward Primer	Reverse Primer
Puro THM	ATCGTTTAAACACCTGCAGCCCA AGCTTACCAT	TCAGACTAGTCATATGAGGTTGAT TGTTCCAGACGCGC
Pre-miR-9_1 THM	TCATACAGCTAGATAACCAAAGAC CTGTCTC	TCATACAGCTAGATAACCAAAGAT TTTTCCTGTCTC
Pre-miR-7_1 THM	TGTACAACGCGTTGGAAGAAGCC TTAACCAAG	TGGAATTCATCGATTCGGACATTA GTAGAACAGAA
Pre-miR-128_1 THM	TGTACAACGCGTTGACAAGTTTGT AGCTTCACC	TGGAATTCATCGATTCCCTATTTCT GAGTATGATGC
Pre-miR-130b THM	TGTACAACGCGTTCAGAGGGCAC CCTTTCC	TGGAATTCATCGATCCAGTCCAGC TTCACATCTG
Pre-miR-9_1 LVX	TAGGGATCCTGTCTCGGACTTCA TTTCTCTCTT	AGTGAATTCTGAAATGTCGCCCGA ACCAGT
Pre-miR-7_1 LVX	TAGGGATCCTGGAAGAAGCCTTA ACCAAG	AGTGAATTCATCGATTCGGACATT AGTAGAACA
GFP LVX	AGTGCGGCCGCAAGCTTCGAATT CTGCAGT	ACTCACGCGTTTACTTGTACAGCT
DN-MAML1 LVX	ACGAGCGGCCGCACGAGCGGCC GCATGGCGCTGCCGCG	ACTACGCGTTTACTTGTACAGCTC GTCCAT
NOTCH1-ICD LVX	TCAGCGGCCGCATGGCACGCAA GCGCCGG	TGAACGCGTACTTACTACTTATCGT CGTCGTCC
NOTCH2-ICD LVX	ACGAGCGGCCGCATGGCACGAA AGCGTAAGCA	ACTACGCGTTCACGCATAAACCTG CATGTT
NOTCH1 3´UTR	ACTCTCGAGACTACGGCGCGCCC CAC	GTACGGCGGCCGCCTGCAGCATC TACAGTTCCTCATGTAGATCAC
NOTCH2 3´UTR	ACTCTCGAGTGAGAGAGTCCACC TCCAGTACTCTCGAGGAGAGTCC ACCTCCAGTGTA	GTACGGCGGCCGCCTGCAG GACTTATATCCCAGTTCCCAATTC
HES1 3´UTR	ACTCTCGAGTCAGGCCACCCCTC CTC	GTACGGCGGCCGCCAAAAGAGTC AATTCCTGAATTACCA

2.1.3.5 Solutions

2.1.3.5.1 Western blot

RIPA lysis buffer 50 mM Tris-HCl (pH=7.5), 1 mM EDTA; 0.5% Deoxycholic acid, sodium salt, 150 mM NaCl, 0.1% lauryl sulfate sodium salt and 1% Igepal in ddH_2O, mixed with 1:100 protease inhibitor cocktail (PI, Roche)

2x Lämmli buffer 100 mM Tris-HCl (pH=6.8), 20% Glycerol, 4% SDS, 0.25% Bromphenolblau in ddH_2O

5x Running Buffer 25 mM Tris-Base; 965 mM Glycin; 0.5% SDS in ddH_2O

10x Transfer Buffer 250 mM Tris-Base; 1.95 M Glycin in ddH_2O

Transfer Buffer 100 ml 10x Transfer Buffer; 200 ml Methanol**;** 700 ml ddH_2O**;** store at 4°C

TBS-T 10 mM TRIS-HCl (ph 7,5), 150 mM NaCl, 0.05% Tween in ddH_2O

Stripping buffer 2% SDS, 62.5 mM Tris-HCl (pH=6.7), 7 mM β-Mercapthoethanol in ddH_2O

2.1.3.5.2 Northern blot

Acetic acid 5% 5% acetic acid (v/v) in DEPC-H_2O

Blocking solution 10% Blocking Reagent of the DIG Luminescent Detection Kit in Maleic acid buffer dissolved by stirring at 65°C, autoclaved, stored at 2-8°C

DEPC-H_2O 1 ml DEPC in 1l ddH_2O, incubate overnight while stirring in the dark under the hood, lid open, autoclaved next day

Destaining solution 0.2 x SSC, 1% SDS in DEPC-H_2O

FDE 10 ml deionized formamide, 200 µl EDTA (0.5 M EDTA), 10 mg Xylenecyanol, 10 mg Bromophenol blue in DEPC-H_2O

FLS 10 ml deionized formamide, 200 µl EDTA (0.5 M EDTA), 1 mg Xylenecyanol, 1 mg Bromophenol blue in DEPC-H_2O

Hybridization buffer 5 x SSC, 50% deionized formamide, 0.1% N-lauroly-sarcosine, 0.02% SDS, 2% Blocking solution in DEPC-H_2O

Maleic acid buffer 0.1 M Maleic acid, 0.15 M NaCl in ddH_2O, pH 7.5

Methylene blue staining solution 0.02% (w/v) Methylene blue, 0.3 M sodium actetate in ddH_2O, pH 5.5

Polyacrylamide-Urea Gel, 15%

40 ml:	
Urea	20 g
10x TBE	5 ml
Acrylamide/Bis 19:1	15 ml
DEPC-H2O	4 ml
10% APS	240 µl
TEMED	16 µl

20x SSC	3 M Sodium chloride, 0.3 M Sodium citrate in dd$H_2$0, pH=7.0
Stringency wash buffer	2 x SSC, 0.1% SDS in DEPC-H_2O
Stripping buffer	50% deioinized formamide, 5% SDS, 50 mM Tris-HCl (pH=7.5) in DEPC-H_2O
10x TBE	0.9 M Tris-HCL, 0.9 M Boric acid, 0.02 M EDTA in DEPC-H_2O

2.1.3.5.3 Immunocytochemistry

Blocking buffer	5% FCS, 0.1% Triton-X-100 in DPBS
Borate buffer	10 mM sodium borate in ddH_2O
Mowiol	6 g Glycerol, 2.49 g Mowiol in 6 ml ddH_2O + 12 ml 0.2 M Tris-HCl (pH=8.5)
NaHCO3 Buffer	10 mM NaHCO3 in ddH_2O
4% PFA	4% Paraformaldehyde in DPBS
Sodium azide solution	1 mg/ml sodium azide in DPBS
Triton-X-100 (1%)	10 mg/ml Triton-X-100 in DPBS

2.1.3.5.4 Luciferase Assay

Passive lysis buffer	1:5 Promega passive lysis buffer 5x in ddH_2O
Luciferin Solution	0.5 mM D-Luciferin Na salt, 30 mM Tricine (pH=7.8), 3.75 mM MgSO4, 0.75 mM ATP, 1.25 mM DTT, 67.5 μM Coenzyme A in ddH_2O
Colenterazine Solution	40 μM Colenterazine, 2% Methanol in ddH_2O

2.1.3.5.5 Others

2x BBS buffer:	50 mM BES, 280 mM NaCl, 1.5 mM Na_2HPO_4 in ddH_2O, pH=6.95, sterilized by filtration, frozen at -20°C

2.1.3.6 Antibodies

2.1.3.6.1 Primary antibodies

Target	Host/Isotype	Company	Dilution
BrdU	mouse IgG	Beckton Dickinson	1:50
βIII tubulin	mouse IgG	Covance	1:2000
FLAG-Tag	mouse IgG	Merck Millipore	1:100
FOXA2	goat IgG	R&D Systems	1:1000
GABA	rabbit IgG	Sigma-Aldrich	1:500
HES1	mouse IgG	Sigma-Aldrich	1:500
Histone 3	rabbit IgG	Cell Signaling	1:100
IgG control	rabbit IgG	Abcam	1:100

Target	Host/Isotype	Company	Dilution
LMX1A	rabbit IgG	Merck Millipore	1:1000
NESTIN	mouse IgG	R&D Systems	1:1000
NOTCH1	rat IgG	DHSB	1:500
NOTCH2	rat IgG	DHSB	1:500
RBPj	rabbit IgG	Abcam	1:100
SOX2	mouse IgG	R&D Systems	1:1000
Serotonin	rabbit IgG	Sigma-Aldrich	1:1000
TH	mouse IgG	Sigma-Aldrich	1:1000

2.1.3.6.2 Secondary antibodies

Target	Host/Isotype	Label	Company	Dilution
Mouse IgG	Goat	Cy3	Jackson Immuno Research	1:250
Mouse IgG	Goat	Alexa488	Invitrogen, Darmstadt	1:1000
Rabbit IgG	Goat	Alexa488	Invitrogen, Darmstadt	1:1000
Rabbit IgG	Goat	Alexa555	Invitrogen, Darmstadt	1:1000
Rat IgG	Mouse	Peroxidase	Jackson Immuno Research	1:1000
Mouse IgG	Rabbit	Peroxidase	Jackson Immuno Research	1:1000

2.2 Methods

2.2.1 Cell culture

2.2.1.1 Culture of pluripotent stem cells

The pluripotent stem cell lines used in this work are human embryonic stem cell lines I3 [91] and H9.2 [92] (kindly provided by Prof. J. Itskovitz-Eldor) and human iPS cell line ILB-C-31F-R1 (kindly provided by Matthias Brandt). Maintenance and differentiation followed established protocols.

2.2.1.1.1 Maintenance of pluripotent stem cells

For pluripotent stem cell propagation, cells were cultivated on MG-coated tissue culture (TC) dishes in mTESR medium. The medium was exchanged daily. Cells were split approximately every third day at a ratio of 1:10 treatment with alfazyme for 5-10 min. Detached cells were transferred into a falcon tube and pelleted by centrifugation at 1000 rpm for 5 min. After resuspension in appropriate volume of fresh mTESR medium containing 10 nM Rock inhibitor, cells were plated on MG-coated dishes. Medium was changed to fresh mTESR daily.

2.2.1.1.2 Differentiation of pluripotent cells into dopaminergic neurons

For neuronal differentiation, pluripotent stem cells were plated onto MG-coated TC plates and cultivated in mTESR until the confluence reached approximately 90%. From this time point on, the cells were treated according to *Kriks et al.* [89]. They were cultured for one day (d0) in KO-SR medium containing 100 nM LDN193189 and 10 µM SB431542 and for the next two days (d1-2) in KO-SR medium containing 100 nM LDN193189, 100 ng/ml SHH, 100 ng/ml FGF8b and 2 µM Purmorphamine. On d3-4 additional 3 μM CHIR 99021 were added to the medium. From d5 on, the cells were slowly adapted to N2 medium, which is beneficial for expansion of neuronal precursors, by adding it in increasing amounts into the previously used KO-SR medium. Therefore, the medium used on days 5 and 6 was prepared to include 75% KO-SR medium and 25% N2 medium containing 100 nM LDN193189, 10 μM SB431542, 100 ng/ml SHH, 100 ng/ml FGF8b, 2 μM Purmorphamine and 3 μM CHIR99021. On days 7 and 8, 50% KO-SR medium and 50% N2 medium were used supplemented with 100 nM LDN193189 and 3 μM CHIR99021. On days 9 and 10, the medium was changed to 25% KO-SR medium and 75% N2 medium while the factors added remained the same. From day 11 on, the cells were switched to a neuronal differentiation medium (NeuroBasal containing 1x B27 supplement devoid of vitamin A (B27-RA), 20 ng/ml BDNF, 20 ng/ml GDNF, 200 μM AA, 0.5 mM dbcAMP, 1 ng/ml TGFβ3 and 10 μM DAPT) plus 3 μM CHIR99021. On day 13, the cultures were split by incubation with accutase for 45 min followed by a spindown in NeuroBasal containing 1x B27-RA at 1200 rpm for 4 min. Afterwards, the cells were resuspended in the neuronal differentiation medium and seeded onto polyornithine (PO)/laminin (LN)/fibronectin (FN)-coated dishes at a ratio of 1:1. The medium was changed to fresh neuronal differentiation medium every other day until day 20 when the cells were passaged again as described. This time the cells were counted, plated at a density of 400000 cells/cm^2 on PO/LN/FN-coated TC dishes and kept in the differentiation medium until day 25 for final analysis. Data on the differentiation of pluripotent stem cells into dopaminergic neurons were generated in collaboration with Laura Stappert with equal contribution from both sides.

2.2.1.2. Culture of neural stem cells

For this study, lt-NES cells derived from the parental human embryonic stem cell lines I3 and H9.2 were used. The cell lines used were derived as described in [7] (used for the experiments in *Results sections 3.1, 3.2, 3.9 and 3.11*) or according to a modified version of that protocol (used for the experiments in *Results sections 3.3-3.8, 3.10 and 3.12*). For the modified version of the lt-NES cell derivation, hESCs were harvested as clumps with 1 mg/ml collagenase. These clumps were cultured in suspension on uncoated petridishes to form embryoid bodies in GMEM medium supplemented with 5 μM SB431542 and 1 μM dorsomorphin, which was changed every other day. After 6 - 14 days the formed embryoid bodies were plated on PO/LN-coated TC dishes in N2 medium with 10 ng/ml FGF2, 2 mg/ml fibronectin, 5 μM SB431542 and 1 μM dorsomorphin. The next day, the medium was changed to N2 medium with 10 ng/ml FGF2 and renewed every second day. After 7 - 10 days in monolayer culture, neural rosettes formed and were selectively detached by addition of 0.15 mg/ml dispase for 3 - 10 min. The rosettes were carefully rinsed off the plate and maintained as spheres on uncoated petridishes in N2 medium containing 20 ng/ml FGF2 for 3 days. Afterwards, the spheres were plated on PO/LN-coated TC dishes containing N2 medium supplemented with 1 μM purmorphamine and 10 ng/ml FGF2. After additional 5 - 7 days the purified rosettes were single cell-suspended with trypsin and plated in high density on PO/LN-coated TC dishes in N2 medium supplemented with 10 ng/ml FGF2 and 10 ng/ml EGF. Maintenance and differentiation followed established protocols [7]. Derivation procedure and validation of the modified protocol for lt-NES cell derivation were established by Johannes Jungverdorben based on [7] and carried out by Katja Hamann.

2.2.1.2.1 Maintenance of neural stem cells

Lt-NES cells were cultivated on PO/LN-coated TC dishes in N2 medium supplemented with growth factors (10 ng/ml of each EGF and FGF2). Growth factors were added daily, while medium was exchanged every second day. Cells were split approximately every third day at a ratio of 1:2 by trypsinisation. To this end, cells were removed from the culture dish surface with Trypsin/EDTA solution followed by neutralization with Trypsin inhibitor. Cells were transferred into a falcon tube and pelleted by centrifugation at 1000 rpm for 5 min. After resuspension in an appropriate

volume of fresh N2 medium including growth factors, the cells were plated on fresh PO/LN-coated TC dishes.

2.2.1.2.2 Growth curve analysis of neural stem cells

For growth curve analysis, 700000 lt-NES cells were seeded onto PO/LN-coated 3.5 cm TC dishes in N2 medium containing 10 ng/ml of each EGF and FGF2. Three separate plates of cells were trypsinized and counted on each of the following 4 days for every condition. The counting was carried out in three independent experiments.

2.2.1.2.3 Differentiation of lt-NES cells

For neuronal differentiation, lt-NES cells were plated onto MG-coated TC plates and cultivated in N2 medium supplemented with 10 ng/ml EGF and 10 ng/ml FGF2 until confluence reached approximately 80%. At this time point, the used medium was switched to NGMC medium including 200 μM ascorbic acid (AA) and 20 ng/ml BDNF. NGMC medium was changed every other day.

2.2.1.3. Culture of cancer cell lines

The cell lines HepG2, U87 and 293FT were cultivated on non-coated TC dishes in RPMI (HepG2 cells) or MEF (U87 and 293FT cells) medium. The cultures were split approximately every third day at a ratio of 1:4 with Trypsin/EDTA. The detached cells were transferred into a falcon tube and pelleted by centrifugation at 1000 rpm for 5 min. After resuspension in appropriate volume of fresh RPMI (HepG2 cells) or MEF (U87 and 293FT cells) medium, the cells were replated on non-coated dishes.

2.2.2 RNA-based analysis methods

2.2.2.1 RNA Isolation

Total RNA used for PCR and Northern blot analyses was isolated using PeqGOLD Trifast. Before harvesting, the cells were washed once with DPBS. One 3.5 cm dish was harvested in 1 ml Trifast (the volume was increased according to the surface harvested) and stored at -80°C at least 24 hours. For extraction, the samples were thawed at room temperature (RT), mixed with 200 μl of chloroform and incubated for 5-10 min at RT. After centrifugation at 13000 rpm for 5 min, the clear supernatant

was transferred to a fresh tube and mixed with 500 µl isopropanol. The RNA was pelleted at 13000 rpm and 4°C for 15 min, washed twice with 70% of ethanol and resuspended in DEPC-H_2O. The resulting RNA was digested with DNaseI according to manufacturers protocol to avoid contamination. Final RNA concentration was determined by microspectrophotometer measurement.

2.2.2.2 Quantitative real-time RT-PCR

2.2.2.2.1 Quantitative real-time RT-PCR of small RNA (qRT-PCR)

Reverse transcription of 250-500 ng of total RNA was carried out in a 10 µl reaction using the miScript reverse transcription kit which polyadenylates the RNA and then reverse transcribes it with a poly(T)-universal tag primer resulting in extended miRNA-cDNAs. 0.25 µl of the synthetized template cDNA was applied for each PCR reaction using the miScript SYBR Green PCR kit in combination with a miRNA-specific forward primer and the sequence complementary to the poly(T) universal tag as the reverse primer (for primers see table in section *2.1.3.4.1 Primers used for Realtime PCR*).

The parameters used were:

Step	Temperature	Time	Cycles
Denaturation	95°C	15 min	1
Denaturation	95°C	30 s	40
Annealing	55°C	30 s	
Elongation	72°C	30 s	
Elongation	72°C	10 min	1

All measurements were carried out in technical duplicates or triplicates. Data were normalized to miR-16 or snRNA RnuB5. Quantitative PCR was performed on an Eppendorf Realplex cycler system using the SYBR green method. The specificity of the PCR products was verified by melting curve analysis and gel electrophoresis. Data were analyzed using the δδCt method.

2.2.2.2.2 Quantitative real-time RT-PCR of mRNA (qRT-PCR)

The cDNA for mRNA based Real-Time PCR was synthesized in a volume of 20 µl from 1 µg total RNA using the iScript cDNA synthesis Kit following manufacturers protocol. For each PCR reaction, 0.1-0.5 µl of the synthetized cDNA were mixed with 1xPCR Buffer, 3 mM $MgCl_2$, 6 µM of each forward and reverse primer (for sequences

see table in section *2.1.3.4.1 Primers used for Realtime PCR*), 200 µM of each dNTP, 1:2000000 SYBR Green, 10 µM Fluorescein and 0.75 U Taq-Polymerase in a total volume of 25 µl. The parameters used were:

Step	Temperature	Time	Cycles
Denaturation	95°C	5 min	1
Denaturation	95°C	15 s	40
Annealing	60°C	15 s	
Elongation	72°C	30 s	
Elongation	72°C	10 min	1

All measurements were carried out in triplicates. Data were normalized to 18S reference levels. Quantitative PCR was performed on an Eppendorf Realplex cycler system using the SYBR green method. The specificity of the PCR products was verified by melting curve analysis and gel electrophoresis. Data were analyzed using the δδCt method.

2.2.2.3 RT-PCR

The cDNA for mRNA based RT-PCR was synthesized in a volume of 20 µl from 1 µg total RNA using the iScript cDNA synthesis Kit following manufacturers protocol. For each PCR reaction, 0.1 µl of the synthetized cDNA was amplified using Invitrogen Taq-DNA Polymerase according to manufacturers protocol. Primers used are listed in section *2.1.3.4.2 Primers used for semiquantitative PCR*.

The parameters used for cycling in a Biorad Thermocycler were:

Step	Temperature	Time	Cycles
Denaturation	95°C	5 min	1
Denaturation	95°C	15 s	35
Annealing	60°C	15 s	
Elongation	72°C	30 s	

For reference gene 18S, the cycle number was reduced to 20. Afterwards, the PCR products were analyzed by electrophoresis on a 1.5% agarose gel.

2.2.2.4 Northern blotting of small RNAs

2.2.2.4.1 miRNA oligonucleotides probes for Northern blots

DIG-labeled RNA probes were synthesized by *in vitro* transcription using the mirVana miRNA Probe Construction Kit. Single-stranded DNA oligonucleotides were designed

according to manufacturers suggestions. For miRNA probes, the sequence of the mature miRNA according to their annotation in miRBase [93] was used (miR-9: UCU UUG GUU AUC UAG CUG UAU GA; miR-9*: AUA AAG CUA GAU AAC CGA AAG U; miR-125b: UCC CUG AGA CCC UAA CUU GUG A) while for loading control snRNA U6 a 21 nt sequence (AAT TCG TGA AGC GTT CCA TAT) was chosen. Furthermore, a sequence complementary to the T7 promoter (5'-CCTGTCTC-3') was added to the 3´ end of sequences and annealed to a T7 promoter specific primer. Afterwards, the oligonucleotides were extended to generate double-stranded DNA templates using the Exo-Klenow polymerase. These templates were then *in vitro* transcribed by T7 phage RNA polymerase in presence of DIG-11-UTP to synthesize DIG-labeled small RNA transcripts.

Unincorporated nucleotides were removed by ammonium acetate/ethanol precipitations. To this end, the reaction was filled up to 50 µl volume by adding nuclease-free water and mixed with 5 µl of 5 M ammonium acetate, 2 µl of glycogen and 3 volumes (150 µl) of 100% ethanol and stored at -20°C over night. The RNA was pelleted by centrifugation at 13000 rpm at 4°C for 30 min, washed two times with 250 µl cold 75% ethanol and air-dried. The resulting pellet was dissolved in 50 µl nuclease-free water and the acetate/ethanol precipitation was repeated a second time. The amount of DIG-labeled RNA probe was quantified by microspectrophotometer measurement, aliquoted to 400 ng (miRNA) or 100 ng (snRNA) probe in 50 µl DEPC-H_2O containing 10 µM EDTA and stored at -80°C.

2.2.2.4.2 Northern Blotting

Northern blot analysis was performed on 40 µg of total RNA isolated with PeqGOLD Trifast according to manufacturers protocol. The 15% acrylamide denaturing gel used was pre-run in 1xTBE at 400 mV for 1 hour (h). Before loading the RNA was mixed 1:1 with FLS, denaturated at 65°C for 20 min and cooled on ice. A RNA low molecular weight marker was used as size control. The loaded gel was run at 400 mV for 2-3 h. For visualization of the separated RNA, the gel was incubated for 10 min in 1xTBE containing 1 µg/ml ethidium bromide, washed with 1xTBE two times and exposed to UV light in a chemiluminometer. After 20 min of equilibration in 20xSSC, the gel was blotted on a nylon membrane using capillary forces created by a stack of paper and 20xSSC as transfer buffer at RT over night. Afterwards, the

membrane was washed with 2xSSC and cross-linked using a UV Hybridizor at 1200 mJ/cm^2. For visualization, the membrane was soaked in 5% acetic acid for 15 min at RT, stained for 5 min in methylene blue staining solution and rinsed several times with DEPC-H_20. After photo-documentation, the membrane was washed with destaining solution for 15 min and equilibrated in 2xSSC.

2.2.2.4.3 Northern blot detection

The membrane was prehybridized in 10 ml hybridization buffer at 65°C for at least 1 h. For each membrane an aliquot of 100 ng snRNA probe or 400 ng miRNA probe was denaturated at 95°C for 2 min, cooled on ice and mixed with 2 ml hybridization buffer. The membrane was hybridized with the DIG-labeled RNA-probes at RT over night. After hybridization, the membrane was rinsed in DEPC-H_20 and washed in 5ml stringency buffer twice at RT for 5 min and once at 40°C for 15 min. The detection was performed using the DIG Luminescent Detection Kit according to manufacturers protocol. Accordingly, the signal was detected by exposure to a CL-XPosure film at -80°C over night and visualized on a X-ray developing machine. For reprobing, the membranes were stripped incubating them twice in 5 ml stripping buffer for 1 h at 80°C followed by washing in 2xSSC for 5 min. Afterwards, the detection procedure for the new probe was started from the beginning as described above.

2.2.3 Protein-based analysis methods

2.2.3.1 Western blot

2.2.3.1.1 Preparation of protein lysates

For lysis, the cells were scraped of the plates in cold DPBS, pelleted at 3500 rpm for 5 min and resuspended in RIPA buffer. After incubation on ice for 15 min, the supernatant was cleared by centrifugation for 15 min at 4°C and 13000 rpm. The collected supernatant was measured by Bradford assay according to manufacturers protocol. Afterwards, loading buffer was added, the mixture was boiled at 95°C for 10 min, aliquoted, and stored at -20°C.

2.2.3.1.2 Gel electrophoresis and blotting

A SDS PAGE gel in the desired percentage of acrylamide was prepared according to the tables below (separating gel: HES1/ FOXA2: 10%, NOTCH1/ NOTCH2: 8%).

Separating gel	**8%**	**10%**
ddH_2O	4.6 ml	4 ml
30% Acrylamide Mix	2.6 ml	3.4 ml
1.5M TrisHCl (pH=8.8)	2.6 ml	2.6 ml
10% SDS	100 µl	100 µl
10% APS	100 µl	100 µl
TEMED	6 µl	4 µl

Stacking gel	
ddH_2O	1.2 ml
30% Acrylamide Mix	330 µl
0.5M TrisHCl (pH=6.8)	500 µl
10% SDS	20 µl
10% APS	20 µl
TEMED	2 µl

40 µg of protein sample were loaded per lane. The gel was run in running buffer at 100 V for 2 h. Afterwards, it was blotted onto a nitrocellulose membrane in blotting buffer with an ice pack at 70 V for 2 h. After blocking the membrane in 10% of milk powder in TBST at RT for 1 h, the first antibody was added in 5% milk powder in TBST at 4°C over night. The next day, the membrane was washed and the secondary antibody was added in 5% milk powder in TBST at RT for 1 h. For antibodies and dilutions see tables in *section 2.1.3.6 Antibodies*. The membrane was washed and detected with a chemiluminometer using Luminata Western HRP substrates.

For reuse, the membrane was stripped in 10 ml of stripping buffer at 50°C for 30 min and washed afterwards. All washes were carried out in TBST by changing it three times after 5 min of incubation each.

2.2.3.2 Chromatin immunoprecipitation

Chromatin immunoprecipitation was carried out in triplicates with the Magna ChIP G Kit according to the manufacturers protocol. The antibodies against RPBj, Flag-Tag and Histone3 were used as well as an IgG control antibody. For antibodies and dilutions see tables in *section 2.1.3.6 Antibodies*.

Subsequent RT-PCR analyses were carried out on 2 µl of sheared chromatin using Invitrogen Taq-DNA Polymerase according to the manufacturers protocol. Primers

used are listed in *section 2.1.3.4.2 Primer used for semiquantitative PCR*. Parameters used for the PCR reaction are described in *section 2.2.2.3 RT-PCR*.

2.2.3.3 Immunofluorescence

For immunofluorescence, the cells were washed, fixed with 4% PFA and washed again. For BrdU staining, the samples were prepared by 30 min of treatment with 0.5% Triton in DPBS and subsequent washing followed by treatment with 2 M HCl for 10 min. The acid was removed by washing and neutralized by treatment with Borane buffer for 10 min, which was washed out as well. For immunofluorescence analysis other than BrdU staining, the PFA fixed samples were used without further pretreatment. Fixed cells were treated with blocking solution at RT for 1 h and subsequently incubated with the first antibody diluted in blocking solution at RT over night. After washing, the secondary antibody was diluted in blocking solution and added to the cells at RT for 1 h. For antibodies and dilutions see tables in *section 2.1.3.6 Antibodies*. After washing out the secondary antibody with DPBS, the samples were counterstained with DAPI and visualized at the fluorescence microscope. All washes were carried out in DPBS by changing it three times after 10 min of incubation each.

2.2.4 Lentivirus-based experiments

2.2.4.1 Cloning of lentiviral constructs

For Pol-III based miRNA overexpression the LVTHM plasmid ([94], kindly donated by Prof. D. Trono) was used. The miRNA genomic loci including the precursor and approximately 150 bp of its upstream and downstream regions were isolated by PCR on genomic DNA of lt-NES cells and cloned under the control of the H1 promoter using restriction endonucleases MluI and ClaI. As short scrambled RNA control the sequence from the pSilencer construct (Ambion, Life Technologies) was cloned using restriction endonucleases MluI and ClaI. For selection the GFP cassette was exchanged for puromycine, neomycine and hygromycine resistance using restriction endonucleases PmeI and SpeI.

The pLVX-Tight-Puro plasmid (part of the Lenti-X™ Tet-On® Advanced Inducible Expression System) was used for Pol-II based ectopic expression of miRNAs. The

respective miRNA loci including the precursor and approximately 150 bp of its upstream and downstream regions amplified from genomic DNA of lt-NES cells and cloned under the control of the Tight promoter using restriction endonucleases BamH1 and EcoR1. For modulation of Notch signaling, human NOTCH1-ICD and NOTCH2-ICD constructs ([95], kindly donated by Prof. A. J. Capobianco), a DN-MAML1-GFP fusion construct ([96], kindly donated by Prof. J. C. Aster) and eGFP (taken from the DN-MAML1-GFP fusion construct) were cloned under the control of the Tight promoter using restriction endonucleases NotI and MluI. To achieve doxycycline-based inducibility, the resulting vectors were combined with a modified pTet-ON advanced vector (part of the Lenti-X™ Tet-On® Advanced Inducible Expression System) carrying an EF1α promoter instead of the original CMV promotor as described in [97]. For primers used in the generation of the lentiviral vectors described see section *2.1.3.4.3 Primers used for cloning*.

2.2.4.2 Expansion of lentiviral constructs

The cloned constructs were expanded in Stbl2, or Stbl3 E. Coli to assure minimum recombination events. For a mini preparation, the bacteria carrying the desired plasmid were expanded in 5 ml TB medium at 30°C, or 37°C respectively, and 225 rpm over night. The DNA of 1.5 ml of the bacterial culture was prepared with PeqGold Miniprep Kit according to manufacturers protocol.

For a maxi preparation, the bacteria carrying the desired plasmid were expanded in 250 (high copy plasmids) to 400 ml (low copy plasmids) TB medium at 30°C, or 37°C respectively, and 225 rpm over night. The resulting bacteria were pelleted and treated according to the NucleoBond Xtra EF Maxiprep Kit guide. The amount of DNA prepared was measured with a microspectrophotometer and validated by endonuclease digestion.

2.2.4.3 Production of lentiviral particles

For each construct, 6-7 x 10^6 293FT cells were plated on a 15 cm TC dish on day one in MEF medium. The next day, calcium-phosphate precipitate (2.5 ml / 15 cm plate) was prepared by mixing 25 μg of the desired construct with 18.75 μg of the packaging plasmid, 6.75 μg of the envelope plasmid and 125 μl 2.5 M $CaCl_2$. This mixture was filled up to 1.25 ml with water. Afterwards, 1.25 ml 2xBBS was added in

a dropwise fashion and incubated at room temperature for 20 - 25 min. The solution was mixed briefly, added dropwise on a plate and agitated gently. 16 hours later, the medium including the precipitate was removed and 15 ml of fresh MEF medium were added to the plate. The next two days, the supernatant was collected. The pooled supernatants of the two harvests were spun at 3000 g for 5 min, filtered through a 0.45 μm syringe filter and concentrated by ultra centrifugation at 20000 g and 4°C for 90 min. The resulting viral pellet dissolved in 1 ml of HBSS, aliquoted, and stored at -80°C.

2.2.4.4 Transduction of lt-NES and HepG2 cells with lentiviral particles

For viral transduction 800000 (lt-NES) or 400000 (HepG2) cells per 3.5 cm TC dish were seeded one day before to reach a start density of approximately 70%. The next day, the medium was changed to 900 μl culture medium including 4 ng/ml Polybrene and 50 μl of virus dissolved in HBSS. The cells were incubated for 16 hours at 37°C and 5% CO2. Afterwards, the medium was changed to normal culture medium. 72 hours after transduction antibiotic selection was started.

2.2.5 Transfection experiments

The cells were seeded one day before transfection to reach a starting density of approximately 70% (65275 lt-NES cells/cm^2 of a PO/LN coated TC dishes). One hour before transfection, the medium was changed to 100 μl Pen/Strep free medium per cm^2. 13 μl Optimem (Gibco) per cm^2 was mixed with either Lipofectamin 2000 (0.13 μl per cm^2) or the oligonucleotide of interest (10 nM for miRNA mimics, 100 nM for miRNA inhibitors or 10 ng/ml luciferase reporter plasmid). These two separate mixes were incubated at RT for 5 min, then pooled and incubated at RT for another 20 min. Afterwards, 26 μl of the mixture per cm^2 was added. After four hours of incubation at 5% CO2 and 37°C, the medium was changed to 52 μl of normal culture medium per cm^2 and the cells were cultured at 5% CO2 and 37°C.

2.2.5.1 Modulation of miRNA levels

The single-stranded, 2'OMe oligonucleotides used for transfection of cells were purchased from Qiagen and are listed in the table in *section 2.1.2.6 miRNA mimics and inhibitors*. Transfections were repeated every 48 hours.

2.2.5.2 Luciferase reporter assays

The plasmids used for transfection were derived from the psicheck2 vector by fusing the respective 3´UTRs of HES1, NOTCH1 and NOTCH2 amplified from lt-NES cell cDNA with the renilla luciferase cDNA using restriction endonucleases XhoI and NotI. The primers used are listed in section *2.1.3.4.3 Primers used for cloning*. 24 h after transfection, the cells were harvested in 100 µl passive lysis buffer and frozen at -20°C for at least four hours. Afterwards, the lysate was harvested and 10 µl were measured with a luminometer in a 96 well plate upon separate addition of substrates for renilla and firefly luciferases. Each of the replicates of the described experiments was done in technical triplicates.

3. Results

3.1 Assessment of endogenous miR-9/9* expression in differentiating lt-NES cells

Proliferating lt-NES cells derived from the I3 hESC line are uniformly immunopositive for the neural stem cell markers SOX2 and NESTIN (Fig. 3.1A). As the self-renewal of lt-NES depends on the growth factors EGF and FGF2, their presence in the culture medium will be from now on referred to as self-renewing conditions. In turn, media devoid of growth factors induce neuronal differentiation of lt-NES cells and are therefore referred to as differentiating conditions. After 15 (ND15) and 30 (ND30) days of culture under these differentiating conditions, the number of neurons derived from lt-NES cells was assessed by staining for the pan-neuronal marker βIII tubulin. Already at day 15, up to 25% of neuronal differentiation could be observed (Fig. 3.1A). After additional 15 days of differentiation more than 50% of the cells stained positive for βIII tubulin (Fig. 3.1A).

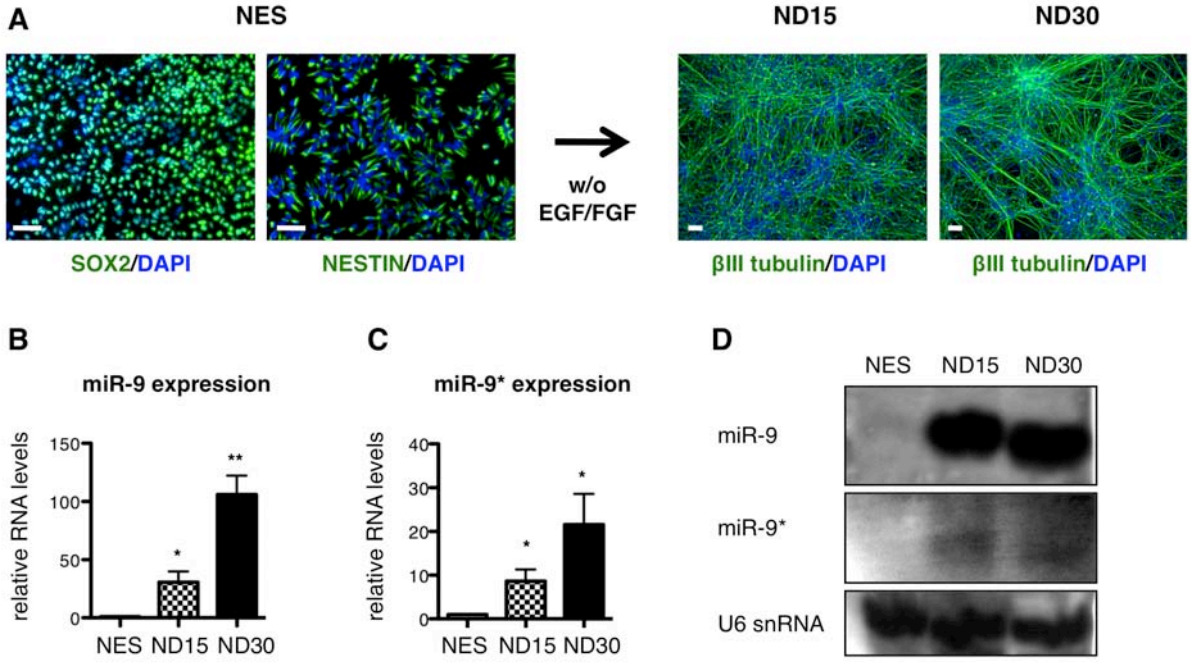

Fig. 3.1: Endogenous expression of miR-9/9* in self-renewing and differentiating lt-NES cells. **(A)** Representative immunostaining for neural stem cell markers SOX2 and NESTIN in proliferating lt-NES cells (NES) and for pan-neuronal marker βIII tubulin in their differentiated progeny after 15 (ND15) and 30 (ND30) days of growth factor withdrawal. DAPI (blue) stains nuclei. Scale bars = 100 μm. **(B, C)** QRT-PCR analyses for relative expression of mature miR-9 **(B)** and miR-9* **(C)** in differentiated lt-NES cultures (ND15, ND30) compared to self-renewing lt-NES cells (NES, equal to 1). Data were normalized to miR-16 reference levels and presented as average changes + SEM (n = 5; Students t-test p-values: *, $p \leq 0.05$; **, $p \leq 0.01$). **(D)** Northern blot analyses of mature miR-9 and miR-9* in the conditions described above. U6 snRNA was used as loading control.

At the described time points RNA was collected to detect the expression of specific miRNAs. Quantitative realtime RT-PCR (qRT-PCR) revealed that expression levels of miR-9 (ND15: 30.68 ± 9.18 fold; ND30: 106.00 ± 16.40 fold) and miR-9* (ND15: 8.66 ± 2.62 fold; ND30: 21.57 ± 7.01 fold) increased significantly during neuronal differentiation of lt-NES cells (Fig. 3.1B, C). The expression patterns of miR-9 and miR-9* were confirmed by non-radioactive Northern blot using snRNA U6 as loading control (Fig. 3.1D).

In humans, miR-9 and miR-9* are expressed from three different genomic loci (Tab. 3.1). The expression of the pri-forms of miR-9/9* in lt-NES cells, glioblastoma cell line U87 as well as commercially available fetal brain RNA (FB) was analyzed by RT-PCR to explore which of them are present in lt-NES cells.

Table 3.1: Genomic loci from which miR-9 and miR-9* are expressed in humans.

Locus name	Mature microRNAs derived	Exact genomic location
9_1	miR-9, miR-9*	Chr.1: 156390133-156390221 [-]
9_2	miR-9, miR-9*	Chr.5: 87962671-87962757 [-]
9_3	miR-9, miR-9*	Chr.15: 89911248-89911337 [+]

While in whole human fetal brain all three genomic loci coding for miR-9/9* are transcribed, in lt-NES and U87 cells only the miR-9_2 locus was detectable by semiquantitative RT-PCR (Fig. 3.2A). Interestingly, the expression of pri-miR-9_2 found in neural stem cells was higher than that detected in the primary glioblastoma cell line U87. The lower expression of pri-miR-9_2 in a malignant, proliferating glioblastoma cell line and the dramatic rise of miR-9/9* expression during differentiation of neural stem cells pointed to a functional role of miR-9 and miR-9* in stem cell maintenance and differentiation.

In order to analyze the effect of miR-9 and miR-9* by ectopic expression in lt-NES cells, lentivirus-based overexpression constructs were designed. As miR-9 and miR-9* are produced from all three genomic loci, the miR-9_1 locus was chosen to be cloned under the control of the H1 polymerase III promoter in the LVTHM vector (LVTHM-miR-9/9*) [94]. Due to its lack in expression in lt-NES cells, the ectopically expressed pre-miR-9_1 was clearly distinguishable from the endogenous pre-miR-

9_2. The vector was modified to carry a puromycin resistance cassette [98] to enable antibiotic selection (Fig. 3.2B). As control construct a hairpin structure carrying a small, scrambled RNA was cloned (LVTHM-ctrl). In lt-NES cells transduced with LVTHM-9/9*, a 48.30 ± 20.00 fold overexpression for miR-9 and 79.80 ± 47.31 fold overexpression for miR-9* were achieved compared to levels in LVTHM-ctrl transduced cells (Fig. 3.2C). Overexpression of miR-9 was additionally validated by Northern blot in the same conditions and compared to untreated lt-NES cells (Fig. 3.2D).

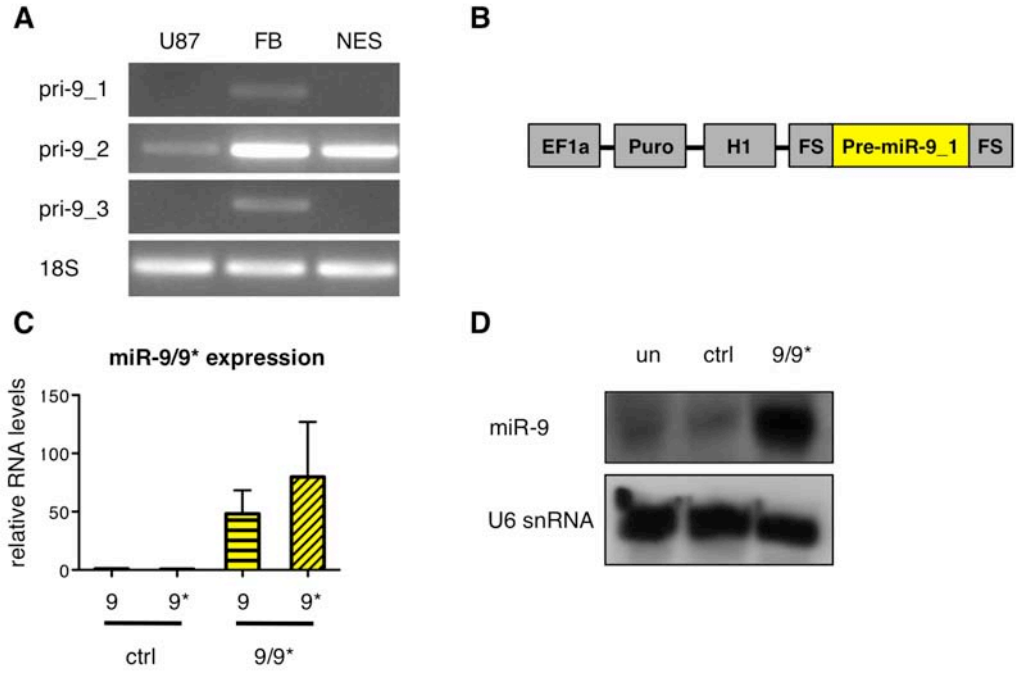

Fig. 3.2: Constitutive overexpression of pri-miR-9/9* in lt-NES cells. (A) Representative gels of RT-PCRs for pri-miR-9_1, -9_2 and -9_3 in proliferating lt-NES (NES) and glioblastoma (U87) cells compared to levels in fetal brain (FB) RNA. 18S rRNA was used as loading control (n=3). **(B)** Scheme of the LVTHM vector modified for overexpression of pre-miR-9_1 including flanking sequences [99]. **(C)** QRT-PCR analysis showing relative expression levels of mature miR-9 (9) and miR-9* (9*) in lt-NES cells transduced with LVTHM-miR-9/9* (9/9*), compared to cells transduced with LVTHM-ctrl (ctrl, equal to 1). Data were normalized to miR-16 reference levels and presented as average changes + SEM (n = 3). **(D)** Northern blot analysis of mature miR-9 in lt-NES cells untreated (un), and transduced with LVTHM-ctrl or LVTHM-miR-9/9*. U6 snRNA was used as loading control.

3.2 Overexpression of miR-9/9* promotes neuronal differentiation and impairs self-renewal of lt-NES cells

First, the impact of miR-9/9* overexpression on lt-NES cell maintenance was analyzed by growth curve and BrdU incorporation assays. Growth curve analyses showed a trend to reduced self-renewal in lt-NES cells overexpressing miR-9/9* compared to untreated cells and cells transduced with a scrambled control construct

(ctrl; Fig. 3.3A). In line with these data, elevated levels of miR-9 and miR-9* reduced the rate of BrdU incorporation significantly to 48.76 ± 2.67% compared to 59.58 ± 1.82% and 58.92 ± 2.64% in untreated and control cultures, respectively (Fig. 3.3B, C).

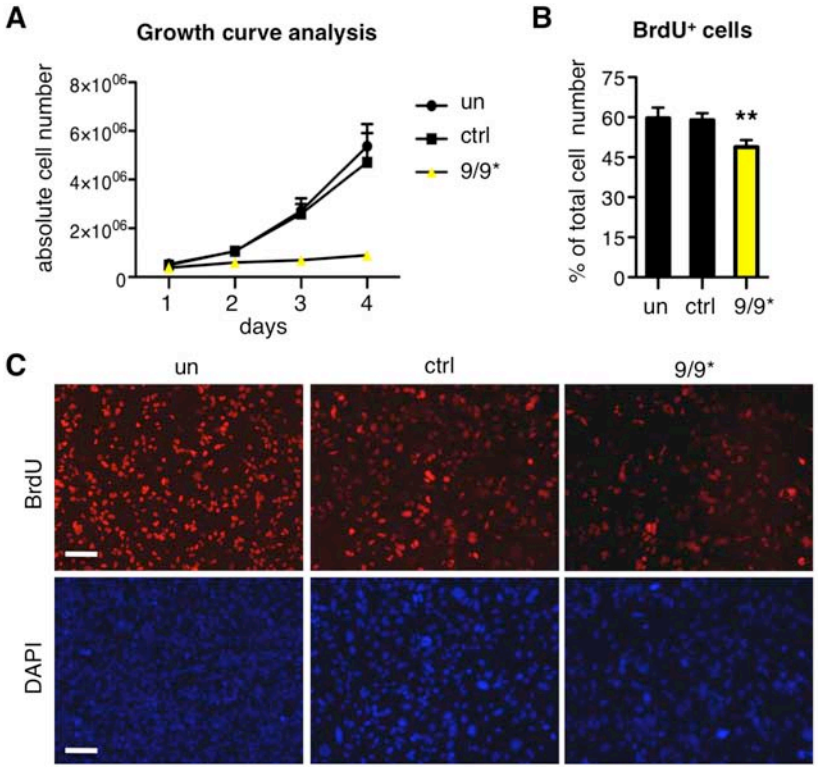

Fig. 3.3: MiR-9/9* overexpression impacts on lt-NES cell self-renewal. (A) Growth curve analysis of untreated lt-NES cells (un), lt-NES cells transduced with LVTHM-ctrl (ctrl) or LVTHM-miR-9/9* (9/9*) under self-renewing conditions. Data are presented as mean + SEM (n=3). **(B)** Quantification of the percentage of BrdU-positive cells in the cell lines described in (A) after 2 days under self-renewing conditions. Data were normalized to the total number of cells and presented as mean + SEM (n = 5). Students t-test p-values: **, $p \leq 0.01$. **(C)** Immunostainings for BrdU in the conditions described in (B). DAPI labels nuclei. Scale bars = 100 μm.

Staining for βIII tubulin in the conditions described revealed that spontaneous differentiation was enhanced significantly by overexpression of miR-9/9* after 4 days under self-renewing conditions. While 0.65 ± 0.10% of the untreated and 0.68 ± 0.10% of the control overexpressing cultures stained positive for βIII tubulin, 3.18 ± 0.06% were positive in lt-NES cells overexpressing miR-9/9* (Fig. 3.4A, B).

Enhanced differentiation was further assessed by looking at neurite outgrowth using the NeuroJ PlugIn for ImageJ to measure their length in μM. Upon miR-9/9* overexpression the neurite length tended to be longer (215.90 ± 15.65 μm) compared to 174.00 ± 11.91 μm in LVTHM-ctrl expressing lt-NES cultures after 7 days under

differentiating conditions (Fig. 3.4C). The observed difference was, however, not significant.

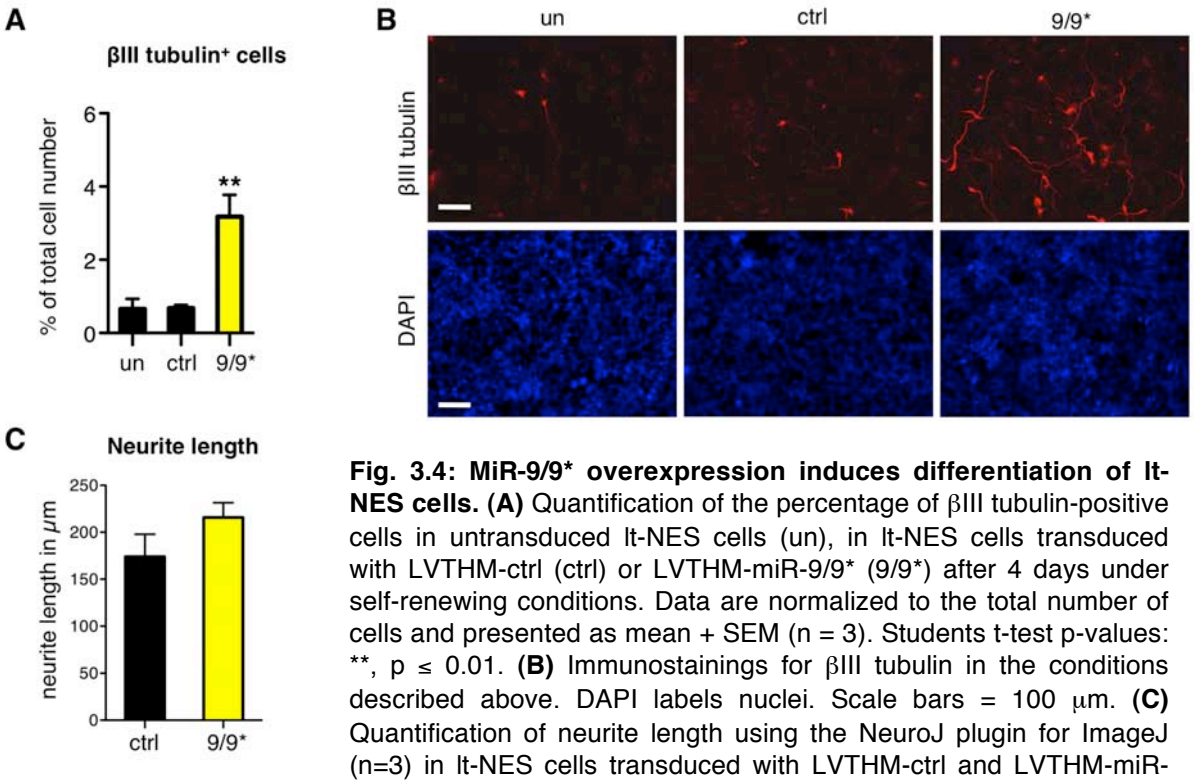

Fig. 3.4: MiR-9/9* overexpression induces differentiation of lt-NES cells. (A) Quantification of the percentage of βIII tubulin-positive cells in untransduced lt-NES cells (un), in lt-NES cells transduced with LVTHM-ctrl (ctrl) or LVTHM-miR-9/9* (9/9*) after 4 days under self-renewing conditions. Data are normalized to the total number of cells and presented as mean + SEM (n = 3). Students t-test p-values: **, $p \leq 0.01$. **(B)** Immunostainings for βIII tubulin in the conditions described above. DAPI labels nuclei. Scale bars = 100 μm. **(C)** Quantification of neurite length using the NeuroJ plugin for ImageJ (n=3) in lt-NES cells transduced with LVTHM-ctrl and LVTHM-miR-9/9* after 7 days under differentiating conditions.

3.3 MiR-9 and miR-9* target components of the Notch pathway

Similar to the impact of miR-9/9*, γ-secretase inhibitor DAPT has been shown to induce premature differentiation and reduce self-renewal of lt-NES cells [22]. These similarities suggested an interplay of miR-9/9* with the Notch signaling pathway. Indeed, target prediction algorithms [100] revealed miR-9 and miR-9* binding sites in the 3´UTRs of various components of the Notch pathway (Tab. 3.2)

	miR-9	miR-9*
NOTCH1	1	0
NOTCH2	3	2
PSEN1	3	1
MAML3	2	0
DLL1	0	1
DLL4	1	0
JAG1	0	2
JAG2	1	0
HES1	2	0
HEY1	0	2
HEY2	1	2

Tab. 3.2: Target prediction for members of the Notch pathway. The two right columns present the number of algorithms predicting binding of miR-9 or miR-9* to the 3´UTRs of the genes indicated. The analysis was done using the miRWALK algorithm [100].

An inducible system for overexpression of miR-9/9* was designed to validate a selection of the predicted targets in cell lines with defined overexpression levels. To

that end, the genomic pre-miR-9_1 including flanking sequences or GFP as control were cloned under the doxycycline-inducible polymerase II promoter of the pTight vector for conditional overexpression (Fig. 3.5A). QRT-PCR analysis showed a robust overexpression of both miR-9 (111.30 ± 18.96 fold) and miR-9* (207.30 ± 88.57 fold) upon doxycycline treatment of lt-NES cells transduced with Tight-miR-9/9* compared to lt-NES cells transduced with Tight-GFP (GFP, equal to 1; Fig. 3.5B, C). In contrast, levels of miR-125b (1.18 ± 0.55 fold), another brain-enriched miRNA, were not affected (Fig. 3.5D).

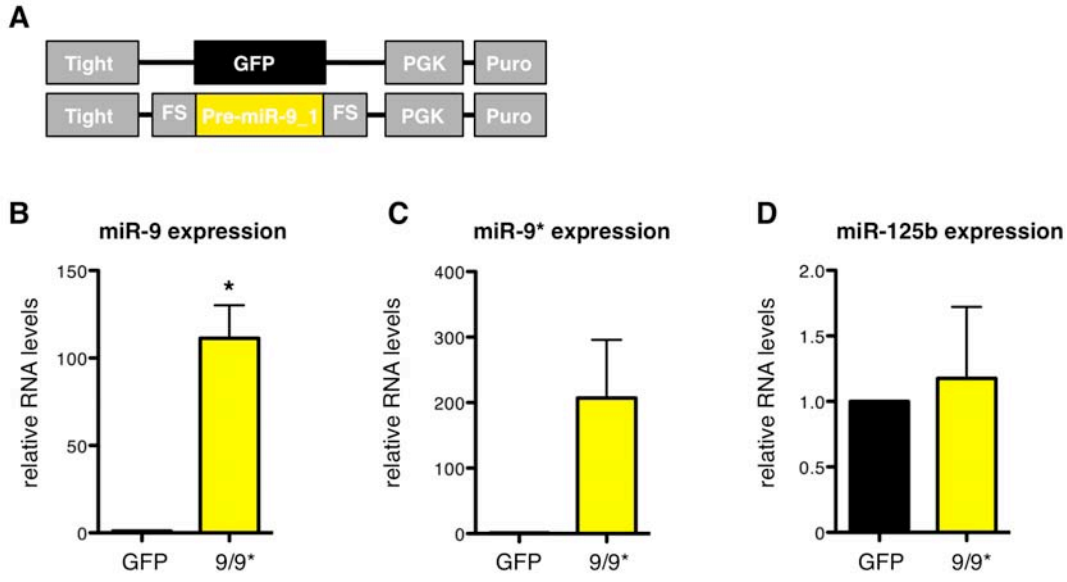

Fig. 3.5: Conditional overexpression of miR-9/9* in lt-NES cells.
(A) Scheme of the lentiviral vector for conditional overexpression of pre-miR-9_1 including flanking sequences [99] or GFP. **(B-D)** QRT-PCR analyses of miR-9 **(B)**, miR-9* **(C)** and miR-125b **(D)** levels in lt-NES cells overexpressing miR-9/9* or GFP after 4 days of doxycycline treatment under self-renewing conditions. Data are normalized to miR-16 reference levels and presented as average changes + SEM relative to GFP transduced lt-NES cells (GFP, equal to 1; n≥ 3; Students t-test p-value: *, p ≤ 0.05).

Next, the mRNA levels of Notch receptors NOTCH1 and NOTCH2 as well as downstream target HES1, which were predicted to be targeted by miR-9/9*, were assessed by qRT-PCR. These targets were chosen for initial analysis due to their known roles in neural development and high expression levels in lt-NES cells [22]. Although a binding site for miR-9 is predicted in its 3´UTR, NOTCH1 levels did not change (1.79 ± 1.01 fold). In contrast, NOTCH2 (0.47 ± 0.31 fold) and HES1 (0.43 ± 0.11 fold) were down-regulated significantly upon miR-9/9* overexpression (Fig. 3.6A-C). The miR-9/9*-induced downregulation of HES1 and NOTCH2 was also observed at the protein level by Western blotting (Fig. 3.6D-F).

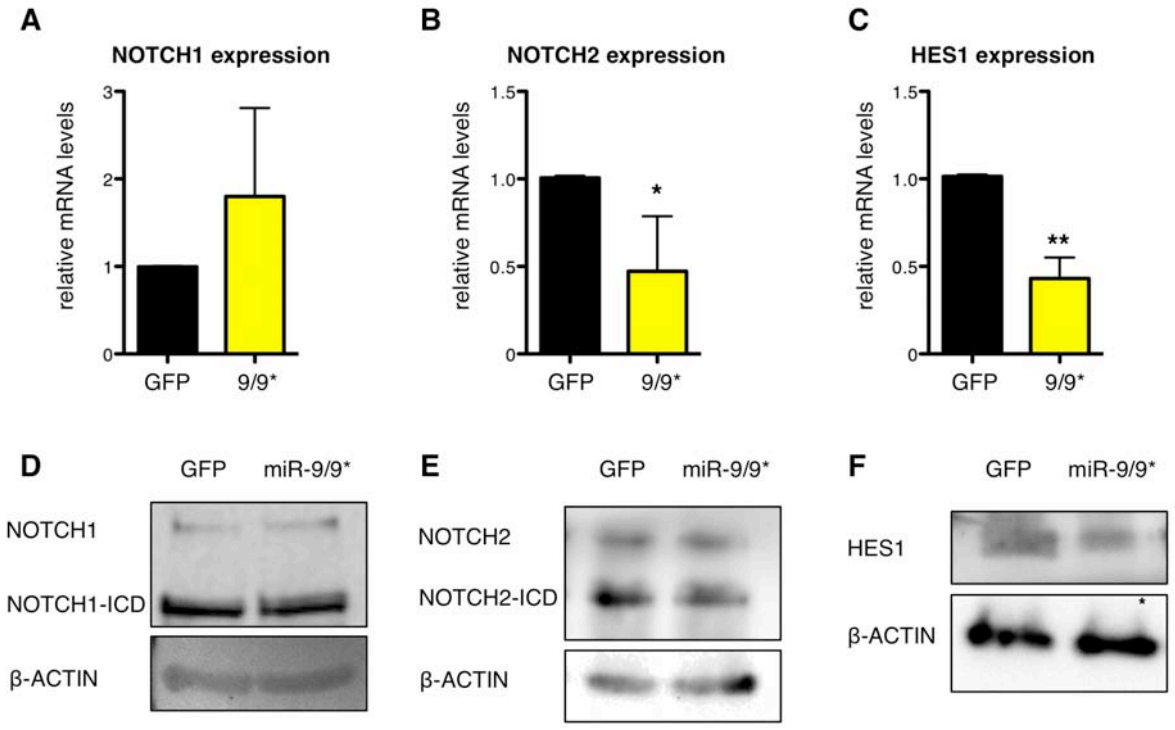

Fig. 3.6: Impact of miR-9/9* overexpression on different members of the Notch signaling pathway. (A-C) QRT-PCR analysis of NOTCH1 **(A)**, NOTCH2 **(B)** and HES1 **(C)** transcript levels in lt-NES cells overexpressing miR-9/9* compared to GFP-overexpressing control cells. Data are normalized to 18S rRNA reference levels and presented as average changes + SEM relative to expression in GFP control cells (equal to 1; n= 6; Students t-test p-values: *, $p \leq 0.05$; **, $p \leq 0.01$). **(D-F)** Representative Western blot analyses of NOTCH1 **(D)**, NOTCH2 **(E)** and HES1 **(F)** in the conditions described above. β-ACTIN was used as loading control.

To assess whether the impact of miR-9/9* on the protein and mRNA levels of NOTCH2 and HES1 was due to direct binding of the 3´UTRs of these targets, a double luciferase reporter construct was designed by fusing the 3´UTRs of NOTCH1, NOTCH2 or HES1 to the 3´end of the renilla luciferase cDNA. Unmodified firefly luciferase cDNA was used as normalizer (Fig. 3.7A). Lt-NES cells were transfected with either synthetic miR-9/9* mimics or a small scrambled control RNA. The next day, a second transfection with the designed dual luciferase constructs was performed. For analysis, data were normalized to the activity of the vectors in lt-NES cells transfected with scrambled control RNA (ctrl, equal to 1; Fig. 3.7B-D). Elevated miR-9/9* levels induced a significant downregulation of renilla luciferase activity for NOTCH2 (0.61 ± 0.08 fold) and HES1 (0.59 ± 0.15 fold) but not NOTCH1 constructs (0.82 ± 0.16 fold) thereby confirming direct binding to their 3´UTRs (Fig. 3.7B-D).

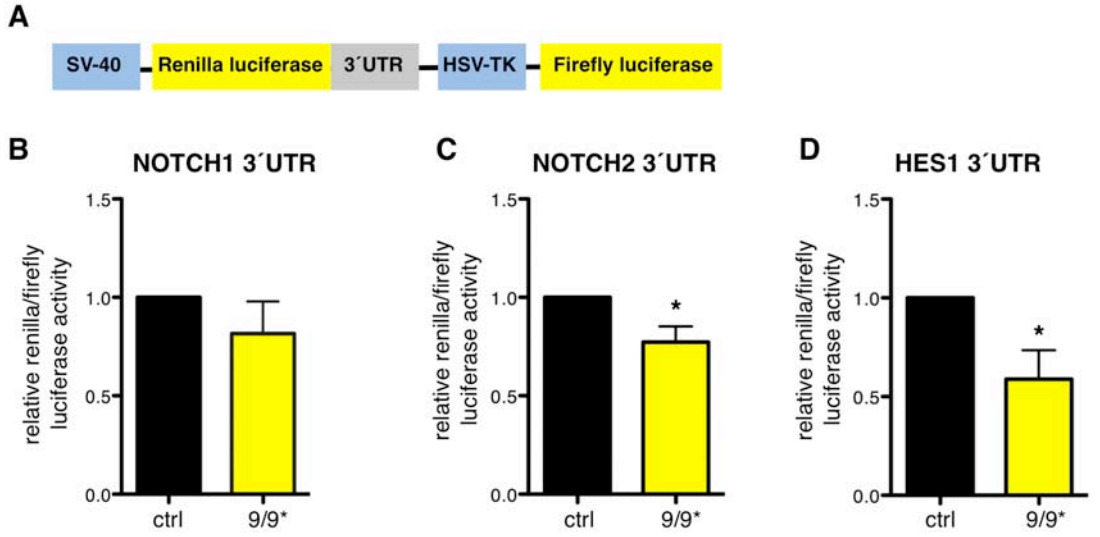

Fig. 3.7: Analysis of direct targeting of NOTCH1, NOTCH2 and HES1 3´UTRs by miR-9/9*.
(A) Scheme of the dual luciferase reporter plasmid used. **(B-D)** Analysis of luciferase activity in lt-NES cells expressing the 3´UTRs of NOTCH1 **(B)**, NOTCH2 **(C)** and HES1 **(D)** cloned downstream of renilla luciferase, and transfected with synthetic mimics for miR-9/9* (9/9*) or a scrambled control (ctrl). Data are normalized to firefly luciferase activity and presented as average changes + SEM relative to activity of a control vector (ctrl, equal to 1; n= 5; Students t-test p-value: *, $p \leq 0.05$).

In order to identify additional true targets of miR-9/9* within the NOTCH signaling cascade among those identified by *in silico* target prediction analysis (Tab. 3.2), further qRT-PCR analyses on lt-NES cell ectopically overexpressing miR-9/9* compared to GFP were performed. Out of 8 genes analyzed only transcript levels of HEY2 were found significantly reduced by 0.74 ± 0.08 fold (Fig. 3.8).

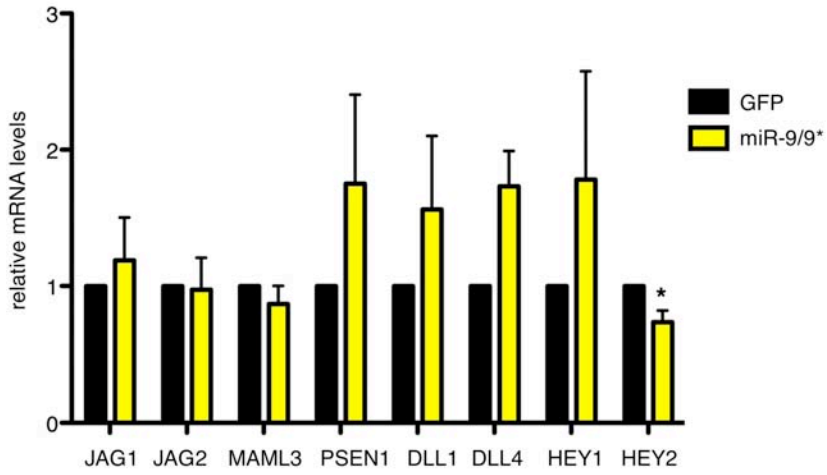

Fig. 3.8: QRT-PCR analysis of transcript levels for additional predicted targets in the Notch signaling pathway.
QRT-PCR analysis of mRNA levels of components of the Notch signaling pathway in lt-NES cells overexpressing miR-9/9*. Data are normalized to 18S rRNA reference levels and presented as average changes + SEM relative to expression in lt-NES cells overexpressing GFP (equal to 1; n= 3; Students t-test p-value: *, $p \leq 0.05$).

Together, these data indicate that in lt-NES cells miR-9/9* affect Notch signaling by targeting of NOTCH2, HES1 and potentially HEY2, but not NOTCH1.

3.4 The impact of miR-9/9* on lt-NES cell differentiation can be abolished by modulation of Notch activity

Notch signaling is an important player in lt-NES cell maintenance and its inhibition by DAPT induces premature lt-NES cell differentiation [22]. In a similar way, lentiviral-based overexpression of miR-9/9* promoted differentiation of lt-NES cells even under self-renewing conditions (Fig. 3.4). In addition, Notch pathway components NOTCH2 and HES1 are directly regulated by miR-9/9*. To address the biological relevance of the interaction between miR-9/9* and Notch in lt-NES cells, modulation of both miR-9/9* and Notch activity was performed, followed by *in vitro* functional assays during lt-NES differentiation. As expected, inhibition of miR-9/9* by transfection of synthetic inhibitors decreased the amount of βIII tubulin-positive cells significantly to 0.55 ± 0.08 fold (Fig. 3.9).

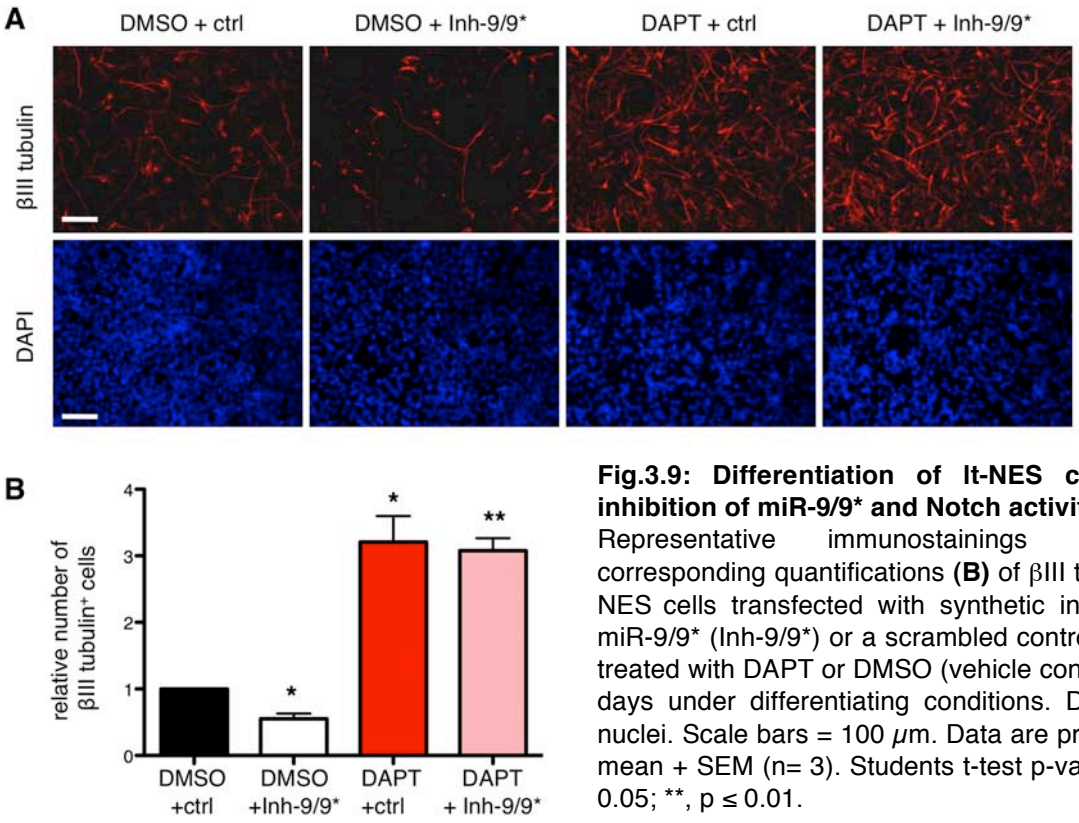

Fig.3.9: Differentiation of lt-NES cells upon inhibition of miR-9/9* and Notch activity. Representative immunostainings **(A)** and corresponding quantifications **(B)** of βIII tubulin in lt-NES cells transfected with synthetic inhibitors for miR-9/9* (Inh-9/9*) or a scrambled control (ctrl) and treated with DAPT or DMSO (vehicle control) after 7 days under differentiating conditions. DAPI stains nuclei. Scale bars = 100 μm. Data are presented as mean + SEM (n= 3). Students t-test p-values: *, $p \leq 0.05$; **, $p \leq 0.01$.

On the contrary, inhibition of Notch signaling via DAPT increased it significantly by 3.21 ± 0.39 fold compared to ctrl cultures (Fig. 3.9). When these two conditions were combined, the amount of βIII tubulin-positive cells was still increased significantly by 3.08 ± 0.19 fold (Fig. 3.9). These data indicate that the block of Notch cleavage

induced by DAPT, which results in a lack of NICDs, prevents the effect of miR-9/9* inhibition conducted via derepression of NOTCH2 and HES1.

In turn, transfection of lt-NES cells with mimics of miR-9 and miR-9* led to a 1.86 ± 0.20 fold increase of the number of βIII tubulin-positive cells in lt-NES cells overexpressing GFP. Conversely, constitutive activation of Notch signaling was achieved by ectopic expression of a NOTCH2-ICD. The pTight-NOTCH2-ICD construct used is not prone to miRNA-9/9* regulation as it lacks the NOTCH2 3´UTR, which harbors the miR-9 and miR-9* binding sites (N2ICD). Ectopic expression of this construct induced a reduction of the relative number of βIII tubulin-positive cells to 0.27 ± 0.01 fold compared to lt-NES cells overexpressing GFP and transfected with a scrambled RNA control (Fig. 3.10).

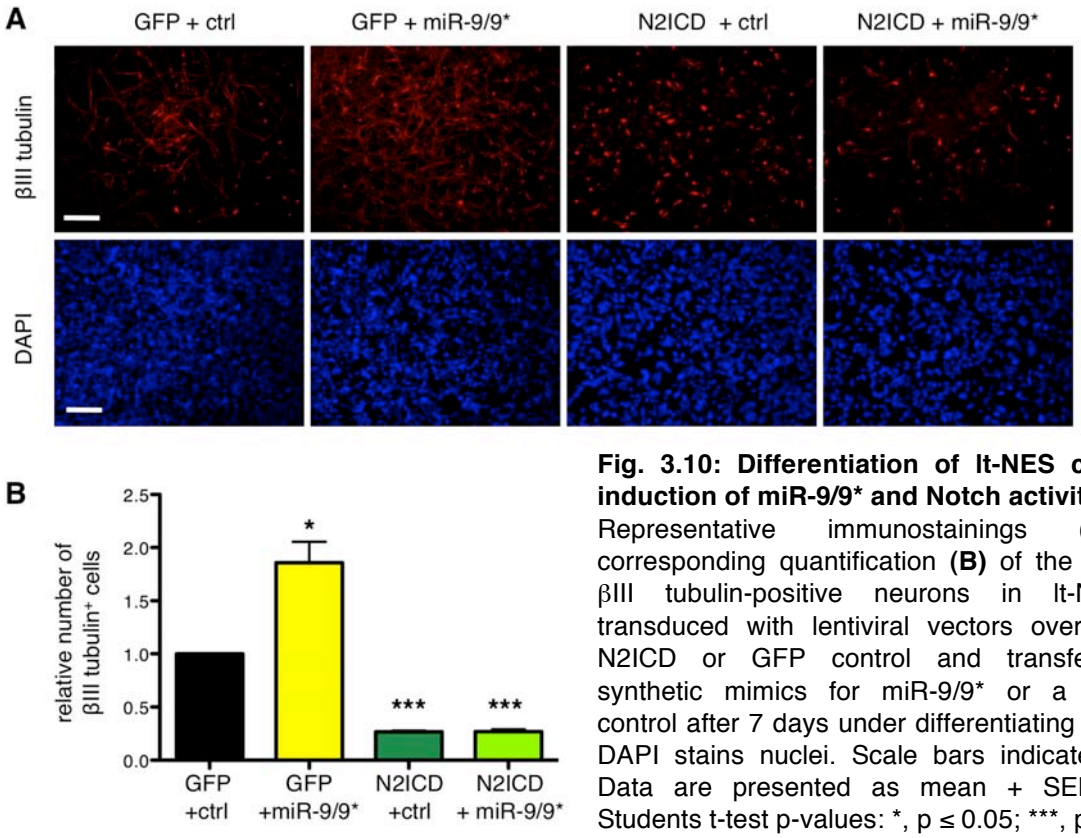

Fig. 3.10: Differentiation of lt-NES cells upon induction of miR-9/9* and Notch activity.
Representative immunostainings **(A)** and corresponding quantification **(B)** of the number of βIII tubulin-positive neurons in lt-NES cells transduced with lentiviral vectors overexpressing N2ICD or GFP control and transfected with synthetic mimics for miR-9/9* or a scrambled control after 7 days under differentiating conditions. DAPI stains nuclei. Scale bars indicate 100 μm. Data are presented as mean + SEM (n= 3). Students t-test p-values: *, $p \leq 0.05$; ***, $p \leq 0.001$.

Interestingly, additional administration of miR-9/9* mimics could not even partially rescue the impairment in differentiation induced by N2ICD overexpression (Fig.3.10; N2ICD + miR-9/9*: 0.27 ± 0.02 fold) indicating that the impact of miR-9/9* is indeed mediated through the Notch signaling pathway.

Taken together, these functional data show that the Notch pathway is an important functional target of miR-9/9* in lt-NES cells and that its modulation accounts, at least in part, for the contribution of these miRNAs to lt-NES cell differentiation.

3.5 Expression of miR-9/9* is decreased upon γ-secretase inhibition

It has been shown that expression of miR-9 is decreased upon knockout of the γ-secretase complex component Presinillin1 in mice [41]. As monitored by Northern blotting, treatment of self-renewing I3 lt-NES cell cultures with γ-secretase inhibitor DAPT for 12, 24 and 48 hours led to down-regulation of miR-9 expression, but not of an additional miRNA analyzed (i.e., miR-125b), compared to treatment with vehicle control (Fig. 3.11A, B).

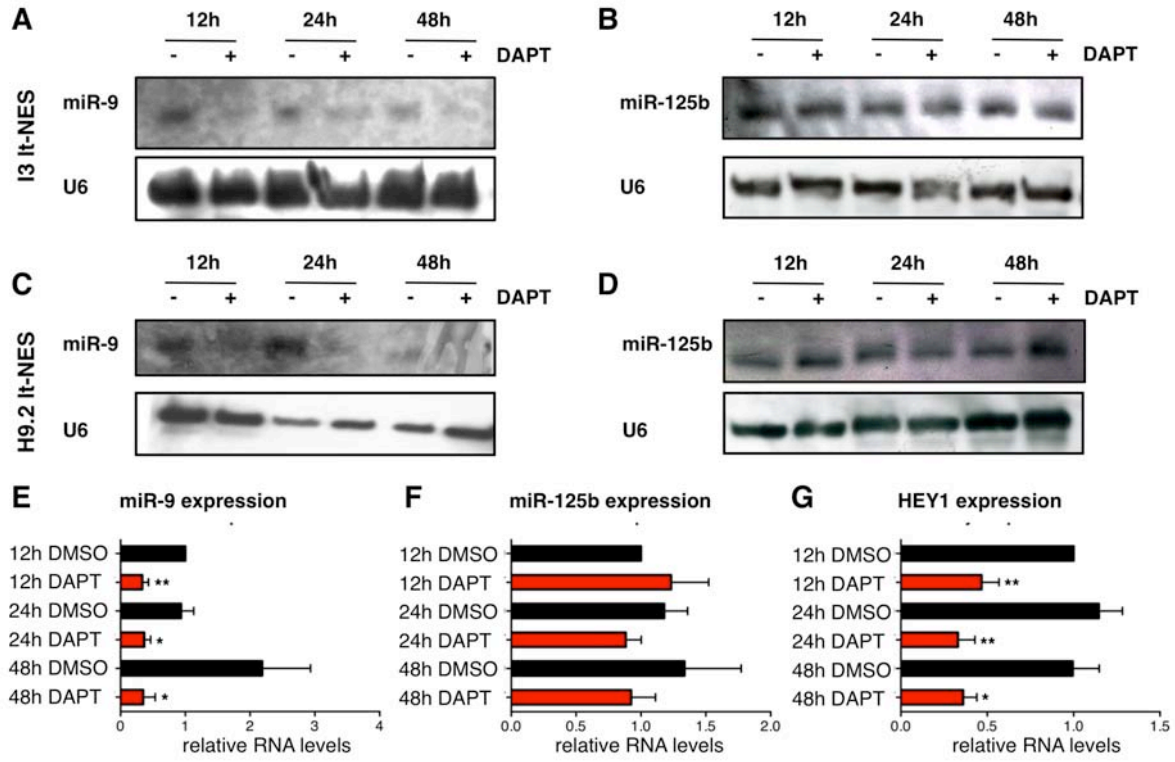

Fig. 3.11: Analysis of miR-9 and miR-125b expression in lt-NES cells treated with the γ-secretase inhibitor DAPT. (A-D) Northern blot analyses showing the expression of miR-9 **(A, C)** and miR-125b **(B, D)** in lt-NES cells derived from I3 **(A, B)** or H9.2 **(C, D)** hESCs treated with DAPT (+) or DMSO (-, vehicle control) for 12, 24 and 48 hours. U6 snRNA was used as loading control. **(E, F)** QRT-PCR analyses monitoring mature miR-9 **(E)** and miR-125b **(F)** in the samples described in (A, B). Data are normalized to miR-16 reference levels and presented as average changes + SEM relative to expression in lt-NES cells treated with DMSO for 12 hours (equal to 1; n= 4). **(G)** QRT-PCR analysis monitoring HEY1 transcript levels in the samples described in (A, B). Data are normalized to 18S rRNA reference levels and presented as average changes + SEM relative to expression in lt-NES cells treated with DMSO for 12 hours (baseline, equal to 1; n= 6). Students t-test p-values: *, $p \leq 0.05$; **, $p \leq 0.01$.

Similar results could be obtained in lt-NES cell cultures derived from H9.2 hESCs (Fig. 3.11C, D). The I3 derived lt-NES cell line was further assessed for miR-9 expression by qRT-PCR analysis, which showed a significant down-regulation of miR-9 expression to 0.34 ± 0.09 fold after 12 hours of DAPT treatment, which was stable at 24 (0.36 ± 0.10 fold) and 48 hours (0.35 ± 0.19 fold; Fig. 3.11E). In contrast, no significant difference was detected in expression levels of miR-125b (Fig. 3.11F; 12h: 1.23 ± 0.29 fold; 24h: 0.88 ± 0.11 fold; 48h: 0.92 ± 0.19 fold) whereas known Notch target HEY1 showed an expression pattern similar to that of miR-9 (Fig. 3.11G; 12h: 0.47 ± 0.10 fold; 24h: 0.33 ± 0.10 fold; 48h: 0.37 ± 0.08 fold) confirming the efficiency of the DAPT treatment. All data were compared to lt-NES cells treated with DMSO as vehicle control (Fig. 3.11E, F; 12h: equal to 1; miR-9: 24h: 0.94 ± 0.20 fold; 48h: 2.19 ± 0.75 fold; miR-125: 24h: 1.18 ± 0.18 fold; 48h: 1.34 ± 0.44 fold; HEY1: 24h: 1.15 ± 0.14 fold; 48h: 1.00 ± 0.15 fold).

In order to assess whether the impact of DAPT on miR-9 expression resulted in an impairment of miR-9 function in lt-NES cells, binding sites for miR-9 were fused to the renilla luciferase cDNA in a double luciferase vector (Fig. 3.12A).

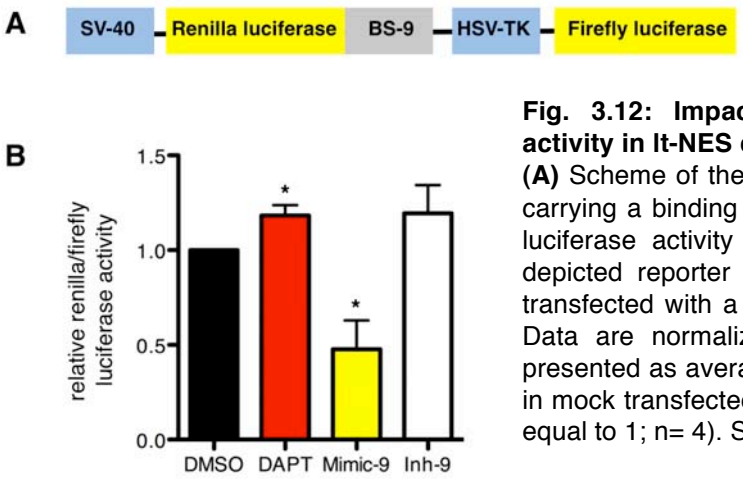

Fig. 3.12: Impact of DAPT treatment on miR-9 activity in lt-NES cells.
(A) Scheme of the double luciferase construct designed carrying a binding site for miR-9 (BS-9). **(B)** Analysis of luciferase activity in lt-NES cells transfected with the depicted reporter construct and treated with DAPT or transfected with a synthetic mimic or inhibitor of miR-9. Data are normalized to firefly luciferase activity and presented as average changes + SEM relative to activity in mock transfected, DMSO treated lt-NES cells (DMSO, equal to 1; n= 4). Students t-test p-value: *, $p \leq 0.05$.

Lt-NES cells were pretreated with DAPT or DMSO or, to validate the sensitivity of the reporter system, transfected with either miR-9 mimic or inhibitor. The next day the luciferase reporter vector harboring binding sites for miR-9 was transfected into the pretreated cells. Changes in renilla luminescence detected were normalized to the activity of an unregulated firefly luciferase. While lt-NES cells transfected with a mimic of miR-9 exhibited a significant relative reduction of renilla luciferase activity to 0.48 ± 0.15 fold, transfection of its inhibitor induced a slight, 1.20 ± 0.15 fold, increase

(Fig. 3.12B), which was not significant. Modulation of mature miR-9 by DAPT, similarly to the transfection of miR-9 inhibitor, led to a slight, yet significant, 1.18 ± 0.06 fold increase in luciferase activity (Fig. 3.12B) confirming that this regulation can cause a detectable difference in binding of miR-9 to its target sites.

Pri-miR-9_2 is the only pri-form of miR-9/9* abundantly expressed in lt-NES cells (Fig. 3.2A). Pri-miR-9_2 expression levels in lt-NES cells treated with DAPT for 12, 24, and 48 hours were analyzed to explore whether DAPT treatment impacts on miR-9 at the level of its transcription. Indeed, similar to miR-9, pri-miR-9_2 was down-regulated to 0.32 ± 0.10 fold after 12 hours of DAPT treatment, and its levels remained low after 24 (0.25 ± 0.01 fold) and 48 hours (0.37 ± 0.14 fold) compared to DMSO-treated samples (Fig. 3.13A; 12h: equal to 1; 24h: 1.27 ± 0.14 fold; 48h: 1.12 ± 0.10 fold).

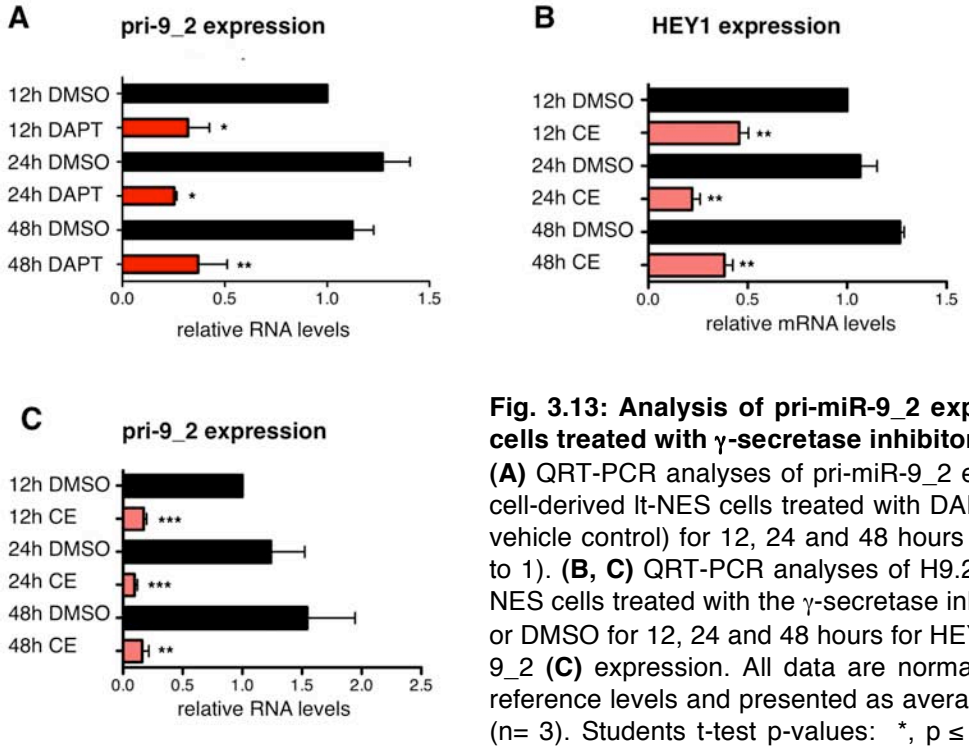

Fig. 3.13: Analysis of pri-miR-9_2 expression in lt-NES cells treated with γ-secretase inhibitors.
(A) QRT-PCR analyses of pri-miR-9_2 expression in I3 ES cell-derived lt-NES cells treated with DAPT (+) or DMSO (-, vehicle control) for 12, 24 and 48 hours (12h DMSO, equal to 1). **(B, C)** QRT-PCR analyses of H9.2 ES cell-derived lt-NES cells treated with the γ-secretase inhibitor compound E or DMSO for 12, 24 and 48 hours for HEY1 **(B)** and pri-miR-9_2 **(C)** expression. All data are normalized to 18S rRNA reference levels and presented as average changes + SEM (n= 3). Students t-test p-values: *, $p \leq 0.05$; **, $p \leq 0.01$; ***, $p \leq 0.001$.

These results were confirmed also when using the alternative γ-secretase inhibitor compound E in lt-NES cells derived from a different hESC line, i.e. H9.2. As shown for DAPT treatment in I3 hESC derived lt-NES cells (Fig. 3.11G), treatment of H9.2 lt-NES cells with compound E also reduced expression of the known Notch target gene HEY1 (12h: 0.46 ± 0.05 fold, 24h: 0.22 ± 0.04 fold and 48h: 0.38 ± 0.04 fold)

compared to treatment with DMSO (Fig. 3.13B; 12h: equal to 1; 24h: 1.07 ± 0.08 fold; 48h: 1.27 ± 0.02 fold). The reduction in levels of pri-miR-9_2 could be recapitulated as well. While pri-miR-9_2 levels did not change upon treatment with DMSO (12h: equal to 1; 24h: 1.24 ± 0.28 fold; 48h: 1.54 ± 0.40 fold), compound E treatment reduced pri-miR-9_2 levels significantly to 0.17 ± 0.02 fold after 12 hours (Fig. 3.13C). The observed reduction remained stable after 24 (0.10 ± 0.02 fold) and 48 (0.16 ± 0.06 fold) hours (Fig. 3.13C). Taken together, the data collected indicate that the downregulation of mature miR-9 and its pri-form upon pharmacological γ-secretase inhibition, recently reported in *Zebrafish* and mouse studies [83, 84], is conserved in human neural stem cells.

3.6 Notch activity regulates expression of miR-9/9*

In addition to the Notch receptors, the γ-secretase complex cleaves a number of other substrates including the amyloid precursor protein which is linked to the pathology of Alzheimer´s disease (reviewed in [101]). To confirm that the observed effects of γ-secretase inhibition on miR-9 transcriptional expression are mediated by Notch signaling, lentiviral constructs for conditional gain and loss of Notch activity in lt-NES cells were generated. More specifically, human NOTCH1-ICD (NICD), described in [95], or a dominant-negative form of the MAML1 (coactivator of transcription of the NICD-RBPj complex, here referred to as DN-MAML1), described in [96], and an eGFP control were cloned under the doxycycline-inducible promoter of the pTight vector (Fig. 3.14A). I3 hESC derived lt-NES cells were transduced with the designed lentiviral vectors and treated with doxycycline for 4 days under self-renewing conditions. First, modulation of Notch signaling upon doxycycline-induced expression of these constructs was validated by qRT-PCR analysis of HEY1 mRNA. HEY1 transcript levels were reduced to 0.52 ± 0.09 fold upon overexpression of DN-MAML1 (Fig. 3.14B). This reduction was comparable to that induced by DAPT (0.59 ± 0.06 fold; Fig. 3.14B). In turn, ectopic expression of NICD increased HEY1 levels 19.36 ± 4.09 fold compared to levels in lt-NES cells transduced with Tight-GFP (GFP, equal to 1; Fig. 3.14B).

Next, the expression of miR-9, miR-125 and miR-9* was assessed under the same conditions. Similarly to HEY1 mRNA, miR-9 showed a 12.18 ± 4.86 fold increase

upon NICD overexpression and a 0.36 ± 0.11 fold or 0.45 ± 0.12 fold decrease upon inhibition of Notch activity by expression of DN-MAML1 or treatment with DAPT, respectively (Fig. 3.14C). In contrast, miR-125b did not show this Notch-dependent behavior (Fig. 3.14D; DAPT: 1.06 ± 0.08 fold; DN-MAML1: 0.99 ± 0.12 fold; NICD: 0.97 ± 0.21 fold).

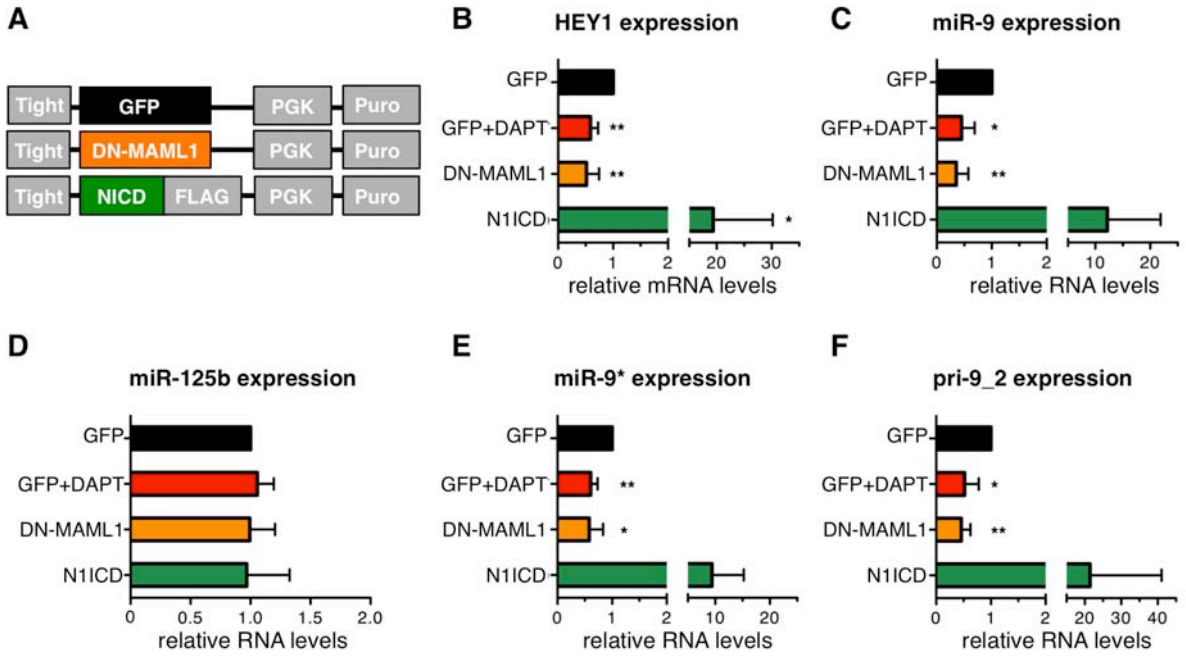

Fig. 3.14: Expression analysis of mature miR-9 and miR-9* as well as pri-miR-9/9* in lt-NES cells upon gain and loss of Notch activity. (A) Scheme of the lentiviral overexpression constructs used for Notch gain (NICD) and loss (DN-MAML1) of function or as control (GFP). **(B, F)** QRT-PCR analyses of HEY1 mRNA **(B)** and pri-miR-9_2 (pri-9_2, **F**) in lt-NES cells transduced with lentiviral vectors overexpressing in a doxycycline-dependent manner GFP, NICD or DN-MAML1, respectively, after 4 days of doxycycline treatment in presence or absence of DAPT. Data are normalized to 18S rRNA reference levels. **(C-E)** QRT-PCR analyses of miR-9 **(C)**, miR-125b **(D)** and miR-9* **(E)** levels in the samples described above. Data are normalized to miR-16 reference levels. All qRT-PCR data are presented as average changes + SEM relative to expression in GFP-expressing lt-NES cells (GFP, equal to 1; n≥ 4). Students t-test p-values: *, p ≤ 0.05; **, p ≤ 0.01.

As expected under these conditions, miR-9* showed a pattern of expression similar to that of its sister strand miR-9 (Fig. 3.14E; DAPT: 0.61 ± 0.06 fold; DN-MAML1: 0.58 ± 0.13 fold; NICD: 9.42 ± 2.92 fold). Pri-miR-9_2 expression also showed a similar dependence on Notch activity (Fig. 3.14F; DAPT: 0.52 ± 0.12 fold; DN-MAML1: 0.46 ± 0.07 fold; NICD: 21.44 ± 8.78 fold). This coinciding expression of pri-miR-9-2 and its progeny further supports the hypothesis of a transcriptional regulation of the miR-9 genomic locus via Notch signaling.

Together, pharmacological inhibition as well as genetic gain and loss of Notch activity show that canonical Notch signaling is involved in the regulation of miR-9/9* transcription in human neural stem cells.

3.7 The miR-9/9* genomic loci are direct transcriptional targets of Notch

A prerequisite for direct regulation of a promoter by Notch transcriptional activity are binding sites for RBPj – the DNA binding component of the NICD/MAML1/RBPj transcriptional complex. Bioinformatic analysis revealed RBPj binding sites in the genomic regions 10 kb upstream of all three miR-9/9* genomic loci and also one site upstream of the miR-125b_2 locus. The number of predicted sites and their genomic location are depicted in the scheme in Fig. 3.15A.

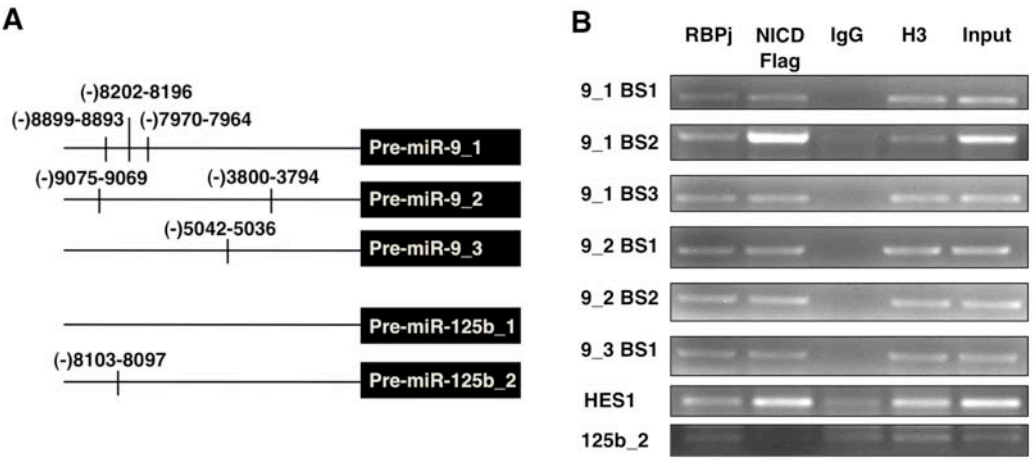

Fig. 3.15: Analysis of RBPj/NICD binding to genomic regions upstream of the loci encoding miR-9/9*. (A) Predicted binding sites for RBPj (strikes) in the genomic loci encoding for miR-9/9* and miR-125b including the region 10 kb upstream of the pre-miRNA. **(B)** Chromatin immunoprecipitation from cross-linked chromatin (Input) of I3 hESC derived lt-NES cells overexpressing a Flag-tagged NICD with antibodies against Flag, RBP-J, IgG (negative control) and H3 (positive control). Representative gel images of PCR analyses for the predicted RBPj binding sites in the genomic regions upstream of the miR-9/9* and miR-125b loci. Binding sites [102] are named after the pri-miRNA or gene regulated (9_1; 9_2; 9_3; 125b_2, HES1) and numbered according to their order of appearance in the genome starting with the one farthest from gene of interest (scheme in A).

The predicted binding sites were tested for direct interaction with the RBPj/MAML1/NICD complex by chromatin immunoprecipitation (ChIP). Specifically, I3 hESC derived lt-NES cells transduced with a construct for conditional overexpression of a Flag-tagged NICD (see scheme Fig. 3.14A) were treated with doxycycline for 4 days under self-renewing conditions. Afterwards, their chromatin was cross-linked to the proteins bound, sonicated, and immuno-precipitated using antibodies against Flag-Tag or RBPj to confirm the binding of the Notch-RBPj-

complex in two independent immunoprecipitations. In addition, an unspecific IgG antibody was used as negative control and an antibody against Histone3 (H3), a protein involved in the chromatin structure, as positive control. PCR reactions on these precipitated samples were carried out with primers designed for the predicted RBPj binding sites (Fig. 3.15A). All primers worked in PCR on chromatin input as well as H3 precipitation, proving their functionality (Fig. 3.15B). The binding sites predicted in front of the three miR-9 loci were all enriched in PCR from immunoprecipitations performed using both anti-Flag (against NICD) and anti-RBPj antibodies when compared to IgG negative control (Fig. 3.15B). This pattern resembled the one found for the known RBPj-binding site in the HES1 promoter region [103] assessed as positive control. No enrichment could be observed for the binding site upstream of the miR-125b_2 locus.

Overall, these results prove that the NICD-RBPj transcriptional complex directly binds genomic regions upstream of the miR-9/9* loci and that miR-9/9* (but not miR-125b) is a direct transcriptional target of Notch.

3.8 Bifunctionality of miR-9/9* in lt-NES cells

The data obtained so far clearly showed that overexpression of a pre-miRNA carrying miR-9 and miR-9* affects lt-NES cell self-renewal and differentiation. To assess the individual contributions of miR-9 and miR-9* to lt-NES cell behavior, the levels of each of these miRNAs were modulated separately. To that end, I3 hESC derived lt-NES cells were transfected with synthetic mimics of either miR-9 or miR-9* or with a scrambled small RNA control (ctrl) every 48 hours. After 2 days under self-renewing conditions, the cells were analyzed for levels of miR-9 and miR-9* by qRT-PCR and after 4 days their differentiation was assessed by immunocytochemistry.

MiRNA levels were found increased 372.60 ± 234.60 fold (miR-9, Fig. 3.16A) and 518.20 ± 249.30 fold (miR-9*, Fig. 3.16B) when compared to levels in mock transfected cells. The intake of the synthetic mimics varied strongly, which led to non-significant mean values. However, the overexpression of miR-9 or miR-9* was always higher than 200 fold, while levels in cells transfected with a scrambled control siRNA did only show mild changes (Fig. 3.16A, B; miR-9: 0.77 ± 0.25 fold; miR-9*: 0.96 ± 0.03 fold). Transfection of each miRNA individually increased the number of

differentiated lt-NES cells. Compared to 2.89 ± 0.11% of βIII tubulin-positive cells in mock control and 2.71 ± 0.04% in control transfected cultures, transfection of miR-9 mimic raised the percentage to 5.13 ± 0.10% (Fig. 3.16C, E). Similarly, transfection of miR-9* increased the percentage of βIII tubulin-positive cells to 4.49 ± 0.9% compared to 1.68 ± 0.34% in mock and 1.67 ± 0.41% in control cultures (Fig. 3.16D, E).

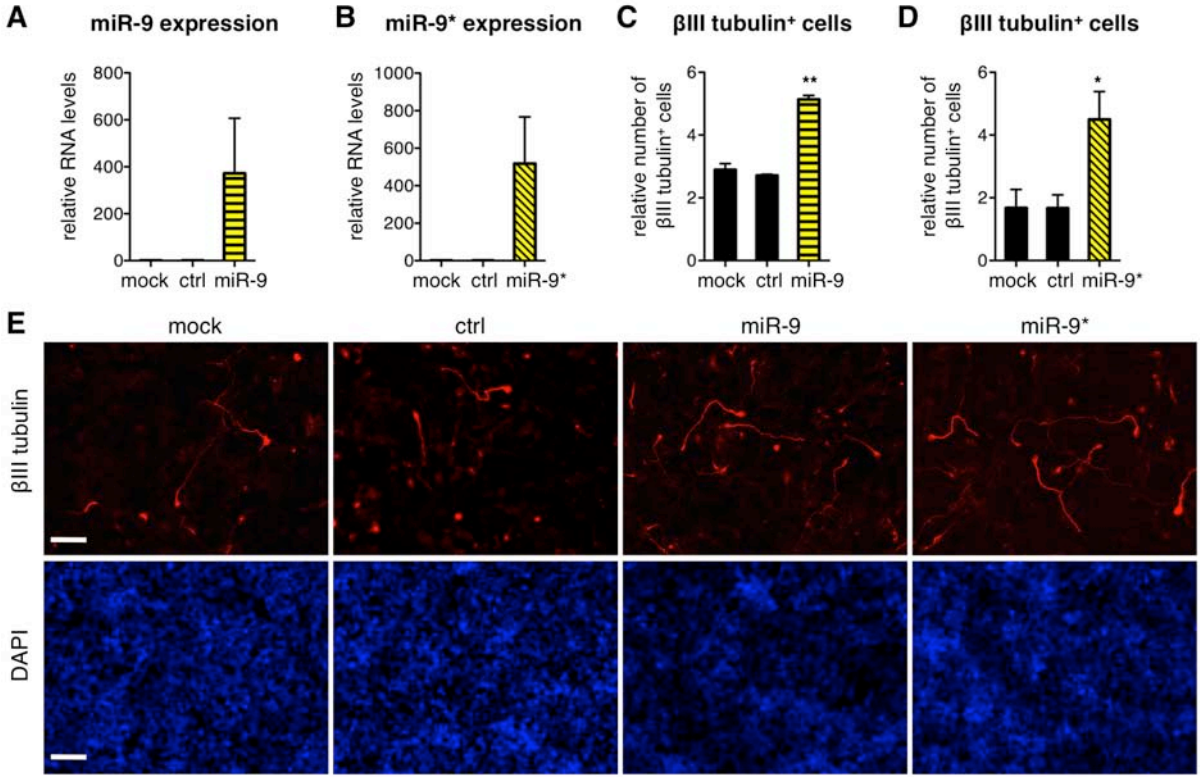

Fig. 3.16: Induced differentiation of lt-NES cells upon transfection of miR-9 or miR-9* mimics. **(A,B)** QRT-PCR analyses of mature miR-9 **(A)** and miR-9* **(B)** in lt-NES cells 48 hours after mimic transfection compared to scrambled control (ctrl) and mock-transfected cells (mock, equal to 1). Data are normalized to miR-16 reference levels and presented as average changes + SEM (n = 3). **(C-E)** Quantification of the percentage of βIII tubulin-positive cells **(C, D)** and corresponding immunostainings **(E)** in mock-transfected lt-NES cells and lt-NES cells transfected with scrambled control or mimic of miR-9 **(C)** or miR-9* **(D)** after 4 days under self-renewing conditions. Data are shown as percentage of total cell number and presented as mean + SEM (n = 3). Students t-test p-values: *, $p \leq 0.05$; **, $p \leq 0.01$. DAPI labels nuclei. Scale bars = 100 μm.

Interestingly, the rate of BrdU incorporation in lt-NES cell cultures was unaffected by miR-9 mimic transfection (Fig. 3.17A, C; un: 44.43 ± 2.64%; ctrl: 42.94 ± 3.32%; miR-9: 42.62 ± 3.36%), whereas it was reduced upon miR-9* mimic transfection to 43.02 ± 2.25% compared to 50.95 ± 0.99% in untreated and 50.40 ± 0.86% in ctrl cultures (Fig. 3.17B, C). This slight impairment of BrdU incorporation was comparable to the

one previously shown to be induced by ectopic expression of pre-miR-9/9* (Fig. 3.3B, C).

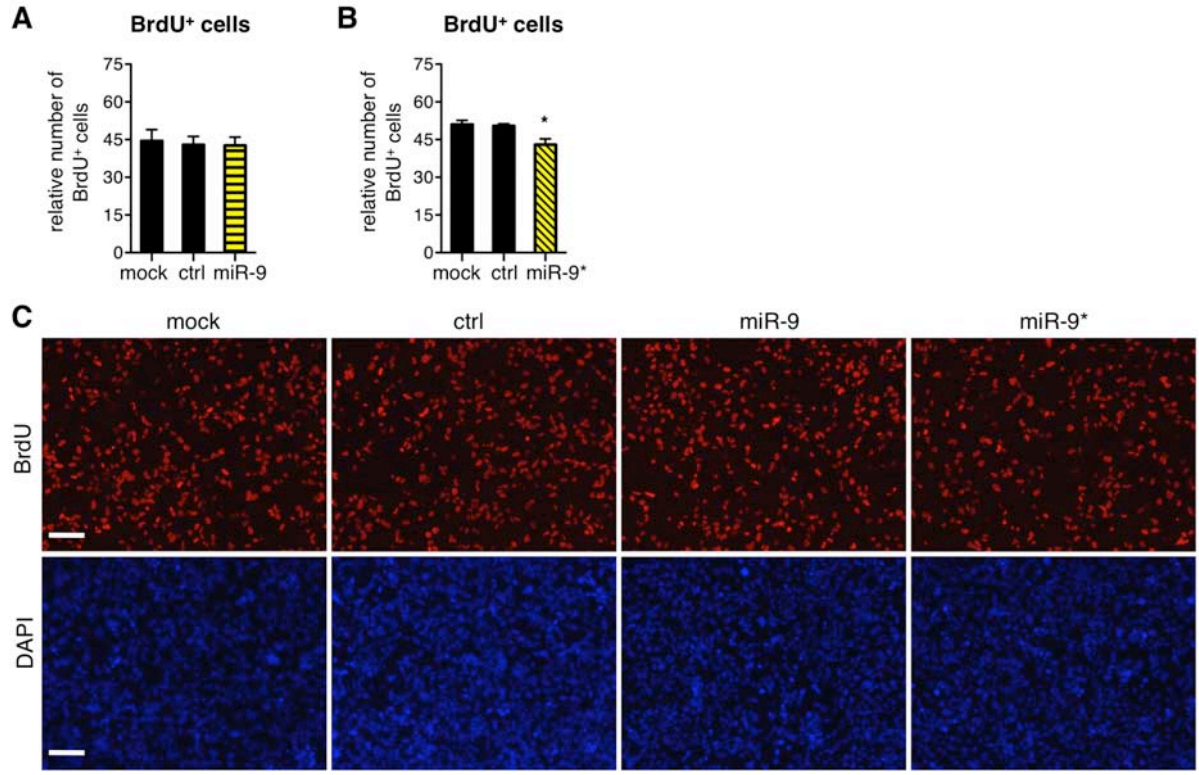

Fig. 3.17: BrdU incorporation rate of lt-NES cells transfected with mimics of miR-9 or miR-9*. Quantification **(A, B)** and corresponding immunostainings **(C)** of BrdU-positive cells in mock-transfected lt-NES cells (mock) and lt-NES cells transfected with scrambled control (ctrl) or mimics of miR-9 **(A)** or miR-9* **(B)** after 2 days under self-renewing conditions. Data are shown as percentage of total cell number and presented as mean + SEM (n = 3). Students t-test p-value: *, $p \leq 0.05$. DAPI labels nuclei. Scale bars = 100 μm.

Remarkably, a comparison of the targets predicted for miR-9 and miR-9* revealed a very small overlap. Only 42 predicted targets out of 855 for miR-9 and 648 for miR-9* were common to the two miRNAs (Fig. 3.18) suggesting that the functions of miR-9 and miR-9* could be exerted through different pathways.

Some of the genes previously shown to be targeted by miR-9/9* overexpression in *section 3.3* were further analyzed in an attempt to assess which of the two miRNAs is responsible for their downregulation. In addition, mRNA levels of the predicted miR-9* target SOX2 were assessed (Fig. 3.18B). SOX2 is known to be important for neural stem cell maintenance (as reviewed in [104]) and has been shown to be regulated by miR-9* in glioblastoma cells [105]. In lt-NES cells, SOX2 levels are down-regulated to 0.59 ± 0.12 fold upon ectopic overexpression of pre-miR-9/9* compared to GFP overexpressing cultures (Fig. 3.18C).

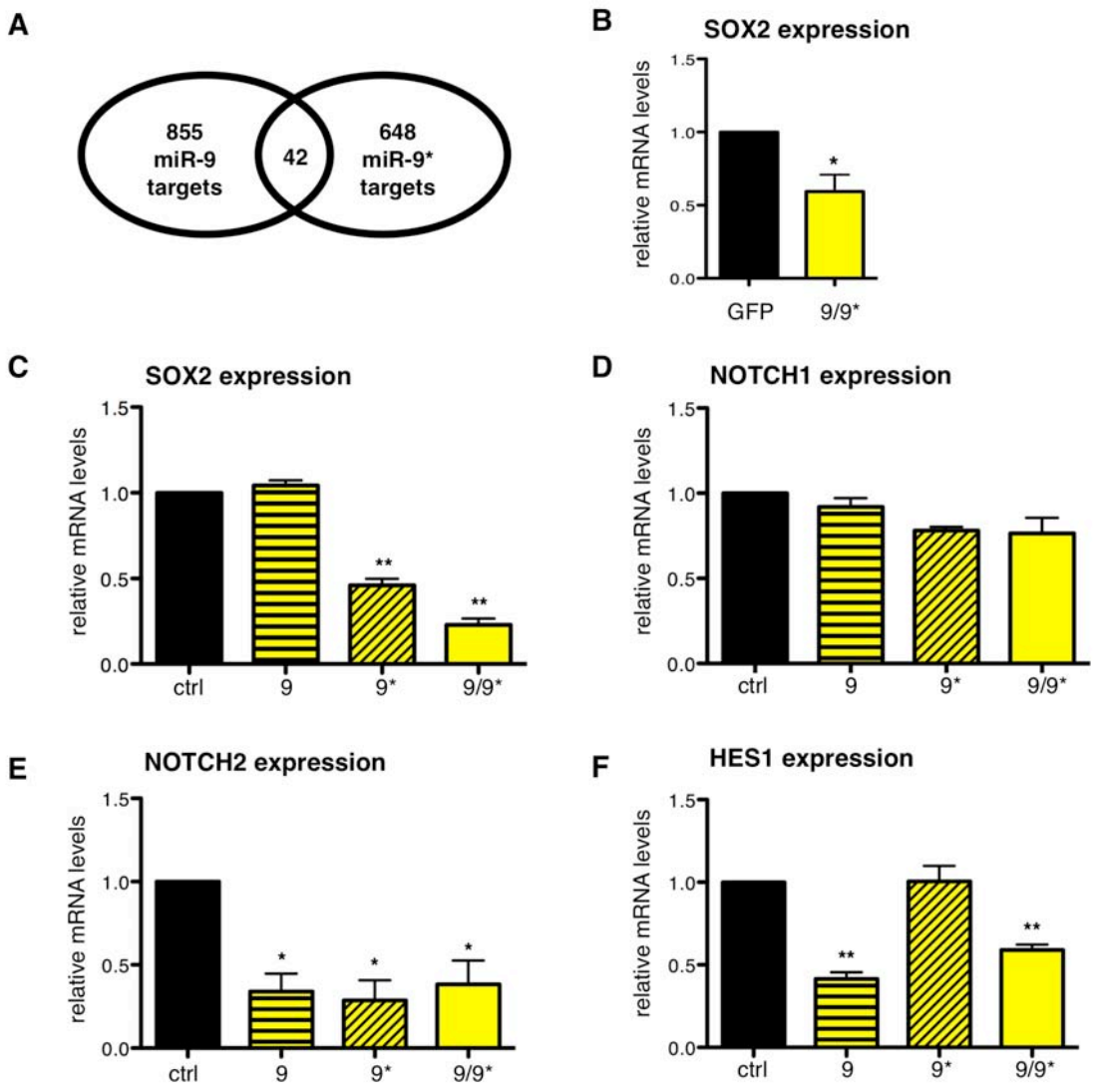

Fig. 3.18: Analysis of SOX2, NOTCH1, NOTCH2 and HES1 mRNA levels upon transfection of miR-9 and miR-9* mimics (A) Venn diagram of the target predictions for miR-9 and miR-9* based on a list of targets annotated using the miRWALK algorithm [100]. **(B)** QRT-PCR analysis of SOX2 mRNA levels in lt-NES cells transduced with Tight-miR-9/9* (9/9*) relative to expression in lt-NES cells transduced with Tight-GFP (equal to 1; n= 3). **(C-F)** QRT-PCR analyses of SOX2 **(C),** NOTCH1 **(D)**, NOTCH2 **(E)** and HES1 **(F)** transcript levels in l3 hESC derived lt-NES cells transfected with synthetic mimics for miR-9 (9), miR-9* (9*) or both (9/9*) compared to cells transfected with a small scrambled RNA (ctrl, equal to 1; n=3). Data are normalized to 18S rRNA reference levels and presented as average changes + SEM (Students t-test p-values: *, $p \leq 0.05$; **, $p \leq 0.01$).

For individual modulation of the two miRNAs, l3 hESC derived lt-NES cells were transfected with mimics for miR-9, miR-9* or both or a scrambled control every other day. After 4 days under self-renewing conditions, mRNA levels of SOX2, NOTCH1, NOTCH2 and HES1 were assessed. Similarly to ectopic overexpression of pre-miR-9/9*, simultaneous transfection of miR-9 and miR-9* mimics significantly reduced the mRNA levels of SOX2 to 0.23 ± 0.04 fold (Fig. 3.18C). Interestingly, transfection of miR-9 mimic alone did not regulate SOX2 significantly, while the transfection of miR-

9* mimic induced a significant reduction of SOX2 levels to 0.46 ± 0.04 fold (Fig. 3.18C, miR-9: 1,04 ± 0.03 fold). In turn, HES1 was regulated by miR-9 but not miR-9* (Fig. 3.18F, miR-9: 0.41 ± 0.04 fold; miR-9*: 1.01 ± 0.10 fold; miR-9/9*: 0.59 ± 0.03 fold), while NOTCH2 was regulated by both miRNAs alone and in combination (Fig. 3.18E, miR-9: 0.34 ± 0.10 fold; miR-9*: 0.29 ± 0.12 fold; miR-9/9*: 0.38 ± 0.14 fold). As expected from the previous data on miR-9/9* overexpression, NOTCH1 mRNA was not regulated significantly by miR-9 or miR-9* (Fig. 3.18D; NOTCH1: miR-9: 0.92 ± 0.05 fold; miR-9*: 0.78 ± 0.02 fold; miR-9/9*: 0.76 ± 0.09 fold). These data are in line with the binding sites for the individual miRNAs presented in Tab.3.2. The 3´UTR of NOTCH2 harbors binding sites for both miR-9 and miR-9*, while the HES1 is only predicted to be targeted by miR-9 and SOX2 only by miR-9*.

The phenotypes caused by individual modulation of miR-9 and miR-9* suggest that both miRNAs regulate differentiation by targeting the Notch signaling pathway and that, in addition, miR-9* affects lt-NES cell maintenance by targeting SOX2.

3.9 Analysis of miR-7, miR-128 and miR-130b in lt-NES cell self-renewal and differentiation

In order to identify additional miRNAs affecting proliferation and differentiation of lt-NES cells, other candidates were picked from group 1 (miRNAs up-regulated in lt-NES cells and upon induction of neuronal differentiation) described in the initial miRNA expression profiling [68]. For validation of the profiling data, qRT-PCR analyses were carried out on lt-NES cells and their differentiated progeny (Fig. 3.19A-C).

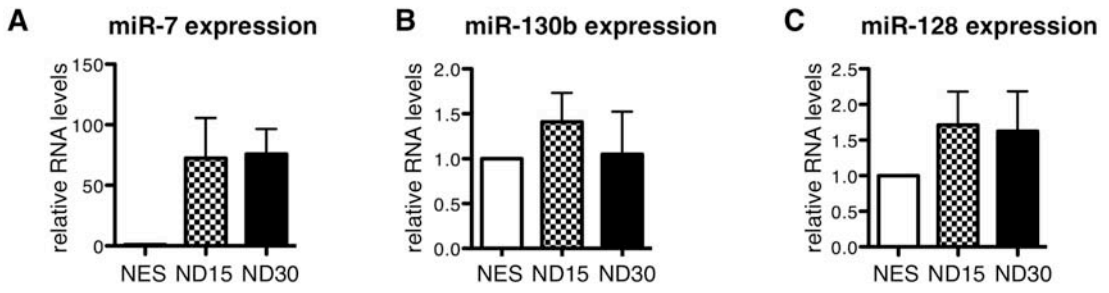

Fig. 3.19: Endogenous expression of miR-7, miR-130b and miR-128 in proliferating and differentiating lt-NES cells. QRT-PCR analyses showing relative expression levels of mature miR-7 **(A)**, miR-130b **(B)**, and miR-128 **(C)** in lt-NES cultures differentiated for 15 days (ND15) and 30 days (ND30) compared to self-renewing lt-NES cells (NES, equal to 1). Data are normalized to miR-16 reference levels and presented as average changes + SEM (n = 3).

In contrast to the miRNA expression profiling data, none of the three miRNAs analyzed was up-regulated significantly. While levels of miR-128 (Fig. 3.19B; ND15: 1.71 ± 0.47 fold; ND30: 1.62 ± 0.56 fold) and miR-130b (Fig. 3.19C; ND15: 1.41 ± 0.32 fold; ND30: 1.05 ± 0.47 fold) did not change, miR-7 expression increased but its expression levels were highly variable (Fig. 3.19A; ND15: 72.29 ± 33.30 fold; ND30: 75.79 ± 20.76 fold).

In the human genome, miR-7 is expressed from three loci, miR-128 from two loci and miR-130b from one locus (Tab.3.3). Like the loci coding for miR-9/9*, the two genomic loci for miR-128 produce the same miRNA species. In contrast, the miRNAs produced from the miR-7 loci differ. Pri-miR-7_1 and pri-miR-7_2 do not only encode miR-7 but also specific miRNAs produced from the passenger strand called miR-7-1* and miR-7-2* (Tab.3.3). Therefore, the transcription of the genomic loci coding for miR-7 was analyzed in lt-NES cells to explore which miRNA species are expressed.

Table 3.3: Genomic loci from which miR-7, miR-128 and miR-130b are expressed in human cells.

Locus name	Mature miRNAs derived	Exact genomic location	Clustered miRNAs
7_1	miR-7, miR-7_1*	Chr.9: 86584663-86584772 [-]	
7_2	miR-7, miR-7_2*	Chr.15: 89155056-89155165 [+]	miR-1179
7_3	miR-7	Chr.19: 4770682-4770791 [+]	
128_1	miR-128	Chr2: 136422967-136423048 [+]	
128_2	miR-128	Chr3: 35785968-35786051 [+]	
130b	miR-130b, miR-130b*	Chr.22: 22007593-22007674 [+]	miR-301b

In lt-NES cells, glioblastoma cell line U87 and cervical cancer cell line HeLa only expression of pri-miR-7_1 was detectable while all pri-miRNAs could be amplified from a mixed tissue positive control. In human fetal brain, expression of pri-miR-7_3 was also detected but at a lower level (Fig. 3.20).

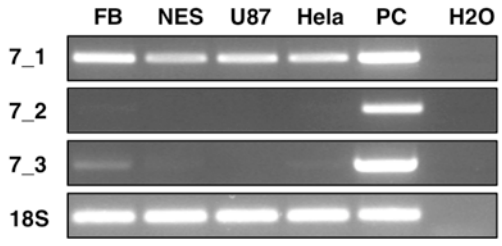

Fig. 3.20: Pri-miR-7_1 is the only pri-form of miR-7 expressed in lt-NES cells.
Representative gel images of RT-PCR for pri-miR-7_1 (7_1), pri-miR-7_2 (7_2), and pri-miR-7_3 (7_3) in proliferating lt-NES (NES), glioblastoma (U87) and HeLa cells as well as fetal brain RNA (FB) and a mixed tissue positive control (PC). 18S rRNA was used as loading control (n=3).

For further analysis, pre-miR-7_1 was chosen to assess the function of the miRNA species endogenously present in lt-NES cells. Pre-miR-7_1 (miR-7) as well as pre-miR-128_1 (miR-128) and pre-miR-130b (miR-130b) including flanking sequences were introduced into the LVTHM vector as described for pre-miR-9_1 (miR-9/9*; Fig. 3.2B). Lt-NES cells were stably transduced with the designed constructs to assess whether elevated levels of these miRNAs impact on their homeostasis. After 4 days under self-renewing conditions, overexpression of miR-7 resulted in a 2.51 ± 0.67 fold increase of βIII tubulin-positive cells compared to lt-NES cultures transduced with LVTHM-ctrl, while overexpression of miR-128 and miR-130b resulted in a 1.81 ± 0.31 and 1.37 ± 0.30 fold change, respectively (Fig. 3.21A). Furthermore, relative BrdU incorporation was not affected significantly by any of these three overexpressed miRNAs (Fig. 3.21B; ctrl equal to 1; miR-9/9*: 0.81 ± 0.01 fold; miR-7: 1.24 ± 0.08 fold; miR-128: 0.84 ± 0.12 fold; miR-130b: 1.05 ± 0.09 fold).

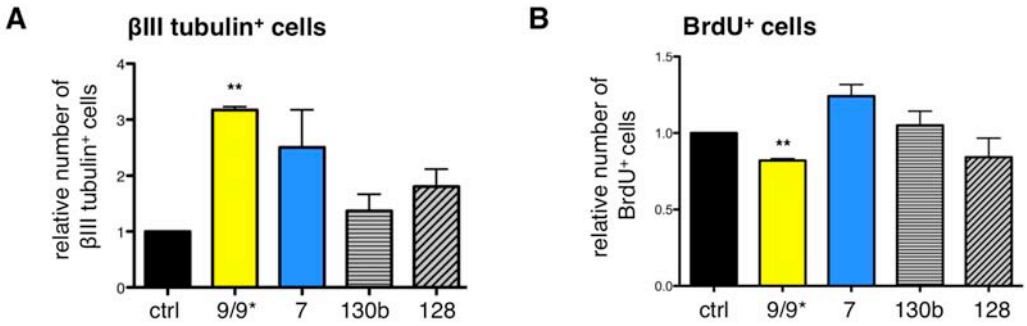

Fig. 3.21: Impact of miR-7, miR-128 and miR-130b overexpression on lt-NES cell proliferation and differentiation. Quantification of the relative number of βIII tubulin-positive **(A)** and BrdU-positive **(B)** cells in lt-NES cultures after 4 **(A)** or 2 **(B)** days under self-renewing conditions. Cells transduced with LVTHM-miR-9/9* (9/9*), LVTHM-miR-7 (7), LVTHM-miR-128 (128) or LVTHM-miR-130b (130b) are compared to lt-NES cells transduced with LVTHM-ctrl (ctrl, equal to 1). Data are presented as mean + SEM (n= 3; Students t-test p-value: **, $p \leq 0.01$).

Under proliferating conditions none of the three candidate miRNAs selected impacted on lt-NES cell maintenance or differentiation. However, miR-7 was, due to its high levels in differentiated lt-NES cells, chosen to assess putative other roles in neural stem cell differentiation.

3.10 Assessment of candidate targets of miR-7 and miR-9/9*

Comparison of target prediction analyses for miR-9/9* and miR-7 revealed that NOTCH2 and HES 1, which are targeted by miR-9/9*, as well as NOTCH3 harbor

binding sites for miR-7 (Fig. 3.22A). In order to analyze if miR-7 impacts on Notch signaling, the genomic pre-miR-7_1 and its flanking sequences were cloned into the pTight vector for conditional overexpression as described for pre-miR-9_1 (Fig. 3.5A). Robust overexpression of miR-9/9* and miR-7 was detected in lt-NES cells transduced with Tight-miR-9/9* (9/9*) and Tight-miR-7 (7) compared to Tight-GFP as control after 4 days of doxycycline treatment under self-renewing conditions (Fig. 3.22B; GFP, equal to 1; 9/9*: 66.01 ± 34.09 fold; 7: 268.69 ± 39.61 fold).

The mRNA levels of potential targets NOTCH2, HES1 and NOTCH3 as well as NOTCH1 and HEY2 were assessed by qRT-PCR in RNA samples of lt-NES cells overexpressing miR-9/9*, miR-7 or GFP.

A

	miR-9	miR-9*	miR-7
NOTCH1	1	0	0
NOTCH2	3	2	3
NOTCH3	0	0	3
HES1	2	0	1
HEY2	1	2	0

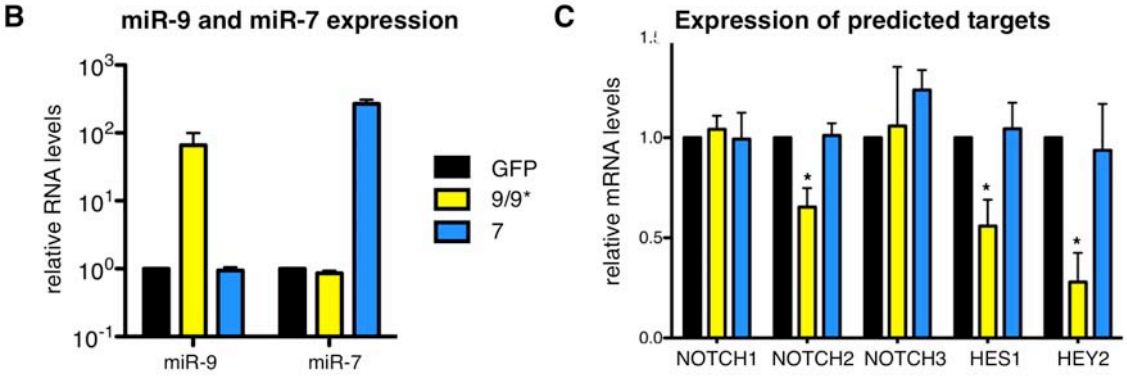

Fig. 3.22: Analysis of predicted targets within the Notch signaling cascade upon miR-7 and miR-9/9* overexpression. (A) Target prediction for members of the Notch pathway. The three right columns present the number of algorithms predicting binding of miR-9, miR-9* or miR-7 to the 3´UTRs of the genes indicated. The analysis was conducted using the miRWALK algorithm [100]. **(B)** QRT-PCR analyses of the expression levels of miR-9 and miR-7 in lt-NES cells transduced with pTight-9/9* (9/9*) or pTight-7 (7) compared to lt-NES cells transduced with pTight-GFP (GFP, equal to 1). Data are normalized to RnuA5 snRNA reference levels. **(C)** QRT-PCR analyses of transcript levels of predicted targets within the Notch signaling pathway in lt-NES cells transduced with pTight-9/9* (9/9*) or pTight-7 (7) compared to lt-NES cells transduced with pTight-GFP (GFP, equal to 1). Data are normalized to 18S rRNA reference levels and presented as average changes + SEM relative to expression in lt-NES cells overexpressing GFP (equal to 1; n= 3; Students t-test p-value: *, $p \leq 0.05$).

Regulation by miR-7 could not be identified for any of these predicted targets (Fig. 3.22C; NOTCH1: 0.99 ± 0.13 fold; NOTCH2: 1.01 ± 0.06 fold; NOTCH3: 1.23 ± 0.10

fold; HES1: 1.04 ± 0.13 fold; HEY2: 0.94 ± 0.23 fold). However, the data confirmed the regulation of NOTCH2, HES1 and HEY2 but not NOTCH1 and NOTCH3 mRNA by miR-9/9* (Fig. 3.22C; NOTCH1: 1.04 ± 0.07 fold; NOTCH2: 0.65 ± 0.09 fold; NOTCH3: 1.06 ± 0.30 fold; HES1: 0.56 ± 0.13 fold; HEY2: 0.28 ± 0.15 fold). As miR-7 did not impact on Notch signaling, additional potential targets were identified based on target prediction analyses and information from previous studies [66, 86, 105-107]. Among the genes with binding sites for miR-9, miR-9* and miR-7 important determinants of stem cell maintenance like Sirtuin1 (SIRT1) and the human homologues of drosophila lin-28 (LIN28A, LIN28B) as well neural stem cell markers SOX2, paired box 6 (PAX6) and NESTIN could be found (Fig. 3.23A).

SIRT1 is a member of the Sirtuin family, which is highly expressed in murine ESCs, subsequently down-regulated during differentiation and up-regulated during reprogramming of mouse embryonic fibroblasts into induced pluripotent stem cells [106]. This expression patterns suggest a role for SIRT1 in the maintenance of ESC stemness. The regulation of SIRT1 levels was shown to be mainly post-transcriptional and carried out by several miRNAs, including miR-9 in mouse [106] and human [77]. Relative levels of SIRT1 were decreased in lt-NES cells upon miR-9/9* (0.61 ± 0.12 fold) but not miR-7 overexpression (1.03 ± 0.19 fold) compared to overexpression of GFP (equal to 1, Fig. 3.23B).

Like SIRT1, both LIN28A and LIN28B are highly expressed in ESCs and their levels decrease with progressing differentiation of several tissues (reviewed in [108]). In mouse ES cells and human cancer cell lines, LIN28 was found targeted by miR-9 and miR-125 [107]. Overexpression of miR-9/9* reduced mRNA levels of both LIN28A and LIN28B significantly in lt-NES cells (LIN28A: 0.72 ± 0.05 fold; LIN28B: 0.59 ± 0.08 fold; Fig. 3.23B). Again, miR-7 overexpression did not impact on mRNA levels (LIN28A: 1.65 ± 0.45 fold; LIN28B: 1.29 ± 0.13 fold; Fig. 3.23B).

In addition, NESTIN, another neural stem cell marker, harbors a miR-9 binding site in its 3´UTR as well. NESTIN is important for the survival and self-renewal of neuronal stem cells [109, 110]. However, neither miR-9/9* (1.30 ± 0.27 fold) nor miR-7 (1.21 ± 0.36 fold) changed NESTIN mRNA levels significantly (Fig. 3.23B). NESTIN interacts with PAX6 to prevent precocious neuronal differentiation and maintain the progenitor pool (reviewed in [111]). The PAX6 3´UTR is predicted to be bound by miR-9/9* as well as miR-7 (Fig. 3.23A). Additionally, studies in mouse indicated that levels of

PAX6 are regulated by both miR-9/9* and miR-7 [66, 86]. However, neither miRNA induced a significant change of its mRNA levels in lt-NES cells (miR-9/9*: 0.84 ± 0.18 fold; miR-7: 1.33 ± 0.30 fold; Fig. 3.23B).

A

	miR-9	miR-9*	miR-7
SIRT1	5	1	2
LIN28A	4	1	1
LIN28B	5	0	0
NESTIN	1	0	0
PAX6	1	1	3

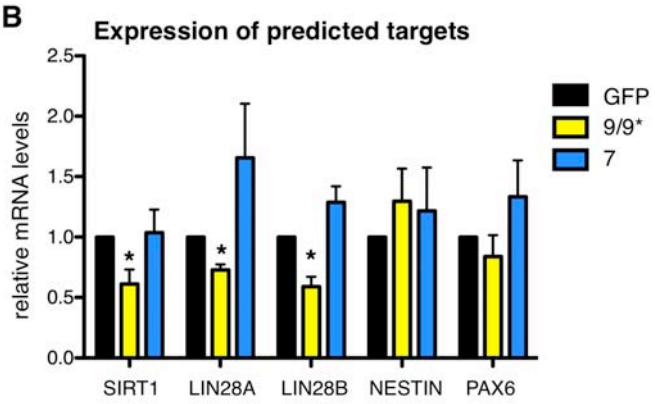

Fig. 3.23: Impact of miR-9/9* and miR-7 overexpression on predicted targets associated with neural stem cell proliferation and differentiation. (A) Target prediction for determinants affecting proliferation and differentiation. The three right columns present the number of algorithms predicting binding of miR-9 or miR-9* to the 3´UTRs of the genes indicated. The analysis was done using the miRWALK algorithm [100]. **(B)** QRT-PCR analyses of transcript levels of predicted targets in lt-NES cells transduced with pTight-9/9* (9/9*) or pTight-7 (7) compared to lt-NES cells transduced with pTight-GFP (GFP, equal to 1). Data were normalized to 18S rRNA reference levels. All qRT-PCR data are presented as average changes + SEM relative to expression in lt-NES cells overexpressing GFP (equal to 1; n= 3; Students t-test p-value: *, $p \leq 0.05$).

Although target sites were predicted in the 3´UTRs of SIRT1, PAX6 and LIN28A, overexpression of miR-7 did not induce a significant change in any of the mRNA levels analyzed. However, translational silencing of these mRNAs is still to be accessed by analyses of the resulting protein levels. In contrast, SIRT1, LIN28A and LIN28B mRNA levels are affected by miR-9/9*. Downregulation of these genes might add to the effects of Notch signaling and SOX2 to cause the reduced self-renewal and enhanced differentiation of lt-NES cells observed upon miR-9/9* overexpression. Future studies have to address whether the identified targets are directly modulated by miR-9, miR-9* or both and explore the impact of the induced reduction of SIRT1, LIN28A and LIN28B levels on human neural stem cell properties.

3.11 Assessment of the impact of miR-9/9* and miR-7 on lt-NES cell-derived dopaminergic neurons

Elevated levels of miR-9/9* were shown to significantly promote differentiation of lt-NES cells under self-renewing conditions (Fig. 3.4). In line with this finding,

endogenous expression of miR-9 and miR-9* was dramatically up-regulated in lt-NES cells after 15 days under differentiating conditions (Fig. 3.1B, C). To explore whether, in addition to an overall enhanced differentiation, also the fate choice of the generated neurons is affected, long-term overexpression of miR-9/9* under differentiating conditions was further assessed to shed light on its impact on neuron subtype specification. For that purpose, I3 hESC derived lt-NES cells were transduced with the LVTHM vector carrying a GFP cassette as optical marker and pre-miR-9/9* or a scrambled control hairpin (ctrl; described in Fig. 3.2.B). To minimize the innate variability of cell culture, an in-dish control was established by mixing lt-NES cells constitutively overexpressing both GFP and miR-9/9* or GFP and control at a ratio of 1:1 with untransduced lt-NES cells. These mixtures of GFP-labeled and wildtype lt-NES cells were cultured for 15 days under differentiating conditions. In line with the data gathered in the short-term studies, at day 15 of differentiation the number of βIII tubulin-positive cells was increased 1.76 ± 0.32 fold upon overexpression of miR-9/9*, compared to overexpression of a scrambled control (Fig. 3.24A, B).

In addition to the general differentiation, the number of the dopaminergic neurons generated in these cultures was assessed by staining for tyrosin hydroxylase (TH) – a rate-limiting enzyme catalyzing the synthesis of dopamine precursor L-DOPA (L-3,4-dihydroxyphenylalanine) [112]. Interestingly, although the overall number of neurons was increased, staining for the dopaminergic neuron marker (TH) was almost absent in the GFP positive population expressing miR-9/9*, while it could be detected in the co-cultured untransduced lt-NES cells.

Quantification of cell numbers revealed a significant difference in distribution of TH positivity between untransduced lt-NES cells (GFP negative) and those with elevated miR-9/9* levels (GFP positive). Only 0.53 ± 0.53% of overall TH-positive cells were also GFP positive, while 99.47 ± 0.53% of them were found in the GFP negative cell population (Fig. 3.24C, D). This indicates that overexpression of miR-9/9* impairs the generation of TH-positive cells, as corresponding control cultures did not show a significant difference in the distribution of TH positivity between cells overexpressing the control construct (GFP positive) and untransduced cells (Fig. 3.24C, D; TH^+ GFP^+ cells: 75.61 ± 13.68%; TH^+ GFP^- cells: 24.39 ± 13.68%).

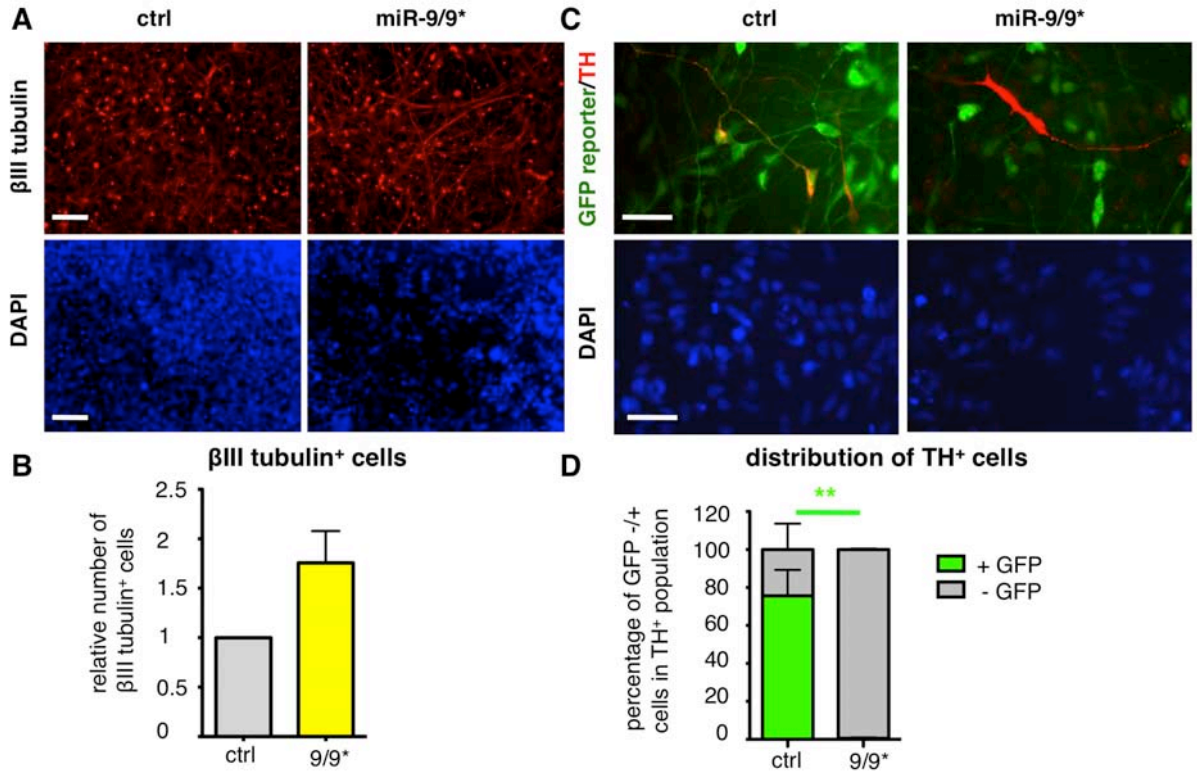

Fig. 3.24: Neuronal differentiation and generation of TH-positive neurons from lt-NES cells upon overexpression of miR-9/9*. (A) Representative immunostaining and quantification **(B)** of βIII tubulin in lt-NES cells transduced with LVTHM-GFP-9/9* (miR-9/9*) or LVTHM-GFP-ctrl (ctrl) after 15 days of differentiation. DAPI labels nuclei. Scale bars = 100 μm. Data are shown relative to ctrl transduced lt-NES cells + SEM (n=3). **(C)** Representative immunostaining and quantification **(D)** for TH [113] in lt-NES cells transduced with LVTHM-GFP-9/9* (miR-9/9*) or LVTHM-GFP-ctrl (ctrl) after 15 days of differentiation. DAPI labels nuclei. Scale bars = 100 μm. **(D)** Relative distribution of TH-positive neurons in mixed cultures of untreated lt-NES cells (gray) and lt-NES cells transduced with either miR-9/9* or scrambled control (green) + SEM (n=3; Students t-test p-value: **, p ≤0.01).

Similarly to miR-9/9*, miR-7, too, tends to be up-regulated in lt-NES cells after 15 days under differentiating conditions and its overexpression slightly increased the rate of lt-NES cell differentiation under self-renewing conditions. However, these data were too variable to be significant. In order to investigate whether miR-7 overexpression impacts on neuronal subtype specification, I3 hESCs derived lt-NES cells were transduced with the LVTHM vector carrying pre-miR-7_1 or a scrambled control hairpin (ctrl) as well as a puromycin resistance gene and assessed by immunostaining. Specifically, after antibiotic selection cultures enriched in transduced cells were differentiated for 15 days and subsequently stained for βIII tubulin and TH. The obtained results were similar to those for miR-9/9* overexpression (Fig. 3.25).

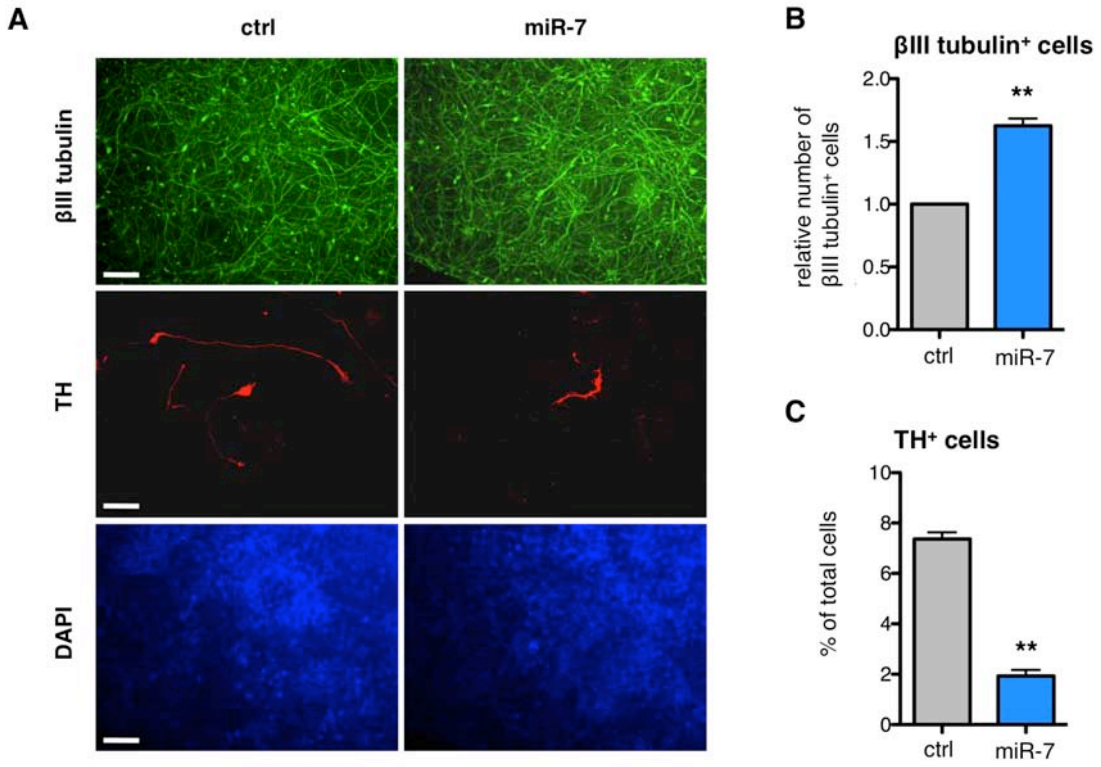

Fig. 3.25: Neuronal differentiation and generation of TH-positive neurons from lt-NES cells upon overexpression of miR-7. (A) Representative immunostainings for βIII tubulin (green) and TH [113] in lt-NES cells transduced with LVTHM-miR-7 (miR-7) or LVTHM-ctrl (ctrl) after 15 days of differentiation in medium devoid of growth factors. DAPI labels nuclei. Scale bars = 100 μm. **(B, C)** Quantification of βIII tubulin-positive (B) and TH-positive (C) cells in the immunostainings described. Data are shown relative to ctrl transduced lt-NES cells + SEM (n=3). Students t-test p-value: **, p ≤0.01.

In cultures overexpressing miR-7, the number of βIII tubulin-positive cells increased significantly by 1.63 ± 0.06 fold in comparison to control transduced cultures (Fig. 3.25B), while the percentage of TH-positive neurons was significantly decreased from 7.37 ± 0.27% of overall cells (in ctrl cultures) down to 1.93 ± 0.24% (Fig. 3.25C).

Therefore, both miR-9/9* and miR-7 enhanced overall differentiation but impaired the generation of TH-positive neurons from lt-NES cells.

3.12 MiR-9/9* and miR-7 target determinants of dopaminergic lineage development

In order to identify genes regulated by miR-9/9* and miR-7 that may underlie their impact on dopaminergic lineage choice, the miRWALK algorithm [100] was used to predict potential targets. Putative binding sites for miR-9/9* and miR-7 were found in

the 3´UTRs of the dopaminergic determinants Engrailed 2 (EN2), FOXA2 and LMX1A (Tab. 3.4).

	miR-9	miR-9*	miR-7
EN2	3	0	3
FOXA2	0	2	2
LMX1A	4	1	2

Table 3.4: Target prediction for dopaminergic determinants. The three right columns present the number of algorithms predicting binding of miR-9, miR-9* or miR-7 to the 3´UTRs of the genes indicated. Analysis was done using the miRWALK algorithm [100].

First, a suitable model to monitor mRNA levels of FOXA2, LMX1A and EN2 had to be identified as lt-NES cells may not express detectable levels of transcription factors involved in dopaminergic lineage choice. In addition to lt-NES cells, liver cell line HepG2, which is known to express FOXA2 [114], and, as positive control, commercially available human fetal brain RNA (FB) were used. While LMX1A could not be amplified from any sample analyzed, EN2 was expressed in proliferating lt-NES cells and at low levels in FB and HepG2 cells. FOXA2 mRNA was detectable in HepG2 cells but not lt-NES cells and very weakly expressed in FB (Fig. 3.26A).

When looking at transcript levels of EN2 in lt-NES cells overexpressing miR-9/9*, miR-7 or GFP (Fig. 3.8C), a significant down-regulation (0.58 ± 0.13 fold) was observed upon miR-9/9* overexpression compared to lt-NES cells overexpressing GFP, while miR-7 overexpression did not induce a significant change (1.07 ± 0.24 fold) (Fig. 3.26B). As FOXA2 was solely detectable in HepG2 cells (Fig. 3.26A) these cells were transduced with the Tight-GFP, Tight-miR-9/9* and Tight-miR-7 constructs. After 4 days of doxycycline treatment miR-9 expression was induced 5.67 ± 0.83 fold, miR-9* expression 93406.38 ± 9062.98 fold and miR-7 expression 1127.21 ± 96.87 fold, compared to cells overexpressing GFP (Fig. 3.26C). In these samples, FOXA2 mRNA expression was slightly down-regulated to 0.75 ± 0.16 fold upon overexpression of miR-9/9* and significantly reduced to 0.67 ± 0.07 fold by miR-7 overexpression, compared to cells overexpressing GFP (Fig. 3.26D). The changes observed were even stronger when looking at FOXA2 protein levels by Western blot analysis (Fig. 3.26E).

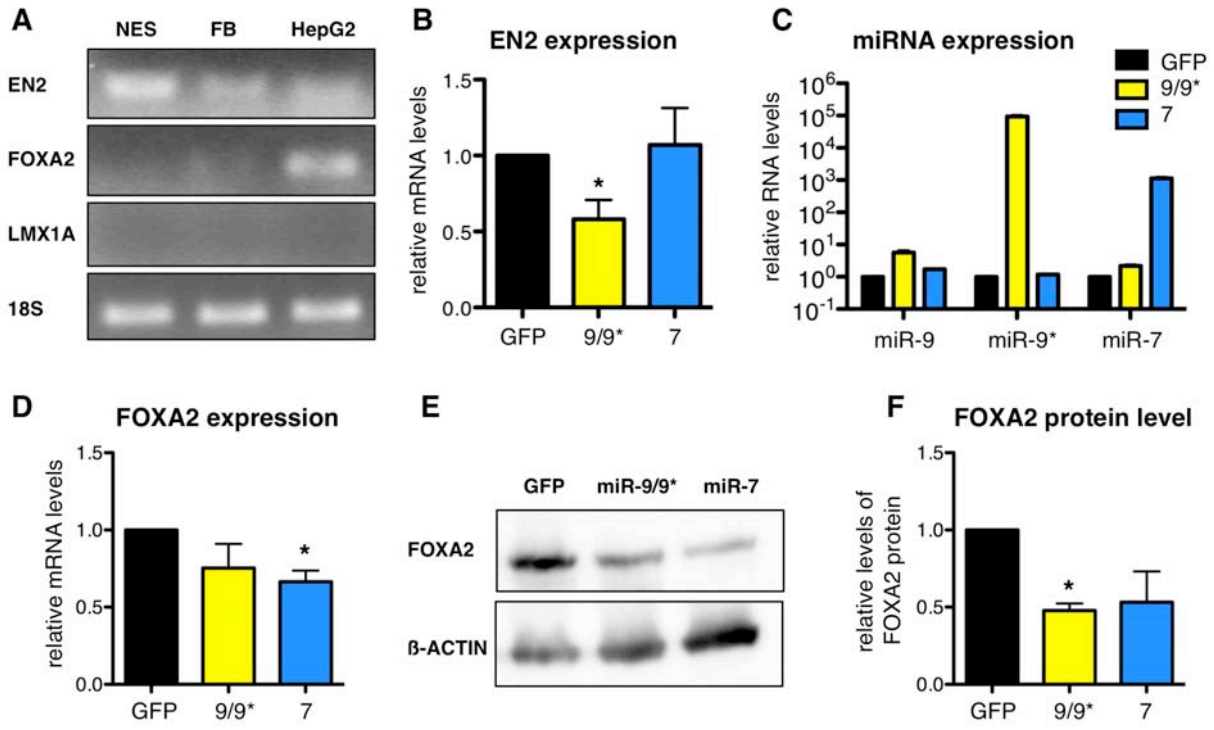

Fig. 3.26: Monitoring the impact of miR-9/9* and miR-7 overexpression on the dopaminergic determinants EN2 and FOXA2. (A) Representative gel images of RT-PCR analyses for FOXA2 and EN2 from proliferating lt-NES cells (NES), fetal brain RNA (FB) and liver cell line HepG2 (HepG2). 18S rRNA was used as loading control (n=3). **(B)** QRT-PCR analysis of EN2 transcript levels in lt-NES cells overexpressing miR-9/9* or miR-7 compared to GFP control (n=5). **(C)** QRT-PCR analysis monitoring induced expression of miR-9, miR-9* and miR-7 in HepG2 cells upon miR-9/9* or miR-7 overexpression, compared to GFP control. Data are normalized to snRNA RnuB5 reference levels and presented as average changes + SEM relative to expression in cells overexpressing GFP (equal to 1; n=3). **(D)** QRT-PCR analysis of FOXA2 transcript levels in the HepG2 cells decribed above (n=3). **(B+D)** Data are normalized to 18S rRNA reference levels and presented as average changes + SEM relative to expression in cells overexpressing GFP (equal to 1). **(E)** Representative Western blot analysis of FOXA2 in the HepG2 cells decribed above. β-ACTIN was used as loading control. **(F)** Quantification of FOXA2 protein expression from Western blot analysis. Data are shown as average changes + SEM relative to cells overexpressing GFP and normalized to β-ACTIN (n=3). **(B, D, F)** Students t-test p-value: *, $p \leq 0.05$.

Quantification of three independent blots revealed a significant reduction of FOXA2 protein to 0.48 ± 0.05 fold upon miR-9/9* overexpression and to 0.53 ± 0.20 fold upon miR-7 overexpression, compared to GFP overexpressing cultures (Fig. 3.26F).

These results on post-transcriptional regulation of FOXA2 and EN2 by miR-9/9* and miR-7 are in line with their antagonistic role in dopaminergic differentiation of lt-NES cells.

3.13 Analysis of miR-9/9* and miR-7 expression during the differentiation of human pluripotent stem cells towards the midbrain dopaminergic lineage

The overall yield of TH-positive neurons in differentiating It-NES cell cultures is rather low (Fig. 3.25C). In order to monitor endogenous expression of miR-9, miR-9* and miR-7 during dopaminergic specification and to further assess their impact on the generation of midbrain dopamine neurons, a different cell culture system specifically designed to enrich these medically relevant neurons was employed. It was recently shown that a high yield of midbrain dopaminergic neurons is achieved when pluripotent stem cells are patterned into floorplate precursors and then further differentiated into neurons. I3 hESCs and ILB-C-31F-R1 hiPSCs were used to implement a protocol described by *Kriks et al.* [89] which follows this line of differentiation. Expression levels of dopaminergic and neuronal determinants were analyzed at every other of the first 13 days of *in vitro* differentiation to monitor proper regionalization and maturation (Fig. 3.27A).

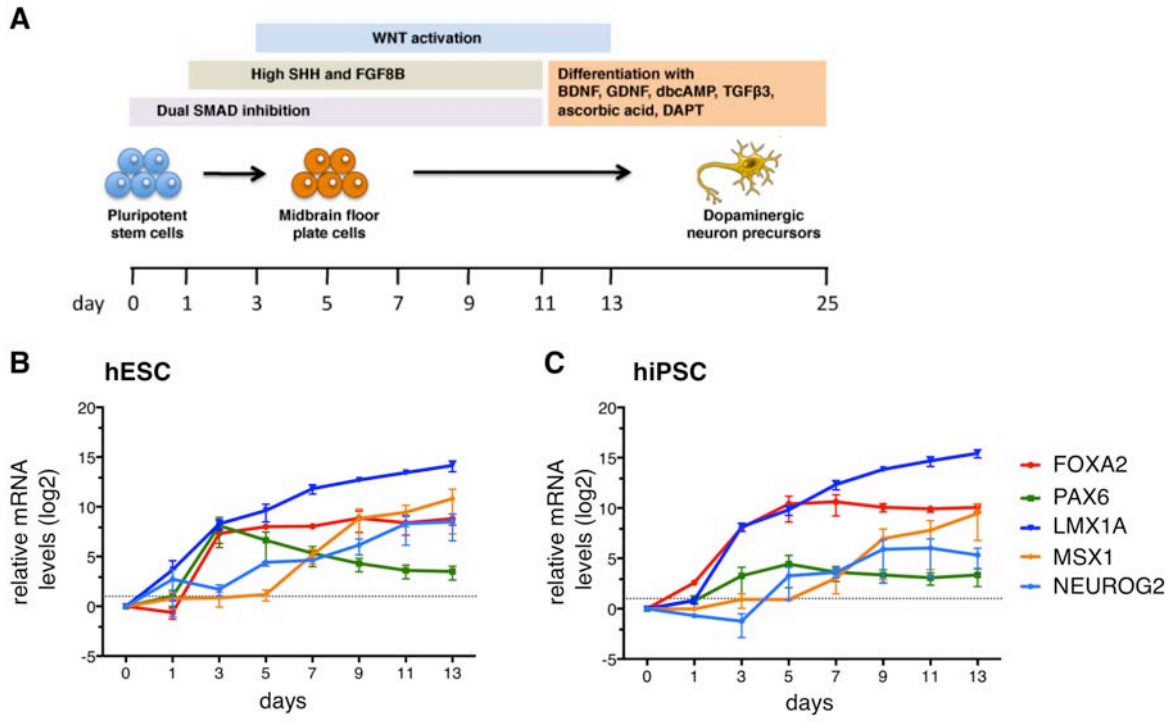

Fig. 3.27: Expression of dopaminergic determinants during the time course of midbrain dopamine neuron induction. (A) Scheme of the induction protocol according to *Kriks et al.* [89]. **(B, C)** QRT-PCR analysis of FOXA2 (red), LMX1A (blue), MSX1 (orange), PAX6 (green), and NEUROG2 (light blue) expression in I3 hESCs **(B)** and ILB-C-31F-R1 hiPSCs **(C)** during the time course of floorplate and dopaminergic precursor induction, compared to expression at day 0 (d0; equal to 1, n = 3). Data are normalized to 18S rRNA reference levels and presented as average changes ± SEM. Data obtained in cooperation with Laura Stappert and Beatrice Weykopf.

Already after 3 days of floor plate induction, qRT-PCR analyses confirmed the up-regulation of the dopaminergic transcription factors FOXA2 and LMX1A in both hESCs and hiPSCs (Fig. 3.27 B, C). Two days later, the expression of MSX1 (MSH homeobox protein 1) started to rise as well. The neural stem cell marker PAX6 and the neuronal marker NEUROG2 (Neurogenin 2) were up-regulated from day 3 on. However, while PAX6 levels remained relatively stable during the first 13 days of the differentiation paradigm, NEUROG2 expression showed a constant increase reflecting the differentiation of these neurogenic cultures (Fig. 3.27 B, C).

At day 25 of differentiation, cultures originating from I3 hESCs were chosen for immunofluorescence analysis and stained for the dopaminergic determinants FOXA2 and LMX1A, as well as for TH and βIII tubulin (Fig. 3.28). The majority of βIII tubulin-positive cells were found also positive for TH, FOXA2 and LMX1A (Fig. 3.28) as expected for dopamine neurons from the midbrain region [89].

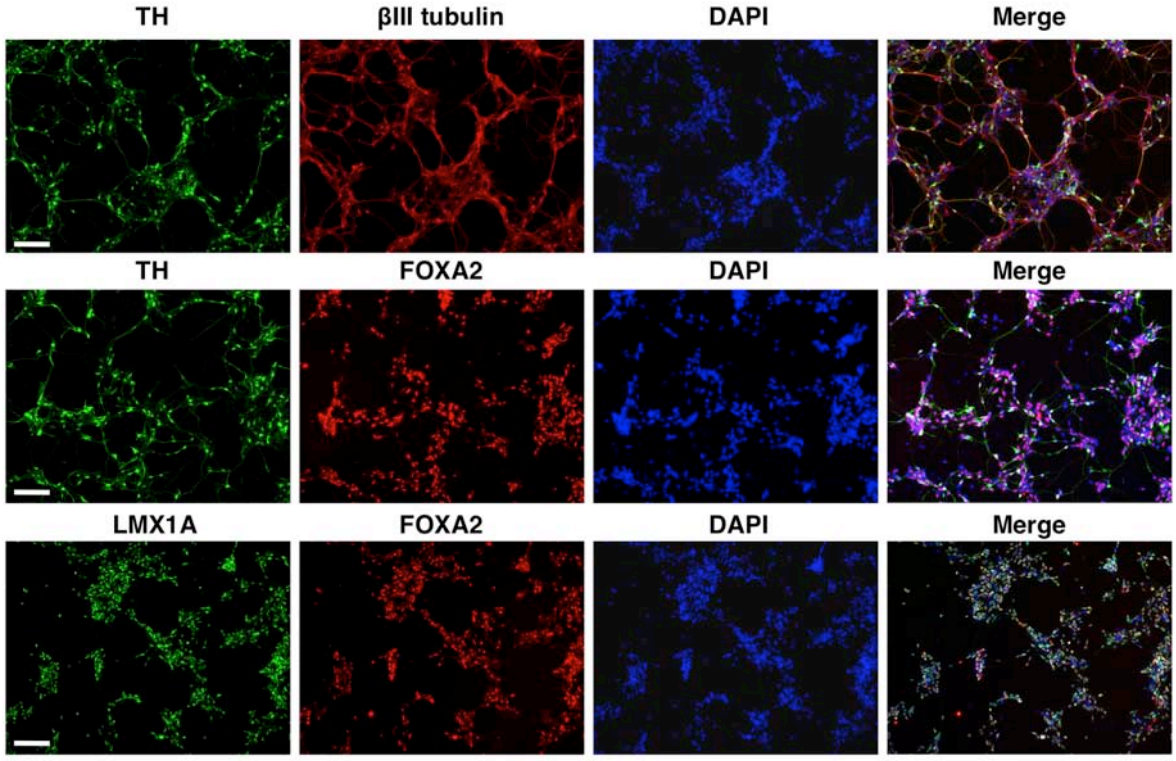

Fig. 3.28: Expression of dopaminergic markers after differentiation of hESC. Representative immunostainings for βIII tubulin, TH, FOXA2 and LMX1A at day 25 of I3 hESC differentiation according to the *Kriks et al.* protocol (n=3). DAPI labels nuclei. Scale bars = 100 μm. Data obtained in cooperation with Laura Stappert and Beatrice Weykopf.

Once the dopaminergic phenotype of the obtained neuronal cultures was confirmed on transcriptional and immunofluorescent levels, expression of miR-9, miR-9*, miR-7 and miR-133b – a miRNA shown to be expressed in dopaminergic neuron

progenitors [65] – were analyzed by qRT-PCR (Fig. 3.29). In contrast to miR-133b levels, that did not clearly change upon induction of a floorplate and later on a dopaminergic fate, levels of miR-9* and miR-7 were found to gradually decrease parallel to the floorplate induction as indicated by the mean expression of LMX1A (Fig. 3.29). MiR-9 expression slightly down-regulated as well; however, this effect was not as distinct (Fig. 3.29 C). Once neuronal differentiation was induced (day 11), levels of miR-7, miR-9 and miR-9* started to rise again, reminiscent of their expression profile in differentiating lt-NES cells.

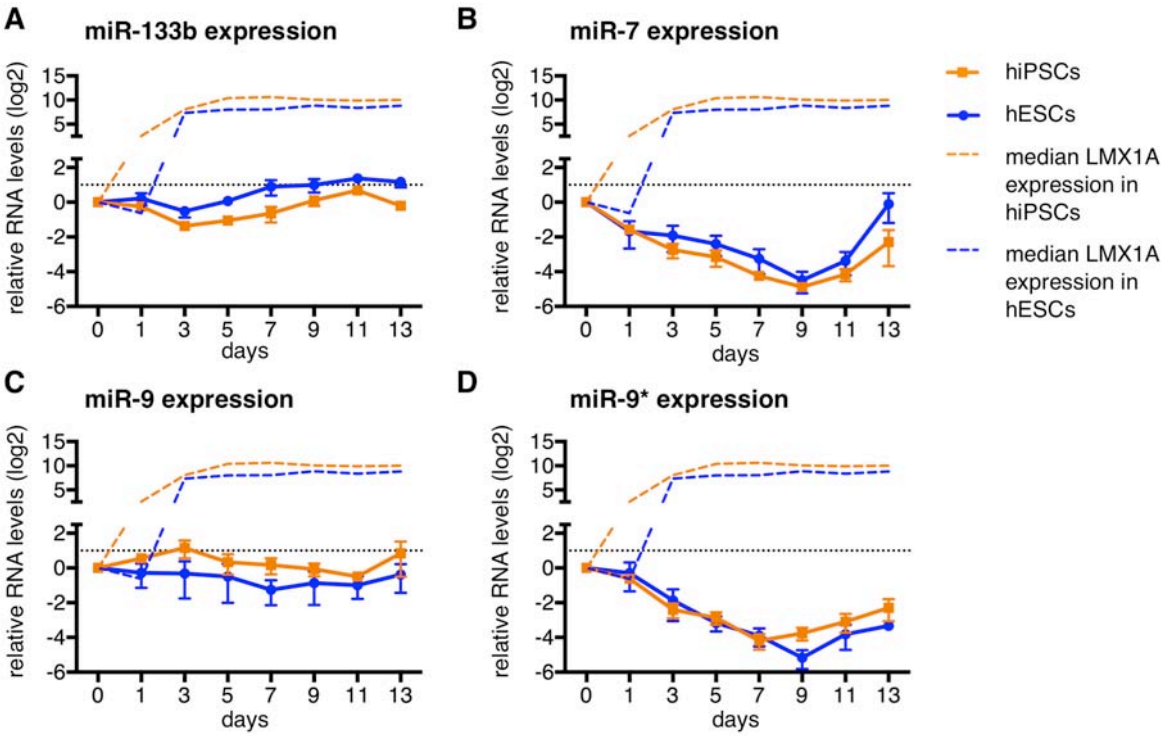

Fig. 3.29: Expression of selected miRNAs during the time course of dopamine neuron lineage induction. QRT-PCR analysis of miR-133b **(A)**, miR-7 **(B)**, miR-9 **(C)**, and miR-9* **(D)** expression levels during the time course of induction of floorplate precursor and dopaminergic progenitors from I3 hESCs and ILB-C-31F-R1 iPSCs compared to expression levels at day 0 of the induction protocol (d0; equal to 1, n=3). Data are normalized to RnuA5 snRNA reference levels and presented as average changes + SEM. Solid lines indicate the levels of miR expression and dashed lines the mean level of LMX1A expression (blue: I3 hESCs; orange: ILB-C-31F-R1 iPSCs). Data obtained in cooperation with Laura Stappert and Beatrice Weykopf.

Taken together, these data show that miR-9/9* and miR-7, which impair dopaminergic differentiation of lt-NES cells, are down-regulated during the induction of floor plate progenitors that later give rise to mesenchephalic dopaminergic neurons. The opposed expression pattern of these miRNAs (Fig. 3.29) and FOXA2 (Fig. 3.27) mRNA observed during the time course of the floor plate induction

protocol is in line with the data gathered in HepG2 cells indicating targeting of the FOXA2 mRNA by miR-9/9* and miR-7. Taken together, the data presented indicate an antagonistic role for miR-9/9* and miR-7 in the specification of dopaminergic fate that may – at least in part – be due to targeting of EN2 and FOXA2.

4. Discussion

In the last years, miRNAs emerged as potential new regulators in neuronal differentiation [53, 115, 116]. They are abundantly expressed in the nervous system, and nearly 50 percent of the known species can be detected in the human brain [117]. To analyze their impact on the human neural system a robust cell culture model is needed since access to primary human material is rather scarce. For this purpose, a homogeneous population of long-term self-renewing neuroepithelial-like stem cells from human ES (lt-NES) cells was employed in this study [7]. The maintenance and differentiation of these neural stem cells into distinct neuronal subtypes depends on highly orchestrated programs of developmental signals that have to be under tight spatial and temporal control. Knowledge on the impact of post-transcriptional regulation by specific miRNAs, like e.g. miR-9/9*, on human neural stem cell behavior is still rather limited. Therefore, the focus of this work was to analyze the role of miRNAs in the maintenance and differentiation of lt-NES cells.

4.1 Modulation of the switch from neural stem cell self-renewal to differentiation by specific miRNAs

The analysis of the expression pattern of a miRNA during a biological process like differentiation is a prerequisite for understanding its function. Although there are available data from other mammalian species like mouse [41], miRNA expression may differ among species. For instance, even though the sequence between *Drosophila* miR-9a and mammalian miR-9 is strongly conserved (reviewed in [71]), their transcriptional regulation differs. While miR-9 is strongly enriched in the mammalian brain (reviewed in [74]), *Drosophila* miR-9a only shows little expression in the nervous system of developing embryos and is highly expressed in ectodermal epithelial cells and in wing disc cells but not in sensory organ precursor cells [73, 118]. Therefore, this work is based on data from an expression profiling comparing levels of miRNAs in hESCs to derived neural stem cells and their differentiated progeny. Five candidate miRNAs up-regulated during this differentiation paradigm, namely miR-7, miR-9, miR-9*, miR-128, and miR-130b, were chosen for further analysis due to their expression pattern and an initial target prediction that revealed potential target genes involved in neural differentiation (data not shown). The increase detected for miR-7, miR-9, miR-9* and miR-128 in the screening resembled

their expression patterns during mouse brain development [41, 42], while expression of miR-130b was not addressed in these studies.

4.1.1 Dependence of miR-7, miR-128 and miR-130b action on spatial and temporal cell identity

Data on the role of the three selected candidate miRNAs (i.e. miR-7, miR-128, miR-130b) in the nervous system are rather scarce. The best-studied one is miR-7, which is expressed moderately in the human brain, while other organs only show sporadic expression [43]. The role of miR-7 in neuronal differentiation is not clear from the studies published so far. Data gathered in neuroblastoma cells suggested a down-regulation of miR-7 expression upon retinoic acid induced differentiation and a reduced neurite outgrowth upon miR-7 overexpression. However, the same study showed that in primary mouse cortical neurons miR-7 is up-regulated during differentiation [119]. Conversely and in line with miR-7 expression in neuronal differentiation of lt-NES cells, data gained from a run-through protocol for short-term differentiation of mouse ESCs did not show a significant regulation [119].

In lt-NES cells, miR-7 expression is mainly due to transcription of the 7_1 genomic locus, whose promoter is predicted to be bound by neural stem cell marker PAX6 [120]. Interestingly, data from the mouse forebrain and pancreas indicate that miR-7 directly targets Pax6 mRNA [66, 119] pointing to a potential feedback loop between miR-7 and PAX6. Although the miR-7 binding sites are conserved in human, PAX6 mRNA levels were not regulated by miR-7 in lt-NES cells. However, in the human system, miR-7 binding to the PAX6 mRNA may not induce degradation but translational silencing. Therefore, detail analyses of PAX6 protein levels as well as a 3´UTR luciferase assays are still to be done.

MiR-128 is highly expressed in the adult brain and enriched in murine neurons similar to well known neuronal miRNAs – like miR-124 and miR-137 [61]. In addition, it was reported to act on neural stem cell self-renewal by targeting Bmi1 [121]. A role for miR-7 and miR-128 in stem cell maintenance is also indicated by their significant downregulation in malignantly proliferating glioblastoma samples [102, 121]. However, there is little knowledge on their role and regulation during the development of the central nervous system. MiR-130b is even less studied in this context. Interestingly, miR-130b is down-regulated in various cancer cell types which might

point to a role in the regulation of proliferatory mechanisms [122-124]. Although the screening for miRNA expression in lt-NES cells and their differentiatied progeny [68] suggested an up-regulation of miR-7, miR-128 and miR-130b during differentiation, these changes could not be validated in our differentiation paradigm.

In addition, elevated levels of miR-7, miR-128 and miR-130b did not impact significantly on lt-NES cell self-renewal and spontaneous differentiation. This lack in regulation and impact of miR-7, miR-128 and miR-130b on lt-NES cells may be due to the developmental stage and regionalization these cells represent. The increase in miR-128 expression found during mouse development does not start before E18, while other brain-enriched miRNAs like miR-9 and miR-9* are already expressed at earlier time points [41]. This indicates a role for miR-128 at developmental stages later than the ones represented by lt-NES cells. The effects of miR-7 might depend on the temporal identity of the neural stem cells analyzed as well, as it was shown that – at least in the rat and human fetal cortex as well as mouse spinal cord – neural stem cells mainly depend on FGF signaling for their propagation at certain developmental stages [125-127]. MiR-7, on the other hand, was found to reduce the stemness of glioblastoma cells by targeting the EGF receptor (EGFR) and its down stream targets [102]. In *Drosophila*, miR-7 employs this regulation of EGF signaling to stimulate the differentiation of photoreceptors [128]. However, in neural stem cells miR-7 overexpression did not induce a reduced self-renewing capacity. Although an expression profiling showed that lt-NES cells express the EGFR on mRNA level [129], the functional relevance of EGF signaling in lt-NES cell maintenance is still to be addressed. As growth factors EGF and FGF2 are both present in the media used for maintenance of lt-NES cells, the effect of miR-7 overexpression on EGF signaling might be masked by the strong induction of proliferation by FGF2.

It is important to note that most of the evidence for roles of miR-128, miR-130b and miR-7 in the nervous system was gathered in cell lines derived from malignantly transformed adult cells like glioblastoma or neuroblastoma cell lines. Further detailed analysis of miR-128, miR-130b and miR-7 in other cell types may shed light on their putative roles in human neurogenesis and homeostasis of the adult nervous system.

4.1.2 MiR-9/9* and its influence on neural stem cell properties

Of all five miRNAs tested, elevated levels of miR-9/9* induced the strongest enhancement of differentiation. Concordantly, in neural precursors derived from mouse ES cells elevated levels of miR-9 shifted the ratio of cells positive for glial cell marker GFAP (glial fibrillary acidic protein) and pan-neuronal marker βIII tubulin in favor of neuronal cells [59]. Accordingly, double-knockout mice for the miR-9_2 and miR-9_3 loci showed a decreased number of early neurons in the cortical region [86] underlining the importance of miR-9 in neuronal differentiation.

Out of the miRNAs tested, miR-9/9* was the only one that additionally reduced the self-renewing capacity of lt-NES cells. This is in contrast to data *Delaloy et al.* gathered in hESC derived neural precursors from the neurosphere stage. They showed that miR-9 is needed for the proliferation of neuronal precursor cells and impairs their migration by targeting microtubuli destabilizing protein STMN1 [77]. However, the neural precursors gained from the neurosphere stage used by *Delaloy et al.* result from a variable run-trough protocol starting from hESCs. Therefore, their regional identity and the purity of the population are not clearly defined. In contrast, the lt-NES cells used here exhibit a stable regionalization marker profile corresponding to a ventral anterior hindbrain identity and represent a stable and pure population of neural stem cells [7]. This difference in regional identity, as well as the presumably earlier developmental stage of the used lt-NES cells, may cause the different phenotypes induced by modulation of miR-9 levels. For instance, the phenotype induced through targeting of HES1 homologue Hairy1 by miR-9 in *Xenopus* neural precursors differs in forebrain versus hindbrain areas [79]. While miR-9 was crucial for cell-cycle exit throughout the regions analyzed, only *Xenopus* forebrain progenitors depended on miR-9 for their survival [79]. A similar regional importance of Stathmin (STMN1) targeting by miR-9 might explain the reduced expansion of neurospheres *Delaloy et al.* observed upon miR-9 inhibition [77].

4.1.3 Targets of miR-9/9* in the Notch signaling cascade

Like observed in the *Xenopus* hindbrain by *Bonev et al.* [79], elevated miR-9/9* levels impaired self-renewal and promoted differentiation of the human neural stem cells analyzed here. In addition, modulation of Hairy1 partially rescued a lack of miR-9 in *Xenopus* neurogenesis [79]. Accordingly, the phenotype induced by miR-9/9*

overexpression resembled what was known from pharmacological inhibition of the Notch signaling cascade in morphology, differentiation enhancement, and impaired self-renewal of lt-NES cells [22]. Therefore, the potential interplay between miR-9/9* and the Notch signaling pathway was further investigated. While this work was prepared, studies in various model organisms further underlined the importance of an interaction between miR-9/9* and Notch [79, 83, 84, 130].

Data from these studies showed that homologues of HES1 are targeted by miR-9/9* in frog [79], fish [83] as well as mouse [79]. HES1 is a downstream effector of the Notch signaling pathway that has been shown to inhibit neuronal differentiation and sustain neural stem cell fate (reviewed in [131, 132]). In mouse neuroepithelial cells as well as in lt-NES cells, HES1 does not show robust dependency on Notch signaling modulation ([22, 133]; reviewed in [132]) indicating additional transcriptional regulation by other signaling pathways, such as Sonic hedgehog [134], c-Jun N-terminal kinase [135] and FGF [136] in various cell types. In addition, post-transcriptional regulation might contribute to the fluctuating levels of HES1 as shown for mouse neural precursors [84]. Data from lt-NES cells validated the targeting of HES1 by miR-9 in the human system.

Although there is no evidence for direct targeting of Notch1 by miR-9 from model organisms so far, it was found in mouse that upon upregulation of miR-9 Notch1 is down-regulated [88]. Furthermore, there were hints towards a potential connection between functional Notch signaling and miR-9 [137]. Even though target prediction revealed a binding site for miR-9 in the 3´UTR of human NOTCH1, an interaction could not be observed, as NOTCH1 mRNA levels did not change significantly upon miR-9/9* overexpression in lt-NES cells.

4.1.4 Direct regulation of NOTCH2 by miR-9/9*

In contrast to NOTCH1, NOTCH2, another member of the Notch receptor family, is regulated by miR-9/9*. While it had not been analyzed as a target of miR-9/9* so far, many algorithms predict target sites for miR-9 and miR-9* in the 3´UTR of NOTCH2. In addition, NOTCH2 was recently predicted to be part of a regulatory loop with miR-9 in glioblastoma cells [138]. The 3`UTR of NOTCH2 consists of ~4 kb compared to ~1kb for NOTCH1 and HES1. Within this long sequence many miRNA target sites are predicted indicating heavy post-transcriptional regulation. Additionally, some

functions of NOTCH2 are opposing the ones of miR-9/9*. While the role of miR-9 in tumor tissue remains a topic of ongoing discussion, it has been found to limit expansion of neural precursors (reviewed in [71]). N2ICD expression on the other hand is not sufficient to induce tumors but leads to a prominent expansion of the neurogenic niche [139]. Furthermore, N2ICD expression in cultured NSCs promotes astrocyte differentiation at the expense of neuronal and oligodendrocyte differentiation [139], while miR-9 overexpression leads to a reduction in GFAP positive cells [59]. These functional connections might all be due to direct targeting of NOTCH2 by miR-9/9*, which was shown here for the first time.

4.2 A feedback loop between miR-9/9* and Notch regulating lt-NES cell behavior

4.2.1 MiR-9/9* as a target of Notch transcriptional activity

Endogenous RNA interference is an elegant mechanism to control the homeostasis of major signaling pathways like Notch. In many cases, this regulation is part of a feedback loop to ensure tight regulation. In model organisms, γ-secretase inhibition had been shown to reduce levels of miR-9 [41, 83]. Pharmacological inhibition of Notch signaling as well as genetic gain and loss of function revealed that indeed miR-9/9* expression depends on Notch activity in lt-NES cells. The data presented showed for the first time, that in human neural stem cells the regulation of miR-9/9* expression is carried out by canonical Notch signaling and is due to direct binding of the NICD recruited transcriptional complex to miR-9/9* promoter regions.

4.2.2 Reciprocal interaction between Notch signaling and miR-9 in neural stem cells

Based on the data gathered in lt-NES cells, this work proposes the model of a Notch-miR-9/9*-feedback loop. While expression of miR-9/9* is directly regulated by the transcriptional complex downstream of Notch, levels of Notch signaling are fine-tuned by miR-9/9*. Therefore, miR-9 and miR-9* regulate different stages of the Notch signaling cascade by targeting Notch receptor NOTCH2 and Notch downstream target HES1 (Fig. 4.1). This hypothesis is supported and complemented by studies in *Zebrafish* and mouse, suggesting that additionally HES1 feedbacks on miR-9

expression [83, 84] (Fig. 4.1).

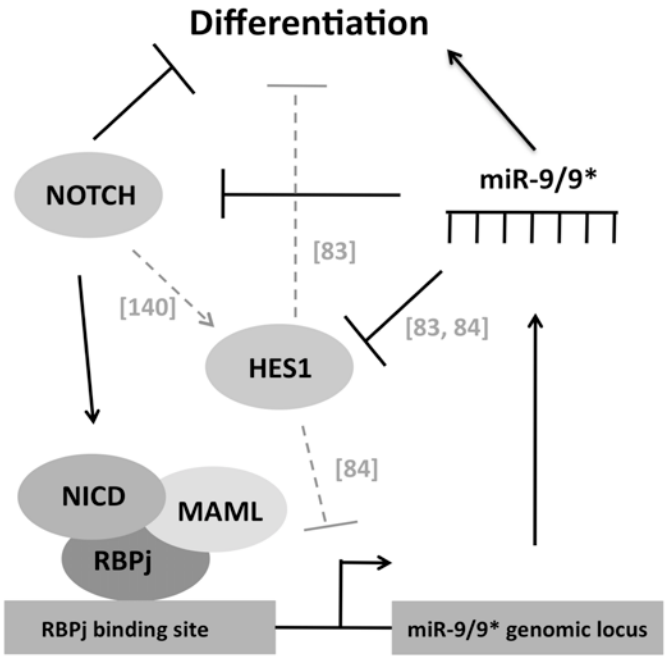

Fig. 4.1: Reciprocal interaction between miR-9/9* and the Notch pathway. Proposed model for the identified interaction between miR-9/9* and the Notch pathway in human neural stem cells, combined with recent findings in other model systems. Dashed lines indicate information integrated from other studies (*Zebrafish* [83] , *Mus Musculus* [84, 140]).

As the dashed lines in the scheme (Fig. 4.1) indicate, HES1 – also found to be targeted by miR-9 in lt-NES cells – was shown to repress miR-9 expression in mouse neural precursors [83]. Although this repression has not been characterized yet in the human system it adds a further layer of complexity to the interplay between Notch and miR-9/9* described here and is to be assessed in future work.

Regulatory mechanisms ensuring tight regulation of Notch activity are crucial for neural stem cell homeostasis. While overactivation of Notch can lead to overproliferation or quiescence [19, 20, 139, 141], too little Notch signaling primes stem cells to differentiate [22]. In granule neuron precursors it was shown that overexpression of NOTCH2 and HES1 blocked the progression to differentiation [141]. This is in agreement with the data obtained from our *in vitro* differentiation studies. Even though elevated levels of miR-9/9* enhanced the differentiation of lt-NES cells this effect is completely suppressed by N2ICD overexpression. In turn, the impairment of lt-NES cell differentiation induced by miR-9/9* inhibition was abolished by blockade of Notch signaling.

The data informing the presented feedback network, in which miR-9/9* and Notch signaling interact at several stages, also indicate that the impact of miR-9/9* on lt-NES cell maintenance is – at least in part – due to targeting of the Notch pathway. In addition to its role in neural stem cell maintenance, reciprocal interaction with miR-9/9* may also buffer the activity of Notch in other cellular systems. For instance, sophisticated control of Notch signaling is needed to avoid pathological cell behavior, since deregulated Notch can lead to tumorigenesis [139, 142-144]. The feedback loop described here might be involved in the neoplastic context as the levels of pri-miR-9_2 detected in the glioblastoma cell line U87 were dramatically lower than in lt-NES cells and miR-9* has already been shown to reduce stemness of glioma cells [105]. The miR-9/9* network regulating neoplastic cells might even expand to other signaling pathways as studies in glioblastoma cells showed that overexpression of miR-9 decreases the levels of Janus kinase 1/3 (JAK1/3) protein levels, the phosphorylation of signal-transducer and activator of transcription protein 3 (STAT3) and expression of the STAT3 downstream target CCAAT/enhancer binding protein (CEBP-β), which interfere with proliferation of glioblastoma cancer stem cells [145]. It has to be explored whether the feedback mechanism described here is part of a bigger regulatory network that includes e.g. the JAK-STAT pathway for regulating self-renewal in a cell type and stage dependent manner. Given its role in the regulation of Notch signaling, its ability to impair neural stem cell proliferation and targeting of JAK-STAT pathway components, one could envision the possibility of manipulating miR-9/9* levels in order to impact on proliferation of cancer cells.

Taken together, the network of miR-9-Notch feedback interactions described may prove as the key-finding of this work as it may be crucial for the regulation of the switch between self-renewal and differentiation of human neural stem cells as well as – potentially – other cell types.

4.3 A network of targets underlies the impact of miR-9/9*

The feedback loop with Notch is not the only mechanism underlying regulation of neural stem cell behavior by miR-9/9*. Data from many studies suggest additional targets for miR-9/9* establishing a network of determinants and regulatory mechanisms that assure proper development of the central nervous system. In

human neural precursors, knowledge on the components of this network is rather scarce. Besides the previously discussed STMN1, there is only one other determinant carefully analyzed in human neural stem cells – REST. REST represses the transcription of pro-neural genes and engages in a feedback loop with miR-9/9* similar to that described for Notch [58].

In an attempt to identify additional genes relevant in the human system, candidate genes targeted by miR-9/9* in model organisms were analyzed for their behavior in lt-NES cells. However, similar phenotypes do not guarantee conservation of targets between species or even different somatic cell types of the same species. This can be due to different reasons. First, variation in the 3´UTR of homologue genes between species may eliminate the underlying miRNA binding sites. For example, parallel to the antiapoptotic effect of miR-9 via the p53 pathway found in the *Xenopus* forebrain [79] its *Drosophila* homologue miR-9a was shown to prevent apoptosis in the development of wings by targeting beadex (dLMO) [146]. Although miR-9 has been shown to regulate apoptosis in both systems, the target site found in *Drosophila* dLMO is neither conserved in *Xenopus* nor in mammalian homologues. Second, the expression of the target mRNAs can differ among the cell types analyzed. In mouse neural progenitors, TLX has been shown to regulate proliferation in a feedback loop with miR-9 [76], which itself is even regulated by another miRNA, let-7d [147]. However, in lt-NES cells TLX is not detectable by qPCR (data not shown) suggesting that other targets underlie the impaired self-renewal and enhanced differentiation of lt-NES cells. Furthermore, TLX regulates the expression of pri-miR-9_1 [76] which is not detectable in lt-NES cells. Expression of pri-miR-9_2, the form dominantly expressed in lt-NES cells, was not significantly changed in TLX -/- mice [76]. Thus, targets and phenotypes known from model organisms or human cell types other than neural stem cells cannot easily be translated to the human nervous system.

As expected, not all candidates picked from literature or target prediction algorithms were targeted by miR-9/9*. As NESTIN is important for survival and self-renewal of neural stem cells [109, 110] and down-regulated upon induction of neurogenesis [148], it was likely to be under the control of brain-enriched miRNAs. Prediction algorithms revealed putative binding sites for miR-9 its 3´UTR, which however were not sufficient to modulate its mRNA levels in lt-NES cell. A recent study showed that post-transcriptional regulation of Nestin is carried out by miR-125b in mice [149]. In lt-

NES cells, brain-enriched miR-125b is up-regulated during differentiation as well [68] and may in part be responsible for the regulation of NESTIN during neuronal differentiation [73].

NESTIN interacts with PAX6 preventing precocious neuronal differentiation to maintain the progenitor pool (reviewed in [111]). Surprisingly, elevated miR-9 levels did not affect PAX6 expression in lt-NES cells. This is in contrast to data from the developing mouse telencephalon, which indicate that Pax6 mRNA levels are regulated indirectly by miR-9 through Meis2 [86]. However, data of an expression profiling revealed that MEIS2 is expressed in lt-NES cells [129]. The reasons underlying this lack of regulation have to be assessed carefully in future work as the regulation of PAX6 by MEIS2 may not be conserved in human cells.

While mRNA levels of NESTIN and PAX6 were not affected, targeting of other important regulators in lt-NES cells was validated. Three of them – SIRT1, LIN28A and LIN28B – are known to be involved in stem cell maintenance and down-regulated upon induction of differentiation [106, 108]. As their dynamic expression across differentiation is inversely correlated to that of miR-9/9*, which promote differentiation, they are likely targets. Indeed, levels of SIRT1 as well as LIN28 were found to be modulated by miR-9 in various murine and human tissues [107]. Analysis of their mRNA levels revealed that they are expressed and affected by miR-9/9* in lt-NES cells as well. Due to their roles in stem cell maintenance, they may contribute to the network of miR-9/9* targets orchestrating human neural stem cell behavior.

LIN28A and LIN28B may even regulate miR-9/9* expression indirectly as they form a reciprocal gradient with the differentiation-promoting miRNA let-7 (reviewed in [108]). In mouse, let-7d has been shown to derepress miR-9 expression by downregulation of TLX levels [147]. However, the relevance of this interaction has still to be addressed in human cells other than lt-NES cells due to their lack in TLX expression. In addition, LIN28A and LIN28B have been shown to be under the control of several miRNAs enriched during brain development (i.e. miR-9, miR-125b, miR-30, miR-181 and let-7) and to regulate the processing of at least let-7 and miR-181 in turn [107, 150]. Therefore, the LIN28 family may present an intersection integrating several post-transcriptional regulatory mechanisms impacting on stem cell maintenance.

The decrease of mRNA levels observed upon miR-9/9* overexpression added SIRT1, LIN28A and LIN28B to the network of miR-9/9* targets regulating human neural stem

cell maintenance (summarized in Fig. 4.2). However, the impact of these targets on the behavior of lt-NES cells is still to be addressed by modulation of their levels and identification of the mechanisms underlying their regulation by miR-9/9*.

4.4 Bifunctionality of miR-9 and miR-9*

Although miR-9 and miR-9* are produced from the same precursor and, therefore, under the same transcriptional control, they differ in their sequence and are predicted to target mostly different gene sets. Also their impact on lt-NES cells differs. While overexpression of miR-9* impairs proliferation and promotes differentiation, miR-9 overexpression enhances differentiation but does not affect proliferation. *Delaloy et al* showed that in neural stem cells originating from the neurosphere stage of a different hESC differentiation paradigm, miR-9 is even required for proper expansion of neural progenitors [77]. Target prediction analysis for the validated components of the Notch signaling pathway revealed that miR-9 alone targets both NOTCH2 and HES1 while miR-9* solely targets NOTCH2. Given that only miR-9* impairs self-renewal of lt-NES cells, this is very likely to be due to regulation of targets differing to the ones affected by miR-9. Indeed, the overlap between putative targets for miR-9 and miR-9* is very small and there are many genes whose modulation could account for the specific effect of miR-9* on lt-NES cell self-renewal.

One of these potential candidates is SOX2 which has been implicated in neural stem cell maintenance [104]. Its constitutive activation maintains neural stem cell characteristics and inhibits neuronal differentiation while its inhibition leads to precocious neuronal differentiation [151, 152]. In glioma cell lines, SOX2 was identified as a direct target of miR-9*, and its expression is in turn derepressed by ID4-mediated transcriptional repression of miR-9* [105]. The finding that only miR-9* and not miR-9 regulates mRNA levels of SOX2 supports the hypothesis that miR-9* might act on lt-NES cell self-renewal by targeting, among other genes, SOX2 (Fig. 4.2). A similar mechanism was recently described for the interaction of Sox2 and the miR-200 family in mouse neural progenitors. The authors showed that reduction of Sox2 levels by the miR-200 family promotes the transition from proliferation to differentiation [153]. This may likely be the case for reduction of SOX2 by miR-9* in neural stem cells. These data indicate that SOX2 is one of the specific miR-9* targets affecting lt-NES cell self-renewal which is not under the control of miR-9.

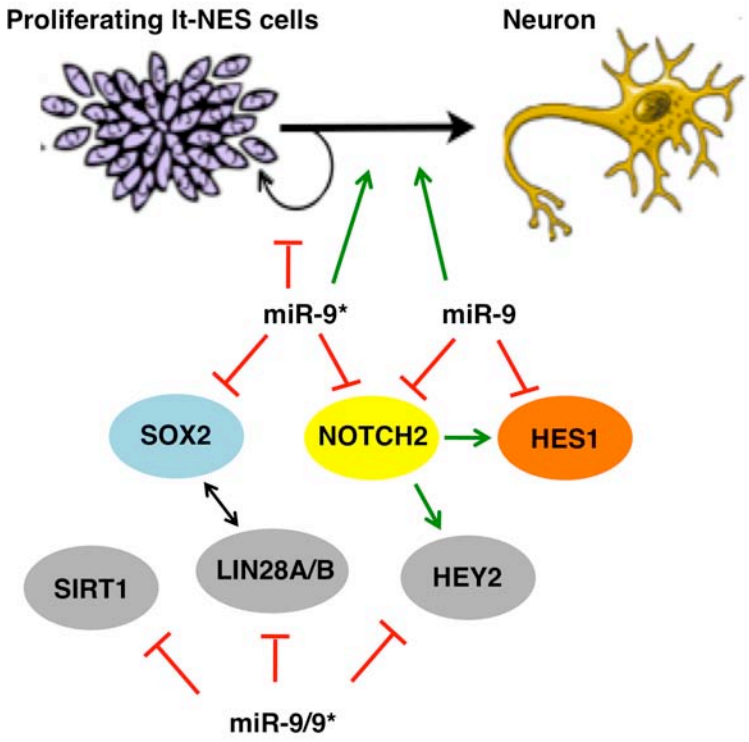

Fig. 4.2: Potential network underlying the role of miR-9/9* in neural stem cell proliferation and differentiation. Schematic summary of the phenotypes induced by miR-9 and miR-9* and potential underlying targets analyzed in lt-NES cells. Colors indicate direct targets of miR-9 (orange), miR-9* (blue) or both (yellow) validated on protein and mRNA level. Gray indicates targets of miR-9/9* that were solely assessed at mRNA level.

4.5 Derivation of specific neuronal subtypes by miRNA modulation

4.5.1 Modulation of lineage choice by miR-9/9* and miR-7

In addition to its impact on self-renewal and differentiation under proliferating conditions, elevated levels of miR-9/9* further increase the yield of neurons generated after induction of neurogenesis by growth factor withdrawal. The beneficial effect on the overall generation of neurons observed is in accordance with data gained from the murine telencephalon and *Zebrafish* hindbrain where miR-9 has been shown to promote differentiation of newly born neurons [78, 86]. In addition, the potential interplay of the JAK-STAT pathway with miR-9/9* and Notch signaling discussed before may not only be important in cancer cells. For instance, it is known that JAK-STAT and Notch signaling cooperate to induce astrocytic fate [154]. Furthermore, miR-9 has the potential to act on neuronal lineage choice as it induces a switch in the subtypes of motor neurons generated by targeting FoxP1 in the chick spinal cord [81] and helps to define the midbrain-hindbrain boundary in *Zebrafish* [78].

Although overexpression of miR-7 did not impact significantly on lt-NES cell maintenance or differentiation in cell culture media containing EGF and FGF, it significantly affected the generation of neuronal cells once differentiation was induced by their withdrawal. The significant enhancement of neuronal generation by miR-7 induction in lt-NES cells observed only at later time points of *in vitro* differentiation supports the hypothesis that miR-7 may be involved at later stages of neural development. This is in line with the described neuroprotective role of miR-7 in defending mature neurons against oxidative stress by targeting *α*-synuclein mRNA [155] and its impact on the generation forebrain dopaminergic neurons in mouse [66].

4.5.2 MicroRNA-based regulation of dopaminergic fate specification

The promoting effect of miR-9/9* and miR-7 on neuronal differentiation and their known influence on neuronal subtype specification called for analysis of the neuronal cultures generated upon their overexpression. Upon induction of differentiation, lt-NES cells give mostly rise to glutamatergic and in small amounts dopaminergic and serotonergic neurons [3]. This work focused on the impact of miR-9/9* and miR-7 on the derivation of dopaminergic neurons. This specific neuronal subtype is very promising for neural replacement since dopaminergic neurons are lost from the substantia nigra pars compacta and consequentially the innervation in the striatum of patients suffering from Parkinson´s disease. Their loss accounts for motor symptoms including rigidity, akinesia, postural instability and tremor which are hallmarks of Parkinson´s disease (reviewed in [156]).

In lt-NES cells, overexpression of miR-9/9* as well as miR-7 led to a reduction of neurons of dopaminergic fate as assessed by staining for tyrosine hydroxylase (TH). This finding is supported by the recent data from the murine forebrain suggesting that miR-7a reduces the number of dopaminergic neurons generated [66]. However, data from the forebrain may not reflect the generation of the dopaminergic neurons lost in Parkinson´s disease, as these originate from the midbrain. Therefore, a detailed analysis of miR-9/9* and miR-7 during dopaminergic lineage choice may help to understand their role. As differentiation of lt-NES cells gives rise to only a small number of TH-positive neurons, another cellular system had to be used. Recently, it was shown that mesenchephalic dopaminergic neurons originate from

mesenchephalic floor plate cells, which represent a specialized cell population that organizes neural tube patterning and axon guidance [157, 158]. This finding was used by *Kriks et al.* to devise a protocol for derivation of dopaminergic neurons from human pluripotent stem cells via induction of floor plate precursor cells [89]. Expression analyses of miR-9, miR-9*, and miR-7 as well as known dopaminergic determinants were performed during the time course of this differentiation paradigm. These data showed that miR-9, miR-9* and miR-7 are down-regulated, while expression of dopaminergic markers like FOXA2, LMX1A, and MSX1 as well as neural stem cell marker PAX6 dramatically increase with progressing differentiation. Both miR-9/9* and miR-7 have been described to target Pax6. MiR-7 reduced the number of mouse forebrain dopaminergic neurons by direct interaction with Pax6 [66], while miR-9 inhibited Pax6 expression indirectly by suppressing Meis2 in the mouse telenchephalon [86]. These data strongly suggested that miR-7 and miR-9/9* converge to regulate the generation of dopaminergic neurons by reducing PAX6 levels. However, as previously discussed, data gained in lt-NES cells did not confirm the impact of miR-9/9* and miR-7 on PAX6 in human neural stem cells.

Other candidates highly expressed in midbrain dopaminergic cells and important for their specification are FOXA2, LMX1A and EN2 [159] which all harbor binding sites for miR-9/9* and miR-7 in their 3´UTRs. Regulation of EN2 mRNA levels by miR- 9/9* in lt-NES cells and FOXA2 mRNA and protein level in HepG2 cells by miR-9/9* and miR-7 could be shown here. Future work has to prove direct binding of miR-9/9* and miR-7 to the mRNAs of EN2 and FOXA2 as well as the predicted regulation of LMX1A und its functional relevance in dopaminergic fate choice. However, the data gathered strongly suggest targeting of EN2 and FOXA2 which may explain, to a certain extent, the impact of miR-9/9* and miR-7 on dopaminergic differentiation. Interestingly, the observed changes in dopaminergic specification could potentially represent an additional connection to the Notch signaling pathway, as Hes1 was indicated to regulate density and location of mouse mesDA neurons [160]. Therefore, the regulation of human HES1 by miR-9/9* described here might further contribute to the impact of these miRNAs on the generation of dopaminergic neurons.

The targeting of dopaminergic fate determinants together with the impaired generation of TH-positive cells from lt-NES cells upon overexpression of miR-9/9* or miR-7 as well as expression patterns of miR-9, miR-9*, and miR-7 during the time

course of mesechephalic dopaminergic precursor induction point to an inhibitory function of these three miRNAs in dopaminergic lineage choice. The absent expression of miR-9 in mouse floor plate cells as shown in [130] further supports the hypothesis of an inhibitory impact of this miRNA on the generation of mesDA neurons also *in vivo*.

4.6 Conclusion

Altogether, the data presented indicate that - in human neural stem cells - miR-9/9* act on the balance between proliferation and differentiation. Interestingly, miR-9 and miR-9* enhanced differentiation, while only miR-9* impaired proliferation (published in [82]). This may be due to the individual targets of the two sister miRNAs. For instance, neural stem cell regulator SOX2 was found to be targeted by miR-9* only. However, the data gathered show that both miRNAs target Notch signaling as it was discovered here that miR-9 as well as miR-9* regulate NOTCH2 levels and direct transcriptional regulation of HES1 by miR-9 could be shown. This interaction was found to be part of a novel feedback loop, in which miR-9/9* expression is under the transcriptional control of Notch signaling in turn. The Notch-miR-9/9* axis described here seems to be part of a bigger network regulating stem cell maintenance. As the role of Notch signaling is not restricted to the neural system, the described interaction may prove to have similar functions in other cellular systems as well.

In addition to its role in proliferating lt-NES cells, miR-9/9* – along with miR-7 – were found to enhance induced differentiation while impairing dopaminergic lineage choice. Modulation of these inhibitory as well as miRNAs known to be beneficial to dopaminergic differentiaton (like miR-181a [68]) may proof useful to increase the yield or accelerate the generation of mesenchephalic dopaminergic neurons from the differentiation paradigms devised so far.

4.7 Outlook

The data presented in this thesis provide new insights on miRNA-based regulation of neural stem cell differentiation and neuron subtype specification. Neurons derived from lt-NES cells may be potentially suitable for high throughput applications, pharmaceutical compound screenings, drug discovery, and neurotoxiticity studies

[129]. In order to shed light on the molecular mechanisms underlying the impact of miR-9/9* on human neural stem cells, the role of transcriptional miR-9/9* repression by HES1 in lt-NES cell maintenance would be interesting to analyze. This interaction might add a second feedback loop to the regulatory role of the NOTCH2-miR-9/9*-axis described. A network that could be further unraveled by validation of direct targeting of HEY2 by miR-9/9*. Parallel to the knowledge gained on NOTCH2, the impact of miR-9/9* targets HES1 and HEY2 could be specifically addressed by modulating them separately. Furthermore, potential interactions with other important signaling pathways like JAK-STAT could be analyzed and the relevance of the observed transcriptional network could be assessed in cell types other than lt-NES cells (e.g. cells with other regional identities like cortical progenitors).

As Notch signaling is known to impact on specification of neuronal versus glial cells dependent on dosage and timing of activation, its interplay with miR-9/9* in lineage decision could be investigated. Furthermore, the effect of miR-7 and miR-9/9* in the specification of neuronal subtypes has to be studied in more detail. These issues could not be addressed in lt-NES cells as the percentage of dopaminergic cells generated upon their differentiation is very small. Therefore, protocols specifically devised to generate mesenchephalic dopaminergic neurons (as described in [89, 161]) might prove useful to follow up on the effect of miR-7 and miR-9/9* overexpression on dopaminergic fate in lt-NES cells. Hence, direct binding of miR-9/9* and miR-7 to the 3´UTRs of FOXA2 and EN2 as well as other potential targets involved in dopaminergic fate like LMX1A has to be assessed to get an insight into the underlying mechanisms. In addition, the analysis on lineage decision could be expanded to other neuronal subtypes like serotonergic and GABAergic neurons.

The knowledge obtained in these experiments should inform future studies on the generation of defined neural cell types for biomedical applications.

5. Literature

[1] Thomson JA, Itskovitz-Eldor J, Shapiro SS, et al. Embryonic stem cell lines derived from human blastocysts. Science. 1998;282(5391):1145-1147.

[2] Meregalli M, Farini A, Torrente Y. Stem Cell Therapy for Neuromuscular Diseases. Stem Cells in Clinic and Research. 2011:437-468.

[3] Koch P, Kokaia Z, Lindvall O, et al. Emerging concepts in neural stem cell research: autologous repair and cell-based disease modelling. Lancet Neurol. 2009;8(9):819-829.

[4] Takahashi K, Tanabe K, Ohnuki M, et al. Induction of pluripotent stem cells from adult human fibroblasts by defined factors. Cell. 2007;131(5):861-872.

[5] Power C, Rasko JE. Will cell reprogramming resolve the embryonic stem cell controversy? A narrative review. Ann Intern Med. 2011;155(2):114-121.

[6] Rolletschek A, Wobus AM. Induced human pluripotent stem cells: promises and open questions. Biol Chem. 2009;390(9):845-849.

[7] Koch P, Opitz T, Steinbeck JA, et al. A rosette-type, self-renewing human ES cell-derived neural stem cell with potential for in vitro instruction and synaptic integration. Proc Natl Acad Sci U S A. 2009;106(9):3225-3230.

[8] Okabe S, Forsberg-Nilsson K, Spiro AC, et al. Development of neuronal precursor cells and functional postmitotic neurons from embryonic stem cells in vitro. Mech Dev. 1996;59(1):89-102.

[9] Reubinoff BE, Itsykson P, Turetsky T, et al. Neural progenitors from human embryonic stem cells. Nat Biotechnol. 2001;19(12):1134-1140.

[10] Zhang SC, Wernig M, Duncan ID, et al. In vitro differentiation of transplantable neural precursors from human embryonic stem cells. Nat Biotechnol. 2001;19(12):1129-1133.

[11] Louvi A, Artavanis-Tsakonas S. Notch signalling in vertebrate neural development. Nat Rev Neurosci. 2006;7(2):93-102.

[12] Yoon K, Gaiano N. Notch signaling in the mammalian central nervous system: insights from mouse mutants. Nat Neurosci. 2005;8(6):709-715.

[13] Gaiano N, Nye JS, Fishell G. Radial glial identity is promoted by Notch1 signaling in the murine forebrain. Neuron. 2000;26(2):395-404.

[14] Zhong W, Jiang MM, Weinmaster G, et al. Differential expression of mammalian Numb, Numblike and Notch1 suggests distinct roles during mouse cortical neurogenesis. Development. 1997;124(10):1887-1897.

[15] Li HS, Wang D, Shen Q, et al. Inactivation of Numb and Numblike in embryonic dorsal forebrain impairs neurogenesis and disrupts cortical morphogenesis. Neuron. 2003;40(6):1105-1118.

[16] Lasky JL, Wu H. Notch signaling, brain development, and human disease. Pediatr Res. 2005;57(5 Pt 2):104R-109R.

[17] Heyer MP, Pani AK, Smeyne RJ, et al. Normal midbrain dopaminergic neuron development and function in miR-133b mutant mice. J Neurosci. 2012;32(32):10887-10894.

[18] Pierfelice T, Alberi L, Gaiano N. Notch in the vertebrate nervous system: an old dog with new tricks. Neuron. 2011;69(5):840-855.

[19] Guentchev M, McKay RD. Notch controls proliferation and differentiation of stem cells in a dose-dependent manner. Eur J Neurosci. 2006;23(9):2289-2296.

[20] Chapouton P, Skupien P, Hesl B, et al. Notch activity levels control the balance between quiescence and recruitment of adult neural stem cells. J Neurosci. 2010;30(23):7961-7974.
[21] Gridley T. Notch signaling in vascular development and physiology. Development. 2007;134(15):2709-2718.
[22] Borghese L, Dolezalova D, Opitz T, et al. Inhibition of notch signaling in human embryonic stem cell-derived neural stem cells delays G1/S phase transition and accelerates neuronal differentiation in vitro and in vivo. Stem Cells. 2010;28(5):955-964.
[23] Lee RC, Feinbaum RL, Ambros V. The C. elegans heterochronic gene lin-4 encodes small RNAs with antisense complementarity to lin-14. Cell. 1993;75(5):843-854.
[24] Rodriguez A, Griffiths-Jones S, Ashurst JL, et al. Identification of mammalian microRNA host genes and transcription units. Genome Res. 2004;14(10A):1902-1910.
[25] Lee Y, Kim M, Han J, et al. MicroRNA genes are transcribed by RNA polymerase II. EMBO J. 2004;23(20):4051-4060.
[26] Borchert GM, Lanier W, Davidson BL. RNA polymerase III transcribes human microRNAs. Nat Struct Mol Biol. 2006;13(12):1097-1101.
[27] Boyd SD. Everything you wanted to know about small RNA but were afraid to ask. Lab Invest. 2008;88(6):569-578.
[28] Yi R, Qin Y, Macara IG, et al. Exportin-5 mediates the nuclear export of pre-microRNAs and short hairpin RNAs. Genes Dev. 2003;17(24):3011-3016.
[29] Hutvagner G, McLachlan J, Pasquinelli AE, et al. A cellular function for the RNA-interference enzyme Dicer in the maturation of the let-7 small temporal RNA. Science. 2001;293(5531):834-838.
[30] Ketting RF, Fischer SE, Bernstein E, et al. Dicer functions in RNA interference and in synthesis of small RNA involved in developmental timing in C. elegans. Genes Dev. 2001;15(20):2654-2659.
[31] Grimson A, Farh KK, Johnston WK, et al. MicroRNA targeting specificity in mammals: determinants beyond seed pairing. Mol Cell. 2007;27(1):91-105.
[32] Lewis BP, Burge CB, Bartel DP. Conserved seed pairing, often flanked by adenosines, indicates that thousands of human genes are microRNA targets. Cell. 2005;120(1):15-20.
[33] Vella MC, Choi EY, Lin SY, et al. The C. elegans microRNA let-7 binds to imperfect let-7 complementary sites from the lin-41 3'UTR. Genes Dev. 2004;18(2):132-137.
[34] Brennecke J, Hipfner DR, Stark A, et al. bantam encodes a developmentally regulated microRNA that controls cell proliferation and regulates the proapoptotic gene hid in Drosophila. Cell. 2003;113(1):25-36.
[35] Doench JG, Sharp PA. Specificity of microRNA target selection in translational repression. Genes Dev. 2004;18(5):504-511.
[36] Lim LP, Lau NC, Garrett-Engele P, et al. Microarray analysis shows that some microRNAs downregulate large numbers of target mRNAs. Nature. 2005;433(7027):769-773.
[37] Wightman B, Ha I, Ruvkun G. Posttranscriptional regulation of the heterochronic gene lin-14 by lin-4 mediates temporal pattern formation in C. elegans. Cell. 1993;75(5):855-862.

[38] Bartel DP. MicroRNAs: target recognition and regulatory functions. Cell. 2009;136(2):215-233.
[39] Krutzfeldt J, Rajewsky N, Braich R, et al. Silencing of microRNAs in vivo with 'antagomirs'. Nature. 2005;438(7068):685-689.
[40] Fineberg SK, Kosik KS, Davidson BL. MicroRNAs potentiate neural development. Neuron. 2009;64(3):303-309.
[41] Krichevsky AM, King KS, Donahue CP, et al. A microRNA array reveals extensive regulation of microRNAs during brain development. RNA. 2003;9(10):1274-1281.
[42] Miska EA, Alvarez-Saavedra E, Townsend M, et al. Microarray analysis of microRNA expression in the developing mammalian brain. Genome Biol. 2004;5(9):R68.
[43] Sempere LF, Freemantle S, Pitha-Rowe I, et al. Expression profiling of mammalian microRNAs uncovers a subset of brain-expressed microRNAs with possible roles in murine and human neuronal differentiation. Genome Biol. 2004;5(3):R13.
[44] Bernstein E, Caudy AA, Hammond SM, et al. Role for a bidentate ribonuclease in the initiation step of RNA interference. Nature. 2001;409(6818):363-366.
[45] Cuellar TL, Davis TH, Nelson PT, et al. Dicer loss in striatal neurons produces behavioral and neuroanatomical phenotypes in the absence of neurodegeneration. Proc Natl Acad Sci U S A. 2008;105(14):5614-5619.
[46] Davis TH, Cuellar TL, Koch SM, et al. Conditional loss of Dicer disrupts cellular and tissue morphogenesis in the cortex and hippocampus. J Neurosci. 2008;28(17):4322-4330.
[47] Schaefer A, O'Carroll D, Tan CL, et al. Cerebellar neurodegeneration in the absence of microRNAs. J Exp Med. 2007;204(7):1553-1558.
[48] De Pietri Tonelli D, Pulvers JN, Haffner C, et al. miRNAs are essential for survival and differentiation of newborn neurons but not for expansion of neural progenitors during early neurogenesis in the mouse embryonic neocortex. Development. 2008;135(23):3911-3921.
[49] Stark KL, Xu B, Bagchi A, et al. Altered brain microRNA biogenesis contributes to phenotypic deficits in a 22q11-deletion mouse model. Nat Genet. 2008;40(6):751-760.
[50] Taft RJ, Glazov EA, Lassmann T, et al. Small RNAs derived from snoRNAs. RNA. 2009;15(7):1233-1240.
[51] Golden DE, Gerbasi VR, Sontheimer EJ. An inside job for siRNAs. Mol Cell. 2008;31(3):309-312.
[52] Giraldez AJ, Cinalli RM, Glasner ME, et al. MicroRNAs regulate brain morphogenesis in zebrafish. Science. 2005;308(5723):833-838.
[53] Bian S, Sun T. Functions of noncoding RNAs in neural development and neurological diseases. Mol Neurobiol. 2011;44(3):359-373.
[54] Maller Schulman BR, Liang X, Stahlhut C, et al. The let-7 microRNA target gene, Mlin41/Trim71 is required for mouse embryonic survival and neural tube closure. Cell Cycle. 2008;7(24):3935-3942.
[55] Schratt GM, Tuebing F, Nigh EA, et al. A brain-specific microRNA regulates dendritic spine development. Nature. 2006;439(7074):283-289.
[56] Choi PS, Zakhary L, Choi WY, et al. Members of the miRNA-200 family regulate olfactory neurogenesis. Neuron. 2008;57(1):41-55.

[57] Yoo AS, Staahl BT, Chen L, et al. MicroRNA-mediated switching of chromatin-remodelling complexes in neural development. Nature. 2009;460(7255):642-646.
[58] Conaco C, Otto S, Han JJ, et al. Reciprocal actions of REST and a microRNA promote neuronal identity. Proc Natl Acad Sci U S A. 2006;103(7):2422-2427.
[59] Krichevsky AM, Sonntag KC, Isacson O, et al. Specific microRNAs modulate embryonic stem cell-derived neurogenesis. Stem Cells. 2006;24(4):857-864.
[60] Makeyev EV, Zhang J, Carrasco MA, et al. The MicroRNA miR-124 promotes neuronal differentiation by triggering brain-specific alternative pre-mRNA splicing. Mol Cell. 2007;27(3):435-448.
[61] Smirnova L, Grafe A, Seiler A, et al. Regulation of miRNA expression during neural cell specification. Eur J Neurosci. 2005;21(6):1469-1477.
[62] Wu L, Belasco JG. Micro-RNA regulation of the mammalian lin-28 gene during neuronal differentiation of embryonal carcinoma cells. Mol Cell Biol. 2005;25(21):9198-9208.
[63] Yoo AS, Sun AX, Li L, et al. MicroRNA-mediated conversion of human fibroblasts to neurons. Nature. 2011;476(7359):228-231.
[64] Eacker SM, Dawson TM, Dawson VL. Understanding microRNAs in neurodegeneration. Nat Rev Neurosci. 2009;10(12):837-841.
[65] Kim J, Inoue K, Ishii J, et al. A MicroRNA feedback circuit in midbrain dopamine neurons. Science. 2007;317(5842):1220-1224.
[66] de Chevigny A, Core N, Follert P, et al. miR-7a regulation of Pax6 controls spatial origin of forebrain dopaminergic neurons. Nat Neurosci. 2012;15(8):1120-1126.
[67] Yang D, Li T, Wang Y, et al. miR-132 regulates the differentiation of dopamine neurons by directly targeting Nurr1 expression. J Cell Sci. 2012;125(Pt 7):1673-1682.
[68] Stappert L, Borghese L, Roese-Koerner B, et al. MicroRNA-Based Promotion of Human Neuronal Differentiation and Subtype Specification. PLoS One. 2013;8(3):e59011.
[69] Cao X, Yeo G, Muotri AR, et al. Noncoding RNAs in the mammalian central nervous system. Annu Rev Neurosci. 2006;29:77-103.
[70] Lagos-Quintana M, Rauhut R, Yalcin A, et al. Identification of tissue-specific microRNAs from mouse. Curr Biol. 2002;12(9):735-739.
[71] Yuva-Aydemir Y, Simkin A, Gascon E, et al. MicroRNA-9: functional evolution of a conserved small regulatory RNA. RNA Biol. 2011;8(4):557-564.
[72] Lagos-Quintana M, Rauhut R, Lendeckel W, et al. Identification of novel genes coding for small expressed RNAs. Science. 2001;294(5543):853-858.
[73] Li Y, Wang F, Lee JA, et al. MicroRNA-9a ensures the precise specification of sensory organ precursors in Drosophila. Genes Dev. 2006;20(20):2793-2805.
[74] Gao FB. Context-dependent functions of specific microRNAs in neuronal development. Neural Dev. 2010;5:25.
[75] Shibata M, Kurokawa D, Nakao H, et al. MicroRNA-9 modulates Cajal-Retzius cell differentiation by suppressing Foxg1 expression in mouse medial pallium. J Neurosci. 2008;28(41):10415-10421.
[76] Zhao C, Sun G, Li S, et al. A feedback regulatory loop involving microRNA-9 and nuclear receptor TLX in neural stem cell fate determination. Nat Struct Mol Biol. 2009;16(4):365-371.

[77] Delaloy C, Liu L, Lee JA, et al. MicroRNA-9 coordinates proliferation and migration of human embryonic stem cell-derived neural progenitors. Cell Stem Cell. 2010;6(4):323-335.
[78] Leucht C, Stigloher C, Wizenmann A, et al. MicroRNA-9 directs late organizer activity of the midbrain-hindbrain boundary. Nat Neurosci. 2008;11(6):641-648.
[79] Bonev B, Pisco A, Papalopulu N. MicroRNA-9 reveals regional diversity of neural progenitors along the anterior-posterior axis. Dev Cell. 2011;20(1):19-32.
[80] Luxenhofer G, Helmbrecht MS, Langhoff J, et al. MicroRNA-9 promotes the switch from early-born to late-born motor neuron populations by regulating Onecut transcription factor expression. Dev Biol. 2013;386(2):358-370.
[81] Otaegi G, Pollock A, Hong J, et al. MicroRNA miR-9 modifies motor neuron columns by a tuning regulation of FoxP1 levels in developing spinal cords. J Neurosci. 2010;31(3):809-818.
[82] Roese-Koerner B, Stappert L, Koch P, et al. Pluripotent Stem Cell-Derived Somatic Stem Cells as Tool to Study the Role of MicroRNAs in Early Human Neural Development. Curr Mol Med. 2013.
[83] Coolen M, Thieffry D, Drivenes O, et al. miR-9 controls the timing of neurogenesis through the direct inhibition of antagonistic factors. Dev Cell. 2012;22(5):1052-1064.
[84] Bonev B, Stanley P, Papalopulu N. MicroRNA-9 Modulates Hes1 ultradian oscillations by forming a double-negative feedback loop. Cell Rep. 2012;2(1):10-18.
[85] Goodfellow M, Phillips NE, Manning C, et al. microRNA input into a neural ultradian oscillator controls emergence and timing of alternative cell states. Nat Commun. 2013;5:3399.
[86] Shibata M, Nakao H, Kiyonari H, et al. MicroRNA-9 regulates neurogenesis in mouse telencephalon by targeting multiple transcription factors. J Neurosci. 2011;31(9):3407-3422.
[87] Packer AN, Xing Y, Harper SQ, et al. The bifunctional microRNA miR-9/miR-9* regulates REST and CoREST and is downregulated in Huntington's disease. J Neurosci. 2008;28(53):14341-14346.
[88] Jing L, Jia Y, Lu J, et al. MicroRNA-9 promotes differentiation of mouse bone mesenchymal stem cells into neurons by Notch signaling. Neuroreport. 2011;22(5):206-211.
[89] Kriks S, Shim JW, Piao J, et al. Dopamine neurons derived from human ES cells efficiently engraft in animal models of Parkinson's disease. Nature. 2011;480(7378):547-551.
[90] Hansen TB, Jensen TI, Clausen BH, et al. Natural RNA circles function as efficient microRNA sponges. Nature. 2013;495(7441):384-388.
[91] Amit M, Itskovitz-Eldor J. Derivation and spontaneous differentiation of human embryonic stem cells. J Anat. 2002;200(Pt 3):225-232.
[92] Amit M, Carpenter MK, Inokuma MS, et al. Clonally derived human embryonic stem cell lines maintain pluripotency and proliferative potential for prolonged periods of culture. Dev Biol. 2000;227(2):271-278.
[93] Kozomara A, Griffiths-Jones S. miRBase: integrating microRNA annotation and deep-sequencing data. Nucleic Acids Res. 2011;39(Database issue):D152-157.

[94] Wiznerowicz M, Trono D. Conditional suppression of cellular genes: lentivirus vector-mediated drug-inducible RNA interference. J Virol. 2003;77(16):8957-8961.
[95] Capobianco AJ, Zagouras P, Blaumueller CM, et al. Neoplastic transformation by truncated alleles of human NOTCH1/TAN1 and NOTCH2. Mol Cell Biol. 1997;17(11):6265-6273.
[96] Weng AP, Nam Y, Wolfe MS, et al. Growth suppression of pre-T acute lymphoblastic leukemia cells by inhibition of notch signaling. Mol Cell Biol. 2003;23(2):655-664.
[97] Ladewig J, Mertens J, Kesavan J, et al. Small molecules enable highly efficient neuronal conversion of human fibroblasts. Nat Methods. 2012;9(6):575-578.
[98] Kefas B, Godlewski J, Comeau L, et al. microRNA-7 inhibits the epidermal growth factor receptor and the Akt pathway and is down-regulated in glioblastoma. Cancer Res. 2008;68(10):3566-3572.
[99] Molofsky AV, Pardal R, Iwashita T, et al. Bmi-1 dependence distinguishes neural stem cell self-renewal from progenitor proliferation. Nature. 2003;425(6961):962-967.
[100] Dweep H, Sticht C, Pandey P, et al. miRWalk--database: prediction of possible miRNA binding sites by "walking" the genes of three genomes. J Biomed Inform. 2011;44(5):839-847.
[101] Wolfe MS. Processive proteolysis by gamma-secretase and the mechanism of Alzheimer's disease. Biol Chem. 2012;393(9):899-905.
[102] Webster RJ, Giles KM, Price KJ, et al. Regulation of epidermal growth factor receptor signaling in human cancer cells by microRNA-7. J Biol Chem. 2009;284(9):5731-5741.
[103] Jarriault S, Brou C, Logeat F, et al. Signalling downstream of activated mammalian Notch. Nature. 1995;377(6547):355-358.
[104] Pevny LH, Nicolis SK. Sox2 roles in neural stem cells. Int J Biochem Cell Biol. 2010;42(3):421-424.
[105] Jeon HM, Sohn YW, Oh SY, et al. ID4 imparts chemoresistance and cancer stemness to glioma cells by derepressing miR-9*-mediated suppression of SOX2. Cancer Res. 2011;71(9):3410-3421.
[106] Saunders LR, Sharma AD, Tawney J, et al. miRNAs regulate SIRT1 expression during mouse embryonic stem cell differentiation and in adult mouse tissues. Aging (Albany NY). 2010;2(7):415-431.
[107] Zhong X, Li N, Liang S, et al. Identification of microRNAs regulating reprogramming factor LIN28 in embryonic stem cells and cancer cells. J Biol Chem. 2010;285(53):41961-41971.
[108] Viswanathan SR, Daley GQ. Lin28: A microRNA regulator with a macro role. Cell. 2010;140(4):445-449.
[109] Park D, Xiang AP, Mao FF, et al. Nestin is required for the proper self-renewal of neural stem cells. Stem Cells. 2010;28(12):2162-2171.
[110] Xue XJ, Yuan XB. Nestin is essential for mitogen-stimulated proliferation of neural progenitor cells. Mol Cell Neurosci. 2010;45(1):26-36.
[111] Osumi N, Shinohara H, Numayama-Tsuruta K, et al. Concise review: Pax6 transcription factor contributes to both embryonic and adult neurogenesis as a multifunctional regulator. Stem Cells. 2008;26(7):1663-1672.
[112] Cuello AC, Priestley JV, Sofroniew MV. Immunocytochemistry and neurobiology. Q J Exp Physiol. 1983;68(4):545-578.

[113] Reddy SD, Ohshiro K, Rayala SK, et al. MicroRNA-7, a homeobox D10 target, inhibits p21-activated kinase 1 and regulates its functions. Cancer Res. 2008;68(20):8195-8200.
[114] Dayoub R, Groitl P, Dobner T, et al. Foxa2 (HNF-3beta) regulates expression of hepatotrophic factor ALR in liver cells. Biochem Biophys Res Commun. 2010;395(4):465-470.
[115] Feng W, Feng Y. MicroRNAs in neural cell development and brain diseases. Sci China Life Sci. 2011;54(12):1103-1112.
[116] Perruisseau-Carrier C, Jurga M, Forraz N, et al. miRNAs stem cell reprogramming for neuronal induction and differentiation. Mol Neurobiol. 2011;43(3):215-227.
[117] Shao NY, Hu HY, Yan Z, et al. Comprehensive survey of human brain microRNA by deep sequencing. BMC Genomics. 2010;11:409.
[118] Stark A, Brennecke J, Bushati N, et al. Animal MicroRNAs confer robustness to gene expression and have a significant impact on 3'UTR evolution. Cell. 2005;123(6):1133-1146.
[119] Chen H, Shalom-Feuerstein R, Riley J, et al. miR-7 and miR-214 are specifically expressed during neuroblastoma differentiation, cortical development and embryonic stem cells differentiation, and control neurite outgrowth in vitro. Biochem Biophys Res Commun. 2010;394(4):921-927.
[120] Alexiou P, Vergoulis T, Gleditzsch M, et al. miRGen 2.0: a database of microRNA genomic information and regulation. Nucleic Acids Res. 2010;38(Database issue):D137-141.
[121] Godlewski J, Nowicki MO, Bronisz A, et al. Targeting of the Bmi-1 oncogene/stem cell renewal factor by microRNA-128 inhibits glioma proliferation and self-renewal. Cancer Res. 2008;68(22):9125-9130.
[122] Yang C, Cai J, Wang Q, et al. Epigenetic silencing of miR-130b in ovarian cancer promotes the development of multidrug resistance by targeting colony-stimulating factor 1. Gynecol Oncol. 2012;124(2):325-334.
[123] Zhao BS, Liu SG, Wang TY, et al. Screening of microRNA in patients with esophageal cancer at same tumor node metastasis stage with different prognoses. Asian Pac J Cancer Prev. 2013;14(1):139-143.
[124] Zhou H, Wang K, Hu Z, et al. TGF-beta1 alters microRNA profile in human gastric cancer cells. Chin J Cancer Res. 2013;25(1):102-111.
[125] Burrows RC, Wancio D, Levitt P, et al. Response diversity and the timing of progenitor cell maturation are regulated by developmental changes in EGFR expression in the cortex. Neuron. 1997;19(2):251-267.
[126] Kato M, Mizuguchi M, Takashima S. Developmental changes of epidermal growth factor-like immunoreactivity in the human fetal brain. J Neurosci Res. 1995;42(4):486-492.
[127] Represa A, Shimazaki T, Simmonds M, et al. EGF-responsive neural stem cells are a transient population in the developing mouse spinal cord. Eur J Neurosci. 2001;14(3):452-462.
[128] Li X, Carthew RW. A microRNA mediates EGF receptor signaling and promotes photoreceptor differentiation in the Drosophila eye. Cell. 2005;123(7):1267-1277.
[129] Falk A, Koch P, Kesavan J, et al. Capture of neuroepithelial-like stem cells from pluripotent stem cells provides a versatile system for in vitro production of human neurons. PLoS One. 2012;7(1):e29597.

[130] Tan SL, Ohtsuka T, Gonzalez A, et al. MicroRNA9 regulates neural stem cell differentiation by controlling Hes1 expression dynamics in the developing brain. Genes Cells. 2012;17(12):952-961.
[131] Shimojo H, Ohtsuka T, Kageyama R. Dynamic expression of notch signaling genes in neural stem/progenitor cells. Front Neurosci. 2011;5:78.
[132] Kageyama R, Ohtsuka T, Kobayashi T. Roles of Hes genes in neural development. Dev Growth Differ. 2008;50 Suppl 1:S97-103.
[133] Haupt S, Borghese L, Brustle O, et al. Non-genetic modulation of Notch activity by artificial delivery of Notch intracellular domain into neural stem cells. Stem Cell Rev. 2012;8(3):672-684.
[134] Wall DS, Mears AJ, McNeill B, et al. Progenitor cell proliferation in the retina is dependent on Notch-independent Sonic hedgehog/Hes1 activity. J Cell Biol. 2009;184(1):101-112.
[135] Curry CL, Reed LL, Nickoloff BJ, et al. Notch-independent regulation of Hes-1 expression by c-Jun N-terminal kinase signaling in human endothelial cells. Lab Invest. 2006;86(8):842-852.
[136] Nakayama K, Satoh T, Igari A, et al. FGF induces oscillations of Hes1 expression and Ras/ERK activation. Curr Biol. 2008;18(8):R332-334.
[137] Kuang Y, Liu Q, Shu X, et al. Dicer1 and MiR-9 are required for proper Notch1 signaling and the bergmann glial phenotype in the developing mouse cerebellum. Glia. 2012.
[138] Sun J, Gong X, Purow B, et al. Uncovering MicroRNA and Transcription Factor Mediated Regulatory Networks in Glioblastoma. PLoS Comput Biol. 2012;8(7):e1002488.
[139] Tchorz JS, Tome M, Cloetta D, et al. Constitutive Notch2 signaling in neural stem cells promotes tumorigenic features and astroglial lineage entry. Cell Death Dis. 2012;3:e325.
[140] Ong CT, Cheng HT, Chang LW, et al. Target selectivity of vertebrate notch proteins. Collaboration between discrete domains and CSL-binding site architecture determines activation probability. J Biol Chem. 2006;281(8):5106-5119.
[141] Solecki DJ, Liu XL, Tomoda T, et al. Activated Notch2 signaling inhibits differentiation of cerebellar granule neuron precursors by maintaining proliferation. Neuron. 2001;31(4):557-568.
[142] Harper JA, Yuan JS, Tan JB, et al. Notch signaling in development and disease. Clin Genet. 2003;64(6):461-472.
[143] Pierfelice TJ, Schreck KC, Eberhart CG, et al. Notch, neural stem cells, and brain tumors. Cold Spring Harb Symp Quant Biol. 2008;73:367-375.
[144] Radtke F, Raj K. The role of Notch in tumorigenesis: oncogene or tumour suppressor? Nat Rev Cancer. 2003;3(10):756-767.
[145] Kim TM, Huang W, Park R, et al. A developmental taxonomy of glioblastoma defined and maintained by MicroRNAs. Cancer Res. 2011;71(9):3387-3399.
[146] Bejarano F, Smibert P, Lai EC. miR-9a prevents apoptosis during wing development by repressing Drosophila LIM-only. Dev Biol. 2010;338(1):63-73.
[147] Zhao C, Sun G, Ye P, et al. MicroRNA let-7d regulates the TLX/microRNA-9 cascade to control neural cell fate and neurogenesis. Sci Rep. 2013;3:1329.
[148] Wiese C, Rolletschek A, Kania G, et al. Nestin expression--a property of multi-lineage progenitor cells? Cell Mol Life Sci. 2004;61(19-20):2510-2522.

[149] Cui Y, Xiao Z, Han J, et al. MiR-125b orchestrates cell proliferation, differentiation and migration in neural stem/progenitor cells by targeting Nestin. BMC Neurosci. 2012;13:116.
[150] Li X, Zhang J, Gao L, et al. MiR-181 mediates cell differentiation by interrupting the Lin28 and let-7 feedback circuit. Cell Death Differ. 2012;19(3):378-386.
[151] Qu Q, Shi Y. Neural stem cells in the developing and adult brains. J Cell Physiol. 2009;221(1):5-9.
[152] Graham V, Khudyakov J, Ellis P, et al. SOX2 functions to maintain neural progenitor identity. Neuron. 2003;39(5):749-765.
[153] Peng C, Li N, Ng YK, et al. A unilateral negative feedback loop between miR-200 microRNAs and Sox2/E2F3 controls neural progenitor cell-cycle exit and differentiation. J Neurosci. 2012;32(38):13292-13308.
[154] Cau E, Blader P. Notch activity in the nervous system: to switch or not switch? Neural Dev. 2009;4:36.
[155] Junn E, Lee KW, Jeong BS, et al. Repression of alpha-synuclein expression and toxicity by microRNA-7. Proc Natl Acad Sci U S A. 2009;106(31):13052-13057.
[156] Correia AS, Anisimov SV, Li JY, et al. Stem cell-based therapy for Parkinson's disease. Ann Med. 2005;37(7):487-498.
[157] Andersson E, Tryggvason U, Deng Q, et al. Identification of intrinsic determinants of midbrain dopamine neurons. Cell. 2006;124(2):393-405.
[158] Ono Y, Nakatani T, Sakamoto Y, et al. Differences in neurogenic potential in floor plate cells along an anteroposterior location: midbrain dopaminergic neurons originate from mesencephalic floor plate cells. Development. 2007;134(17):3213-3225.
[159] Wallen A, Perlmann T. Transcriptional control of dopamine neuron development. Ann N Y Acad Sci. 2003;991:48-60.
[160] Kameda Y, Saitoh T, Fujimura T. Hes1 regulates the number and anterior-posterior patterning of mesencephalic dopaminergic neurons at the mid/hindbrain boundary (isthmus). Dev Biol. 2011;358(1):91-101.
[161] Kirkeby A, Grealish S, Wolf DA, et al. Generation of regionally specified neural progenitors and functional neurons from human embryonic stem cells under defined conditions. Cell Rep. 2012;1(6):703-714.

6. Appendix

6.1 Acknowledgements

First, I would like to thank Prof. Dr. Oliver Brüstle for giving me the opportunity to work on such an interesting topic as well as for his supervision and support.

I also thank Prof. Dr. Waldemar Kolanus for agreeing to be my second supervisor.

In addition, I would like to thank my direct supervisor Dr. Lodovica Borghese for her advice and encouragement throughout the course of this thesis. I thank her for the effort she put into training me in the scientific field and her guidance.

Many thanks also go to the lab members of the Reconstructive Neurobiology department who became friends and made work so much more fun - especially the members of the "AG Lodo" and my "coffee/lunch-buddys". I want to thank Katja and Monika for their technical assistance to my project and Laura and Beatrice for the collaboration on the data presented. Thanks to all colleagues for the nice working atmosphere and support, all the help and the discussions (both work and not work related).

Special thanks also goes to my family and friends outside the lab for all their support, help and understanding. Especially, I would like to thank my parents and sister, which were always there for me and on which I know I can always rely. It is a good feeling to know that you are there to back me up.

Last but not least, I am deeply grateful for Lutz, Nils and Lars - my own little family. Lutz, I am not sure, how I would have survived my time at the university without you and all your love, encouragement and understanding!

6.2 Declaration/Erklärung

I, Beate Katharina Roese-Koerner, hereby confirm that this work submitted is my own. This thesis has been written independently and with no other sources and aids than stated. The presented thesis has not been submitted to another university and I have not applied for a doctorate procedure so far.

Hiermit versichere ich, dass diese Dissertation von mir persönlich, selbständig und ohne jede unerlaubte Hilfe angefertigt wurde. Die Daten, die im Rahmen einer Kooperation gewonnen wurden, sind ausnahmslos gekennzeichnet. Die aus anderen Quellen direkt oder indirekt übernommenen Daten und Konzepte sind ebenfalls unter Angabe der Quelle gekennzeichnet. Die Ergebnisse dieser Arbeit trugen in Teilen zu folgenden Veröffentlichungen bei:

Roese-Koerner B, Stappert L, Koch P, Brüstle O, Borghese L. (2013) Pluripotent Stem Cell-Derived Somatic Stem Cells as Tool to Study the Role of MicroRNAs in Early Human Neural Development. Curr Mol Med. 2013 Jun 1;13(5):707-22.

Roese-Koerner B, Borghese L, Stappert L, D'Araio S, Jungverdorben, Evert B, Peitz M, Brüstle O (2014) A feedback loop between bifunctional miR-9/9* and its direct transcriptional modulator Notch regulating human neural stem cell self-renewal and differentiation Stem Cell Rep. Manuscript in preparation

Die vorliegende Arbeit wurde an keiner anderen Hochschule als Dissertation eingereicht. Ich habe früher noch keinen Promotionsversuch unternommen. Diese Dissertation wurde an der nachstehend aufgeführten Stelle auszugsweise veröffentlicht.

Bonn, den

_____

(Beate Katharina Roese-Koerner)